Dynamic Modeling and Control of Multi-Machine Power System with FACTS Devices for Stability Enhancement

A thesis submitted in partial fulfillment of the requirements for the degree of

Doctor of Philosophy
in
Electrical Engineering

by

Jose P. Therattil
ROLL NO. 509EE703

Under the Guidance of

Prof. P. C. Panda

Department of Electrical Engineering

National Institute of Technology

Rourkela-769008 (Odisha)

July 2012

DEPARTMENT OF ELECTRICAL ENGINEERING
NATIONAL INSTITUTE OF TECHNOLOGY, ROURKELA-769 008
ODISHA, INDIA

CERTIFICATE

This is to certify that the thesis entitled "Dynamic Modelling and Control of Multi-machine Power System with FACTS Devices for Stability Enhancement", being submitted by Shri Jose P. Therattil, is a record of bonafide research carried out by him at Electrical Engineering Department, National Institute of Technology, Rourkela, under my guidance and supervision. The work incorporated in this thesis has not been, to the best of my knowledge, submitted to any other university or institute for the award of any degree or diploma.

Dr. P. C. Panda
Professor
Department of Electrical Engineering
National Institute of Technology
Rourkela-769 008 (Odisha)

Acknowledgements

This thesis is a result of research that has been carried out at National Institute of Technology, Rourkela. During this period, I came across with a great number of people whose contributions in various ways helped my field of research and they deserve special thanks. It is a pleasure to convey my gratitude to all of them.

In the first place, I would like to express my deep sense of gratitude and indebtedness to my supervisor Prof. P. C. Panda for his advice, and guidance from early stage of this research and providing me extraordinary experiences throughout the work. Above all, he provided me unflinching encouragement and support in various ways which exceptionally inspire and enrich my growth as a student, a researcher and a scientist. I am proud to record that I had opportunity to work with an exceptionally experienced scientist like him.

I am grateful to Director, Prof. S.K. Sarangi and Prof. Bidyadhar Subudhi, Head of Electrical Engineering Department, National Institute of Technology, Rourkela, for their kind support and concern regarding my academic requirements.

I am thankful for the opportunity to be a member of National institute of technology of Electrical Engineering Department. I express my gratitude to the members of Doctoral Scrutiny Committee, Prof. K.B. Mohanty and Prof. K.K. Mohapatra for their advice and care.

I express my thankfulness to the faculty and staff members of the Electrical Engineering Department for their continuous encouragement and suggestions. Thanks are also due to my co-scholars at National Institute of Technology, Rourkela, for their whole hearted support and cooperation during the duration of this work.

My parents deserve special mention for their inseparable support and prayers. They are the persons who show me the joy of intellectual pursuit ever since I was a child. I thank them for sincerely bringing up me with care and love.

The completion of this work came at the expense of my long hours of absence from home. Words fail me to express my appreciation to my wife Jerry Jose and my sons Paul Therattil

and Anthony Therattil for their understanding, patience and active cooperation throughout the course of my doctoral dissertation. I thank them for being supportive and caring.

Last, but not the least, I thank the one above all of us, the omnipresent God, for giving me the strength during the course of this research work.

Jose P. Therattil
Roll No. 509EE703

Abstract

Due to environmental and economical constraints, it is difficult to build new power lines and to reinforce the existing ones. The continued growth in demand for electric power must therefore to a great extent be met by increased loading of available lines. A consequence of this is reduction of power system damping, leading to a risk of poorly damped power oscillations between generators. This thesis proposes the use of controlled active and reactive power to increase damping of such electro-mechanical oscillations.

The focus of this thesis is a FACTS device known as the Unified Power Flow Controller (UPFC). With its unique capability to control simultaneously real and reactive power flows on a transmission line as well as to regulate voltage at the bus where it is connected, this device creates a tremendous quality impact on power system stability. These features turn out to be even more significant because UPFC can allow loading of the transmission lines close to their thermal limits, forcing the power to flow through the desired paths. This providdes the power system operators much needed flexibility in order to satisfy the demands.

A power system with UPFC is highly nonlinear. The most efficient control method for such a system is to use nonlinear control techniques to achieve system oscillation damping. The nonlinear control methods are independent of system operating conditions. Advanced nonlinear control techniques generally require a system being represented by purely differential equations whereas a power system is normally represented by a set of differential and algebraic equations.

In this thesis, a new method to generate a dynamic modeling for power network is introduced such that the entire power system with UPFC can be represented by purely differential equation. This representation helps us to convert the nonlinear power system equations into standard parametric feedback form. Once the standard form is achieved, conventional and advanced nonlinear control techniques can be easily implemented.

A comprehensive approach to the design of UPFC controllers (AC voltage control, DC voltage control and damping control) is presented. The damping controller is designed using nonlinear control technique by defining an appropriate Lyapunov function. The analytical expression of the nonlinear control law for the UPFC is obtained using back stepping method. Then, combining the nonlinear control strategy with the linear one for the other variables, a complete linear and nonlinear stabilizing controller is developed.

Finally, an adaptive method for estimating the uncertain parameters is derived. This relaxes the need for approximating the uncertain parameters like damping coefficient, transient synchronous reactance etc., which are difficult to be measured precisely.

The developed controller provides robust dynamic performance under wide variations in loading condition and system parameters, and provides a significant improvement in dynamic performance in terms of peak deviations. The proposed controller is tested on different multi-machine power systems and found to be more effective than existing ones.

Dedicated to

My Wife and Children

Contents

List of Tables

List of Figures

Nomenclature

δ_i, ω_i : Rotor angle and angular speed of the i^{th} machine

P_{mi} : Input mechanical power of the i^{th} machine

E_{gi} : Internal generator voltage of the i^{th} machine

M_i : Machine inertia of the i^{th} machine

D_i : Damping coefficient

H_i : Inertia constant

P_e : Electrical power of the generator

X_d :Direct axis steady state reactance of the generator

X_q : Quadrature axis steady state reactance of the generator

X'_d : Direct axis transient reactance of the generator

T'_{do} : Direct axis open circuit time constant of the generator

C_{dc} : DC link capacitor

V_{dc} : Voltage at DC link

m_{SH} : Modulation index of shunt converter

φ_{SH} : Phase angle of shunt-converter voltage

m_{SR} : Modulation index of series converter

φ_{SR} : Phase angle of series-converter voltage

I_{SH} : Current through shunt converter

T_1, T_2, T_3, T_4 : Time constants of Lead-Lag controller

f : Frequency

P_{Li}, Q_{Li} : Active and reactive load at each bus

V_i : Voltage magnitude of the i^{th} bus

Φ_i : Phase angle of the i^{th} bus voltage

X_{Li} : Reactance of transmission line

X_{SH}, X_{SR} : Reactance of shunt and series transformer

V_{Ti} : Terminal voltage at bus i

X_{ti} : Reactance of the step-up transformer

V_B : System side base voltage in KV

E_{fd} : Field voltage of generator

K_A : Excitation system gain

T_A : Excitation system time constant

Δ : Incremental operator

T_W : Wash out filter time constant

Ψ_i : Uncertain parameters

Abbreviation

FACTS	: Flexible AC Transmission Systems
SVC	: Static VAR Compensator
TCSC	: Thyristor Controlled Series Capacitor
STATCOM	: Static Synchronous Compensators
SSSC	: Static Synchronous Series Compensators
UPFC	: Unified Power Flow Controllers
IPFC	: Interline Power Flow Controllers
PSS	: Power System Stabilizer
HVDC	: High Voltage Direct Current
EPRI	: Electric Power Research Institute
QFT	: Quantitative feedback theory
CSC	: Controllable Series Capacitor
SSR	: Sub-synchronous Resonance
GTO	: Gate Turn Off
SVD	: Singular Value Decomposition
PWM	: Pulse Width Modulation
VSC	: Voltage Source Converter
SISO	: Single-input Single-output

MIMO	: Multi-input Multi-output
PI	: Proportional and Integral
COI	: Center of Inertia
SMIB	: Single Machine Infinite Bus
GA	: Genetic Algorithm

Chapter 1

Introduction

Chapter 1

Introduction

The available power generating plants are often located at distant locations for economic, environmental and safety reasons. For instance, it becomes cheaper to install a thermal power station at pit-head instead of transporting coal to load centers. Hydro power is generally available in remote areas and a nuclear plant may be located at a place away from urban areas. Additionally, modern power systems are highly interconnected. Sharing of generation reserves, exploiting load diversity and economy gained from the use of large efficient units without sacrificing reliability are the advantages of interconnection. Thus power must consequently be transmitted over long distances. To meet the load and electric market demands, new lines should be added to the system, but due to environmental reasons, the installation of electric power transmission lines are often restricted. Hence, the utilities are forced to rely on already existing infra-structure instead of building new transmission lines. In order to maximize the efficiency of generation, transmission and distribution of electric power, the transmission networks are very often pushed to their physical limits, where outage of lines or other equipment could result in the rapid failure of the entire system.

The power system may be thought of as a nonlinear system with many lightly damped electromechanical modes of oscillation. The three modes of electromechanical oscillations are:

- Local plant mode oscillations
- Inter-area mode oscillations
- Torsional modes between rotating plant

In local mode, one generator swings against the rest of the system at 1.0 to 2.0 Hz. The impact of the oscillation is localized to the generator and the line connecting it to the

grid. The rest of the system is normally modeled as a constant voltage source whose frequency is assumed to remain constant. This is known as the SIMB model

Inter-area mode of oscillations is observed over a large part of the network. It involves two coherent groups of generators swinging against each other at 1Hz or less. This complex phenomenon involves many parts of the system with highly non-linear dynamic behavior. The damping characteristic of the inter-area mode is dictated by the tie-line strength, the nature of the loads and the power flow through the interconnection and the interaction of loads with the dynamics of generators and their associated controls.

Torsional mode oscillations is associated with a turbine generator shaft system in the frequency range of 10-45 Hz. Usually these modes are excited when a multi-stage turbine generator is connected to the grid system through a series compensated line. A mechanical torsional mode of the shaft system interacts with the series capacitor at the natural frequency of the electrical network. The shaft resonance appears when network natural frequency equals synchronous frequency minus torsional frequency.

If the damping of these modes becomes too small, it can impose severe constraints on the system's operation. It is thus important to be able to determine the nature of those modes, find stability limits and in many cases use controls to prevent instability. The poorly damped low frequency electromechanical oscillations occur due to inadequate damping torque in some generators, causing both local-mode oscillations and inter-area oscillations (0.2 Hz to 2.5 Hz) [1], [2].

The basic function of an excitation system is to provide direct current to the synchronous machine field winding. In addition, the excitation system performs control functions essential to the satisfactory performance of the power system by controlling the field voltage and there by the field current. The control functions include the control of voltage and reactive power flow, and the enhancement of system stability. Excitation system helps to improve synchronizing torque where as under heavy loading conditions it introduces negative damping. This is because the excitation system introduces a large

phase lag at low system frequencies just above the natural frequency of the excitation system. Thus it can often be assumed that the voltage regulator introduces negative damping. These are the situations in which dynamic stability is of concern.

The traditional approach employs power system stabilizers (PSS) on generator excitation control systems in order to damp those oscillations. PSSs are effective but they are usually designed for damping local modes. In large power systems, they may not provide enough damping for inter-area modes. So, more efficient substitutes are needed other than PSS.

In late 1980s, the Electric Power Research Institute (EPRI) had introduced a new technology program known as Flexible AC Transmission System (FACTS) [3]. The main idea behind this program is to increase controllability and optimize the utilization of the existing power system capacities by reliable and high-speed power electronic devices. The latest generation of FACTS controllers is based on the concept of the solid state synchronous voltage sources (SVSs) introduced by L. Gyugyi in the late 1980s [4]. The SVS behaves as an ideal synchronous machine, i.e., it generates three-phase balanced sinusoidal voltages of controllable amplitude and phase angle with fundamental frequency. It can internally generate both inductive and capacitive reactive power. If coupled with an appropriate energy storage device, i.e., DC storage capacitor, battery etc., SVS can exchange real power with the AC system. The SVS can be implemented by the use of the voltage source converters (VSC).

The major advantages of SVS-based compensators over mechanical and conventional thyristor compensators are:

- Improved operating and performance characteristics
- Uniform use of same power electronic device in different compensation and control applications
- Reduced equipment size and installation labor.

The SVS can be used as shunt or series compensator. If operated as a reactive shunt compensator, it is called static synchronous compensator (STATCOM); and if operated as a reactive series compensator, it is called static synchronous series compensator (SSSC). A special arrangement of two SVSs, one connected in series with the AC system and the other one connected in shunt with common DC terminals, is called Unified Power Flow Controller (UPFC). The UPFC is a combination of the two in a single device. UPFC is the most promising device in the FACTS concept. It has the ability to adjust all the three control parameters, *i.e.,* the bus voltage, transmission line reactance and phase angle between two buses, either simultaneously or independently. A UPFC performs this through the control of the in-phase voltage, quadrature voltage and shunt compensation.

1.1 Review of literature

In this section a literature survey of topics related to power system operation, modeling and control is highlighted. A power system may be thought to be a large interconnected system with many lightly damped electro-mechanical oscillations. During such oscillations, mechanical kinetic energy is exchanged between synchronous generators as electric power flows through the network. The oscillations can be seen in many variables, where the rotor velocities of the generators and the power flows in the network are the most important. The rotor velocity variation causes strain to mechanical parts in the power plant and should be limited. The power flow oscillations may amount to the entire rating of a power line. As they are superimposed on the stationary line flow, they limit the transfer capacity by requiring increased safety margins. Power system stability is defined as the ability of an electrical power system, for a given initial operating condition, to regain a state of operating equilibrium after being subjected to physical disturbance [1], [6].

A. Conventional methods

As a convenient approach to control synchronous generator and stabilize power systems, excitation controller design has drawn sizable consideration [7], [8]. The operation of excitation control continues to maintain generator voltage and reactive power output. A high response exciter is helpful in adding synchronizing torque. However, on account of performing, it introduces negative damping. An efficient method to meet the conflicting exciter behavior with respect to system stability is to assign a PSS. The elementary usage of power system stabilizer is to supplement damping to the generator rotor oscillations by governing its excitation employing auxiliary stabilizing signals [9], [10], [11]. The PSS classically uses shaft speed, active power output or bus frequency as input [12]. The stabilizer shown in Figure 1.1 consists of two lead-lag filters. These are used to compensate for the phase lag introduced by the AVR and the field circuit of the generator. Other filter sections are usually added to reduce the impact on torsional dynamics of the generator, and to prevent voltage errors due to a frequency offset. The lead-lag filters are tuned so that speed oscillations give a damping torque on the rotor. By varying the terminal voltage the PSS affects the power flow from the generator, which efficiently damps local modes. Figure 1.1 shows the block diagram representation of a conventional PSS. Where K_S is the stabilizer gain, while T_w and T_1 to T_4 are the time constants of washout and lead-lag filters respectively. The PSS output is added to the difference between reference V_{ref} and actual value V_{act} of the terminal voltage.

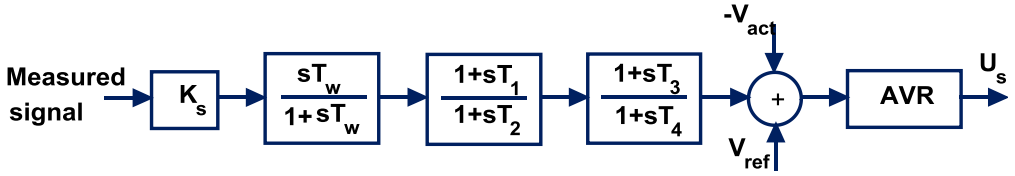

Figure 1.1: **Block diagram of conventional power system stabilizer**

A difficulty of PSS tuning, except for the trade-off with voltage regulation, is that the dynamics that should be compensated by the lead-lag filters vary with the operating point and the network reactance [12].

The effect of PSS on inter-area modes differs from the local modes in two ways. Firstly, the achievable damping of inter-area modes is less than that of local modes. Secondly, inter-area modes are affected mainly through modulation of voltage sensitive loads. This makes assumptions on load characteristics critical both for investigations and for field tuning [13], [14]. Damping of both local and inter-area modes requires suitable phase compensation over a wider frequency range, which may be difficult to achieve and therefore, other efficient substitutes are needed in addition to PSS.

B. FACTS devices

In the late 1980s, the Electric Power Research Institute (EPRI) formulated the vision of the FACTS in which various power-electronics based controllers regulate power flow and transmission voltage, and they mitigate dynamic disturbances. Generally, the main objectives of FACTS are to increase the useable transmission capacity of lines and control power flow over designated transmission routes. Hingorani and Gyugyi [5] and Hingorani [15], [16] proposed the concept of FACTS and Edris et al. [17] proposed terms and definitions for different FACTS controllers. Due to recent advances in power electronics, the FACTS devices have gained a great interest during the last few years.

There are two generations for realization of power electronics-based FACTS controllers: the first generation employs conventional thyristor-switched capacitors and reactors, and quadrature tap-changing transformers, and the second generation employs gate turn-off (GTO) thyristor-switched converters as voltage source converters (VSCs). The first generation has resulted in the Static VAR Compensator (SVC), the Thyristor- Controlled Series Capacitor (TCSC), and the Thyristor-Controlled Phase Shifter (TCPS) [18], [19]. The second generation has produced the Static Synchronous Compensator (STATCOM), the Static Synchronous Series Compensator (SSSC), the Unified Power Flow Controller

(UPFC), and the Interline Power Flow Controller (IPFC) [20], [21], [22], [23]. The two groups of FACTS controllers have distinctly different operating and performance characteristics.

(a) First generation FACTS

First generation FACTS employs capacitor and reactor banks with fast solid-state switches in traditional shunt or series circuit arrangements. The thyristor switches control the on and off periods of the fixed capacitor and reactor banks and thereby realize a variable reactive impedance. Except for losses, they cannot exchange real power with the system.

Static VAR Compensator (SVC)

The SVC is a reactive shunt device that uses its reactive capability to alter the bus voltage. It enables a regulated voltage support. An SVC for continuous control contains a thyristor switched capacitor bank in parallel with a bank of phase angle controlled reactors and is connected to the transmission voltage level via a transformer.

The SVC influences electro-mechanical oscillations like the PSS: it changes the line transfer (by controlling V) as well as modulates voltage sensitive loads. Depending on which of these effects dominate, the SVC is placed either at the midpoint of a long transmission line or near the load centre.

It is known that the SVCs with an auxiliary injection of a suitable signal can considerably improve the dynamic stability performance of a power system [24]–[36]. In the literature, SVCs have been applied successfully to improve the transient stability of a synchronous machine [24]. Hammad [25] presented a fundamental analysis of the application of SVC for enhancing the power systems stability. Then, the low frequency oscillation damping enhancement via SVC has been analyzed [26], [27], [28], [29]. It shows that the SVC enhances the system damping of local as well as inter-area oscillation modes. Self-tuning and model reference adaptive stabilizers for SVC control

have been also proposed and designed [30], [31], [32]. Robust SVC controllers based on H_∞, uncertainty representation cannot treat situations where a nominal stable system becomes unstable after being perturbed [35]. Moreover, the pole-zero cancellation structured singular value μ, and Quantitative Feedback Theory QFT has been presented to enhance system damping [33], [34]. However, the importance and difficulties in the selection of weighting functions of H_∞ optimization problem have been reported. In addition, the additive and/or multiplicative phenomenon associated with this approach produces closed loop poles whose damping is directly dependent on the open loop system (nominal system) [36]. Apart from the above-mentioned disadvantage, the major disadvantage of SVC is that its maximum compensation current depends upon the system voltage. During fault, compensation decreases due to voltage drop which is an unhealthy situation. Maximum capacitive VAR output decreases with the square of voltage decrease.

Controllable Series Capacitor (CSC)

The Controllable Series Capacitor (CSC) is connected in series with long transmission lines. In the first place its presence is motivated by the need to effectively shorten the line electrically, which increases the power transfer capability.

A CSC affects electro-mechanical oscillations by modulating the transfer reactance of a line. The impact of this control action increases with line loading [37], which is a desirable property. The CSC is more effective than the SVC for damping purposes [37], which is explained by how they are connected. The series device affects the entire line flow, and the shunt device only changes a part [38]. While fixed series capacitors are common, only a few CSCs are currently in operation. An important reason is the constructional difficulties with a main circuit on line potential. The voltage rating of a CSC is typically a fraction of the normal voltage drop over the line where it is installed. As this is far less than the voltage resulting from a three-phase short-circuit on the line, protection circuits that by-pass the compensator are critically important. Due to the low

number of CSCs in operation, no statements about the measurements commonly used by damping controllers can be made. The major disadvantage is that sustained oscillation below the fundamental system frequency can be caused by series capacitive compensation. The phenomenon, referred to as sub-synchronous resonance (SSR).

High Voltage Direct Current Link

In a High Voltage Direct Current (HVDC) link the AC voltage is rectified, transmitted as DC, and converted back to AC. The absence of reactive transmission losses makes HVDC the preferred technique for connections with submarine cables longer than 30 km and for overhead lines longer than 600 km [1]. The DC transmission also provides an asynchronous connection between two power systems, which is of particular value when the systems have different frequencies such as 50 and 60 Hz.

An HVDC link is controlled at the rectifier and the inverter through their firing angles and through the tap changer of the transformer at each converter station. The control system operates in a number of control modes, where certain variables are held constant. The ability to directly affect power flow makes HVDC links very powerful for damping of electro-mechanical oscillations.

The active power modulation is typically controlled by the frequency at the converter station(s) [40], [41], the frequency of a nearby generator [13] or a line flow [1]. Since the converters are line commutated, reactive power consumption is associated with the active power flows. The dependence between the modulations of active and reactive power is governed by the control mode. It may either support the active power modulation or counteract it [41].

(b) Second generation of FACTS

The technologies described above are in operation today, but new power electronic devices with a potential for damping of electro-mechanical oscillations are constantly suggested [3]. The voltage source converter (VSC) type FACTS controller group

employs self-commutated DC to AC converters, using GTO thyristors, which can internally generate capacitive and inductive reactive power for transmission line compensation, without the use of capacitor or reactor banks. The converter with energy storage device can also exchange real power with the system in addition to the independently controllable reactive power. The VSC can be used uniformly to control transmission line voltage, impedance, and angle by providing reactive shunt compensation, series compensation, and phase shifting, or to control directly the real and reactive power flow in the line [23].

Static Synchronous Compensator (STATCOM)

The emergence of FACTS devices and in particular GTO thyristor-based STATCOM has enabled such technology to be proposed as serious competitive alternatives to conventional SVC [42]. From the viewpoint of power system dynamic stability, the STATCOM provides better damping characteristics than the SVC as it is able to transiently exchange active power with the system. The effectiveness of the STATCOM to control the power system voltage was presented [43]. However, the effectiveness of the STATCOM to enhance the angle stability has not been addressed. Abido [44] presented a singular value decomposition (SVD) based approach to assess and measure the controllability of the poorly damped electromechanical modes by STATCOM different control channels. It was observed that the electromechanical modes are more controllable via phase modulation channel. It was also concluded that the STATCOM-based damping stabilizers extend the critical clearing time and enhance greatly the power system transient stability. Haque [45] demonstrated that by the use of energy function, a STATCOM can to provide additional damping torque to the low frequency oscillations in a power system.

Static Synchronous Series Compensator (SSSC)

The SSSC has been applied to different power system studies to improve the system performance. There has been some work done to utilize the characteristics of the SSSC

to enhance power system stability [46], [47]. Wang [46] investigated the damping control function of an SSSC installed in power systems. The linearized model of the SSSC integrated into power systems was established and methods to design the SSSC damping controller were proposed. Kumkratug and Haque [47] demonstrated the capability of the SSSC to control the line flow and to improve the power system stability. A control strategy of an SSSC to enlarge the stability region has been derived using the direct method. The effectiveness of the SSSC to extend the critical clearing time has been confirmed though simulation results on a single-machine infinite bus system.

Unified Power Flow Controller (UPFC)

The UPFC, which was proposed by L. Gyugyi in 1991 [5], [48], [49], is superior to the FACTS devices in terms of performance. UPFCs have been chosen in recent days to unify the bus bar voltage regulation ability of STATCOM and power flow control capability of SSSC in a single device. It is primarily used for independent control of real and reactive power in transmission lines for a flexible, reliable and economic operation and loading of power system. Further, the UPFC can be used for voltage support, transient stability improvement and damping of low frequency power system oscillations. The elementary ideas on how bus bar voltage regulation, reactive power compensation, and power flow control can be obtained by a UPFC [49], [50]. The interest measure of FACTS is shown in Figure 1.2. The literature survey carried out in [58] shows that the number of publications, applications of FACTS to power system stability in particular, has a tremendous increment. From Figure 1.2, it is clear that the interest in the 2^{nd} generation of FACTS has drastically increased while the interest in the 1^{st} generation has decreased.

The response time of second generation FACTS devices are shorter than that of first generation FACTS devices, mainly due to the fast switching times provided by the IGBTs of voltage converter. The typical dynamic response times of first generation FACTS devices are of the order of few milliseconds where as that of second generation

FACTS devices are in the range of microseconds.

Table 1.1 shows the performance analysis of FACTS devices. First column of Table 1.1 shows that series compensator is good for load flow control. Second column of the same table shows shunt compensator is good for voltage stability. Third column of Table 1.1 shows that all FACTS devices are good enough for the case of transient stability. A combination of shunt and series can better perform load flow control, voltage stability and transient stability. From the above analysis it is clear that UPFC is one of the most promising devices in FACTS concept.

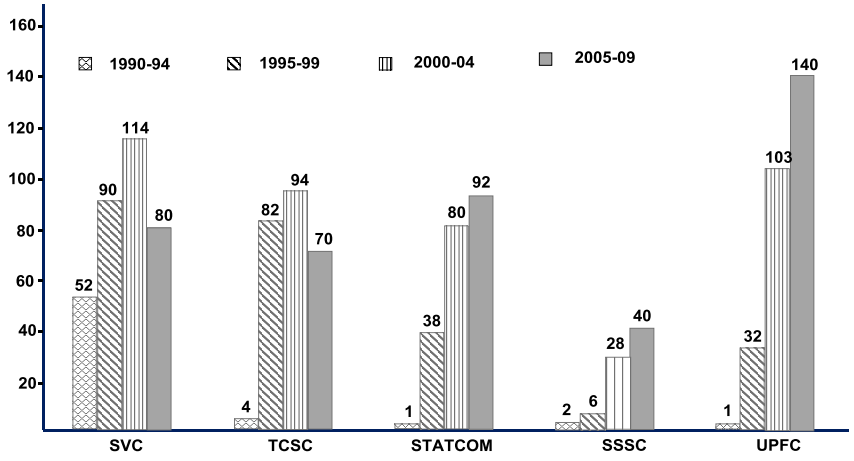

Figure 1.2: **Statistics for FACTS applications to power system stability**

Table 1.1: **Performance Analysis of FACTS devices [20]**

	Load Flow Control	Voltage Stability	Transient Stability
SVC	★	★ ★ ★	★
TCSC	★ ★	★	★ ★
STATCOM	★	★ ★ ★	★ ★
SSSC	★ ★ ★	★	★ ★
UPFC	★ ★ ★	★ ★ ★	★ ★

Many approaches have been achieved to the modeling and control of the UPFC. The foremost recurrent approach continues to model the UPFC as a power injection model [51], [52]. The power injection model ignores the dynamics of the UPFC and employs the UPFC active and reactive power injection as the control inputs into the power system. In the case where UPFC dynamics are involved, the superior approach to controlling the UPFC is to use PI control [53], [54], [55]. However PI control is less productive in damping oscillations that include multiple modes. For multiple mode damping, many lead-lag blocks are necessary that demand extra coordinated tuning. Another drawback is PI control shows poor performance as the system conditions shift from the operating point at which the controller was tuned. FACTS devices have been examined in [56],[57] using energy functions to formulate the controllers and compute the critical clearing time. This method is not suitable for controller formation since it constrains the assessment of the derivatives of power system bus voltages and angles as well as needs numerical differentiators or approximations. A feedback linearization based UPFC is explained in [10]. The nonlinear dynamic model is transformed into a linear one by coordinate transformation. From thence, the linear control technique is used in the transformed linear model. However, the details of the dynamic models must be known exactly when the exact feedback linearization techniques are used. It is very difficult to perform this task because errors and external disturbances are inherent in power systems. To overcome the above-mentioned challenges, the following contributions are made in this thesis.

1.2 Research objective

Though technological barriers exist, as in most technology areas, it is important to overcome them by developing proper understanding of the process with related attributes. The next chapters explain the various efforts directed for improving the inter-area oscillation damping applied to multi-machine power system. Exhaustive literature review reveals that the nonlinear controllers are least explored out of different methods.

Similarly, current work emphasizes the nonlinear control technique applied to multi-machine power system.

Based on these guiding principles, the objectives of the current research are as follows:

- Explore the existing methods and models for power system stability study.
- Develop an advanced nonlinear controller for transient stability improvement using UPFC as a stabilizing device.
- Derive an adaptive law for uncertain parameters which are otherwise difficulty to be measured precisely.
- Develop the software program to simulate small scale and transient phenomena.

1.3 Thesis outline

The other chapters of this thesis are organized as follows:

Chapter 2 gives an overview of basic operation, modeling and interfacing of power system components. In order to implement computer control of a power system, it is imperative to gain a clear understanding of the representation of the power system components. This chapter explains the mathematical models for synchronous generators, associated excitation systems, interconnecting transmission network including static loads and other devices such as UPFC. The chapter explains the basic operation and characteristics of different power system components. The basic knowledge of these devices is essential for controller development in the subsequent chapters

Chapter 3 deals with the Lead-Lag control design for multi-machine power system with UPFC. This chapter explores the conventional methods available for oscillation damping. A procedure for linearizing power system equations including UPFC is explained in this chapter. Phillips-Heffron model explained in this section helps to study the impact of control functions of the UPFC up on system oscillation stability. The eigen-values corresponding to electromechanical mode of oscillation are identified using participation

factor method. The procedure for calculating the controllability index is explained in this chapter. The most relevant control signal is used for the development of damping controller. Along with simulation results the advantages and disadvantages of the traditional methods are also outlined.

Chapter 4 introduces the dynamic modeling and adaptive control of single machine-infinite bus (SMIB) system with UPFC. A new method to generate a nonlinear dynamic representation of the power network is introduced to enable more sophisticated control design. The dynamic model is developed using generator terminal currents. The developed dynamic representation helps to convert nonlinear power system equations into standard parametric feedback form. Once the new representation is obtained, suitable adaptive laws for control signal and uncertain parameters are derived. Simulation results are given to validate the theoretical conjectures. The main disadvantage of this method is the assumption of infinite bus. The infinite bus assumption required for this approach is not valid for large multi-machine systems when the fault affects the power system. The adaptive law derived in this section is used in the sixth chapter to improve the efficiency of the controller.

Chapter 5 provides the dynamic modeling and nonlinear control of multi-machine power system with UPFC. First part of this chapter deals with a new nonlinear dynamic modeling for power system with UPFC to enable more sophisticated control design. Once the new modeling is obtained, an advanced nonlinear control design using back stepping methodology is explained in the second part of the chapter. The effectiveness of this approach is presented in a case study on a two-machine power system.

Chapter 6 introduces an integrated linear-nonlinear control of multi-machine power system with UPFC. This chapter begins with the disadvantages of the method developed in the previous chapter. Design of an integrated linear-nonlinear controller is explained to fully utilize the multi-functional UPFC. An adaptive law for uncertain parameters is derived in the second part of the chapter which is otherwise very difficult to be measured precisely. In the case studies, we explore all the three degrees of freedom for UPFC,

namely AC voltage control, DC voltage control and oscillation damping using newly developed hybrid controller.

Chapter 7 provides conclusion and suggestions for future work. It is a summary of the work done and concluded the present study. It explains the importance of the proposed dynamic representation for the development of nonlinear controller. Moreover, some suggestions on the extensions to potential topics for future research are proposed.

1.4 Conclusions

This chapter highlights the reasons for inter-connections and the difficulties that occur while constructing a new transmission line. The full utilization of the transmission lines without proper controllers could result in the rapid failure of the entire system. The chapter also explains the consequences of the low frequency inter-area mode of oscillations. Section 1.1 provides the insight into various past developments in the area of power system stability. For the sake of simplicity, it is divided into two main sections. Section A focuses on the brief history of conventional methods. Section B describes FACTS devices. This section is divided into two sub-sections. The first sub-section explains the existing techniques and the second sub-section explains the emerging ones. The interest measure of FACTS shows the importance of UPFC. It is the most promising device in the FACTS concept. It has the ability to adjust the three control parameters, *i.e.*, the bus voltage, transmission line reactance and phase angle between two buses, either simultaneously or independently, and how a UPFC performs these functions are explained in the next chapter.

Chapter 2

Basic Operation, Modeling and Interfacing of Power System Components

Chapter 2

Basic Operation, Modeling and Interfacing of Power System Components

2.1 Introduction

In order to implement computer control of a power system, it is imperative to gain a clear understanding of the basic operation and representation of the power system components. In the first part of this chapter, we briefly review the basic operation of UPFC and PWM techniques used for VSCs. Voltage-source converter is the building block of UPFC. The UPFC consists of two voltage-source converters. These back-to-back converters are operated from a common DC link provided by a DC storage capacitor. The basics of the VSCs are briefly discussed in the beginning of the chapter.

In the second part, development of the mathematical models of power system components is explained. Before the power systems network can be solved, it must first be modeled. Single phase representation is used for balanced system. In this section, we present simple models for generators, loads, transmission lines, UPFC, etc. The interface of the UPFC with the power network is explained at the end of this chapter.

2.2 Basic operation of UPFC

UPFC is a device placed between two buses referred to as the UPFC sending bus and the UPFC receiving bus. It consists of two voltage-source converters, as illustrated in Figure 2.1. The back-to-back converters, labeled "shunt converter" and "series converter" in the figure, are operated from a common DC link provided by a DC storage capacitor. The shunt converter is primarily used to provide active power demand of the series converter through the common DC link. Shunt converter can also generate or absorb reactive power, if it is desired, and thereby it provides independent shunt reactive compensation for the line.

Series converter provides the main function of the UPFC by injecting a voltage with controllable magnitude and phase angle in series with the line. For the fundamental frequency model, the VSCs are replaced by two controlled voltage sources [60]. The UPFC is placed on the high-voltage transmission lines. This arrangement requires step-down transformers in order to allow the use of power electronics devices for the UPFC.

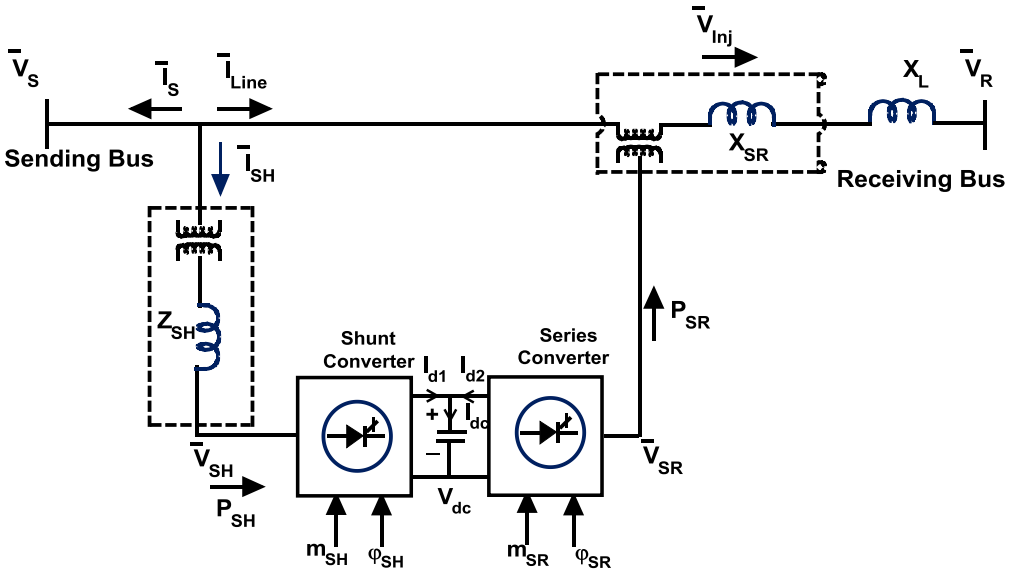

Figure 2.1: **Basic Circuit Configuration of the UPFC**

Applying the Pulse Width Modulation (PWM) technique to the two VSCs the following equations for magnitudes of shunt and series injected voltages are obtained

$$\begin{cases} V_{SH} = \dfrac{m_{SH} V_{dc}}{2\sqrt{2} V_B} \\ V_{SR} = \dfrac{m_{SR} V_{dc}}{2\sqrt{2} V_B} \end{cases} \tag{2.1}$$

The phase angles of $\bar{V}_{SH}$ and $\bar{V}_{SR}$ are

$$\begin{cases} \phi_{SH} = \angle(\phi_S - \varphi_{SH}) \\ \phi_{SR} = \angle(\phi_S - \varphi_{SR}) \end{cases} \tag{2.2}$$

The series converter injects an AC voltage $\bar{V}_{SR} = V_{SR}\angle(\phi_S - \varphi_{SR})$ in series with the transmission line. Series voltage magnitude V_{SR} and its phase angle φ_{SR} with respect to the sending bus are controllable in the range of $0 \le V_{SR} \le V_{SR\max}$ and $0 \le \varphi_{SR} \le 360^0$ respectively. The shunt converter injects controllable shunt voltage such that the real component of the current in the shunt branch balance the real power demanded by the series converter. The real power can flow freely in either direction between the AC terminals. On the other hand, the reactive power cannot flow through the DC link. It is absorbed or generated locally by each converter. The shunt converter operated to exchange the reactive power with the AC system provides the possibility of independent shunt compensation for the line. If the shunt injected voltage is regulated to produce a shunt reactive current component that will keep the sending bus voltage at its pre-specified value, then the shunt converter is operated in the Automatic Voltage Control Mode**.** Shunt converter can also be operated in the VAR control mode**.** In this case shunt reactive current is produced to meet the desired inductive or capacitive VAR request. The basics of VSCs and PWM techniques are briefly discussed in the next section.

A. Basic concepts of voltage source converters and PWM technique

The typical three-phase VSC is shown in Figure 2.2 [5]. It is made of six valves, (1-1') to (6-6') each consisting of a gate turn off device (GTO) paralleled with a reverse diode, and a DC capacitor. The designated order 1 to 6 represents the sequence of valve operation in time. It consists of three-phase legs, which operates in concert, 120 degrees apart. An AC voltage is generated from a DC voltage through sequential switching of the GTOs. Being an AC voltage source with low internal impedance, a series transformer is essential to ensure that the DC capacitor is not short-circuited and discharged rapidly into a capacitive load such as transmission line. The DC voltage always has one polarity and the DC current can flow in either direction. Controlling the angle of the converter output voltage with respect to the AC system voltage controls the real power exchange between the converter and the AC system.

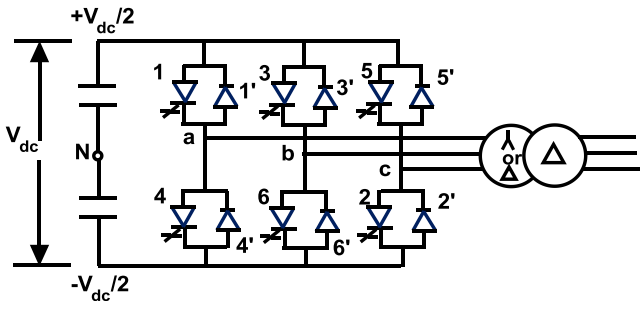

Figure 2.2: **Three Phase Voltage Source-Converter**

The real power flows from the DC side to AC side (inverter operation) if the converter output voltage is controlled to lead the AC system voltage. If the converter output voltage is made to lag the AC system voltage, the real power will flow from the AC side to DC side (rectifier operation). Inverter action is carried out by the GTOs while the rectifier action is carried out by the diodes.

Controlling the magnitude of the converter output voltage controls the reactive power exchange between the converter and the AC system. The converter generates reactive power for the AC system if the magnitude of the converter output voltage is greater than the magnitude of the AC system voltage. If the magnitude of the converter output voltage is less than that of the AC system, the converter will absorb reactive power. The converter output voltage can be controlled using various control techniques. Pulse Width Modulation (PWM) techniques can be designed for the lowest harmonic content. It should be mentioned that these techniques require large number of switching per cycle leading to higher converter losses. Therefore, PWM techniques are currently considered unpractical for high voltage applications. However, it is expected that recent developments on power electronic switches will allow practical use of PWM controls on such applications in the near future. Due to their simplicity many authors, viz., [58], [59], [60], have used PWM control techniques in their UPFC studies. Hence, the same approach is used in this thesis.

When sinusoidal PWM technique is applied, turn on and turn off signals for GTOs are generated comparing a sinusoidal reference signal V_R of amplitude A_R with a saw tooth carrier waveform V_C of amplitude A_C as shown in Figure 2.4 [5]. The frequency of the saw tooth waveform establishes the frequency at which GTOs are switched.

Consider a phase-leg as shown in Figure 2.3. In Figure 2.4, $V_R > V_C$ results in a turn on signal for the device 1 and gate turn off signal for the device 4 and $V_R < V_C$ results in a turn off signal for the device 1 and gate turn on signal for the device 4. The fundamental frequency of the converter output voltage is determined by the frequency of the reference signal. Controlling the amplitude of the reference signal controls the width of the pulses. In two-level or multilevel converters, there is only one turn-on, turn-off per device per cycle. With these converters, the AC output voltage can be controlled, by varying the width of the voltage pulses, and / or the amplitude of the DC bus voltage. It goes without saying that more pulses means more switching losses, so that the gains from the use of PWM have to be sufficient to justify an increase in switching losses.

For FACTS technology with high power in the tens of megawatts and converter voltage in KVs and tens of KVs, low frequencies in the few hundred Hertz or may be the low kilohertz range may seem feasible and worth considering. The least cost and simplest controllable three-phase converter would seem to be a six-valve converter with one turn-off device / diode per valve. In FACTS applications, there will usually be a need for a transformer between the converter valves and the AC system; there is therefore a certain flexibility provided by the transformer turn ratio to match the available device current and voltage rating.

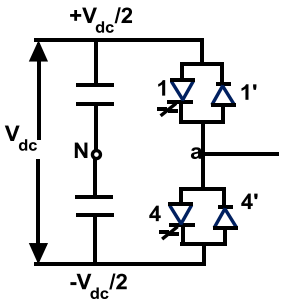

Figure 2.3: **A Phase-leg**

The amplitude modulation index is defined as ratio of A_R to A_C

$$m = \frac{A_R}{A_C} \tag{2.3}$$

For $m \leq 1$ the peak magnitude of the fundamental frequency component of the converter output voltage can be expressed as

$$V = \frac{mV_{dc}}{2} \tag{2.4}$$

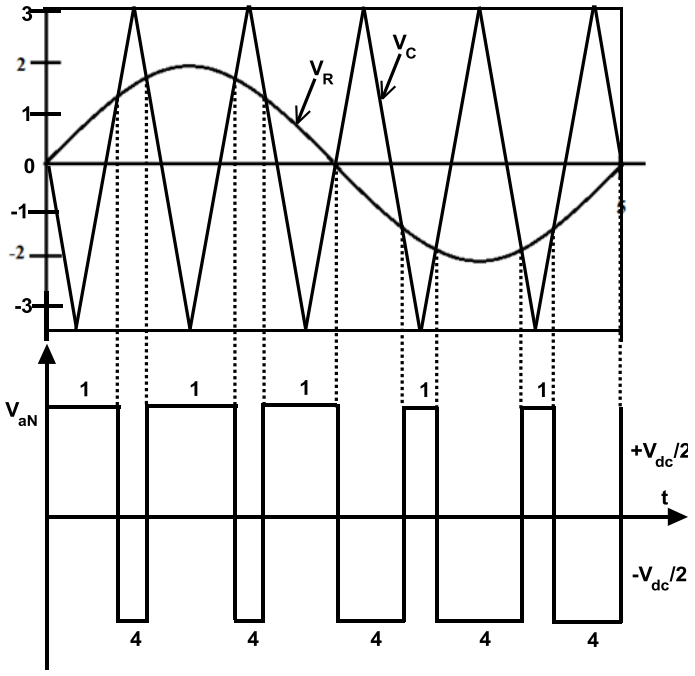

Figure 2.4: **PWM Waveforms**

B. Power flow on a transmission line

The knowledge of power flow on a transmission line is helpful to understand the characteristics of the UPFC. Therefore in this section, power flow on a transmission line between two buses S and R (line sending and receiving buses), as shown in Figure 2.5, is reviewed. For the system shown in Figure 2.5, the RMS phasor voltages of the sending and receiving buses are $\bar{V}_S = V_S \angle \phi_S$ and $\bar{V}_R = V_R \angle \phi_R$, $\bar{I}_{Line}$ is the phasor current on the line, R and X are resistance and reactance of the line respectively.

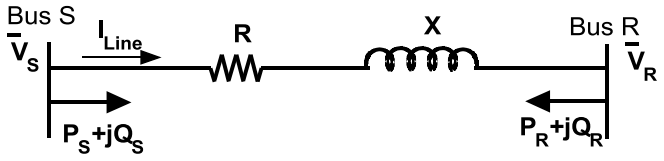

Figure 2.5: **Transmission Line**

The complex power injected into the sending bus is given by

$$S_S = P_S + jQ_S = \bar{V}_S \bar{I}^*_{Line} \tag{2.5}$$

where P_S and Q_S are the real and reactive powers injected into the sending bus, * denotes conjugate complex value. Using Ohm's law, line current can be written as

$$\bar{I}_{Line} = \frac{\bar{V}_S - \bar{V}_R}{R + jX} = (\bar{V}_S - \bar{V}_R)(G - jB) \tag{2.6}$$

where $G = \frac{R}{R^2 + X^2}$ is line conductance and $B = \frac{X}{R^2 + X^2}$ is line susceptance.

Taking the complex conjugate of (2.5) and using (2.6) the following expression can be obtained

$$S^*_S = P_S - jQ_S = (V_S^2 - \bar{V}^*_S \bar{V}_R)(G - jB) \tag{2.7}$$

Using Euler's identity, which states that $V\angle -\phi = V(\cos\phi - j\sin\phi)$, to write

$$\bar{V}_S^* \bar{V}_R = (V_S \angle -\phi_S)(V_R \angle \phi_R) = V_S V_R \angle -(\phi_S - \phi_R) = V_S V_R(\cos(\phi_S - \phi_R) - j\sin(\phi_S - \phi_R)) \quad (2.8)$$

and separating real and imaginary parts of (2.7) the following expressions for the real and reactive powers injected into the sending bus are obtained

$$\begin{cases} P_S = V_S^2 G - V_S V_R G\cos(\phi_S - \phi_R) + V_S V_R B\sin(\phi_S - \phi_R) \\ Q_S = V_S^2 B - V_S V_R B\cos(\phi_S - \phi_R) - V_S V_R G\sin(\phi_S - \phi_R) \end{cases} \quad (2.9)$$

Similarly, the real and reactive powers received at the receiving bus are

$$\begin{cases} P_R = V_S^2 G - V_S V_R G\cos(\phi_R - \phi_S) + V_S V_R B\sin(\phi_R - \phi_S) \\ Q_R = V_R^2 B - V_S V_R B\cos(\phi_R - \phi_S) - V_S V_R G\sin(\phi_R - \phi_S) \end{cases} \quad (2.10)$$

The power losses on the line are given by

$$\begin{cases} P_{Loss} = P_S + P_R = G(V_S^2 + V_R^2) - 2V_S V_R G\cos(\phi_S - \phi_R) \\ Q_{Loss} = B(V_S^2 + V_R^2) - 2V_S V_R B\cos(\phi_S - \phi_R) \end{cases} \quad (2.11)$$

For typical transmission line $X >> R$. Therefore, the conductance G is usually neglected and susceptance B is replaced by $B = -\frac{1}{X}$. Using these approximations, the expression for real power transmitted over the line from the sending to the receiving bus becomes

$$P_S = -P_R = \frac{V_S V_R}{X}\sin(\phi_S - \phi_R) = \frac{V_S V_R}{X}\sin\phi \quad (2.12)$$

where $\phi = \phi_S - \phi_R$ is called the power angle.

$$\begin{cases} Q_S = \frac{V_S^2}{X} - \frac{V_S V_R}{X}\cos(\phi_S - \phi_R) \\ Q_R = \frac{V_R^2}{X} - \frac{V_S V_R}{X}\cos(\phi_R - \phi_S) \end{cases} \quad (2.13)$$

It can be seen from equation (2.12) that the amount of the real power transmitted over the line can be increased by

- increasing the magnitude of the voltages at either end, i.e., voltage support,
- reducing the line reactance, i.e., line compensation, and
- increasing the power angle, i.e., phase shift.

Power flow can be reversed by changing the sign of the power angle, i.e., a positive power angle corresponds to a power flow from the sending to the receiving bus, while a negative power angle corresponds to a power flow from the receiving to the sending bus. Hence, the four parameters that affect real and reactive power flow are V_S, V_R, X and ϕ.

C. Series converter: Four modes of operation

As mentioned earlier, the UPFC can control, independently or simultaneously, all parameters that affect power flow on the transmission line. This is illustrated in the phasor diagrams shown in Figure 2.6 [5].

Voltage regulation is shown in Figure 2.6 (a). The magnitude of the sending bus voltage $\bar{V}_S$ is increased (or decreased) by injecting a voltage $\bar{V}_1$, in phase (or out of phase) with $\bar{V}_S$. Similar regulation can be accomplished with a transformer tap changer. Series reactive compensation is shown in Figure 2.6 (b). It is obtained by injecting a voltage $\bar{V}_2$, orthogonal to the line current $\bar{I}_{Line}$. The effective voltage drop across the line impedance X is decreased (or increased) if the voltage $\bar{V}_2$ lags the current $\bar{I}_{Line}$ by 90^0 (or $\bar{V}_2$ leads current $\bar{I}_{Line}$ by 90^0). A desired phase shift is achieved by injecting a voltage $\bar{V}_3$, that shifts V_S by $\pm\theta$ while keeping its magnitude constant as shown in Figure 2.6 (c).

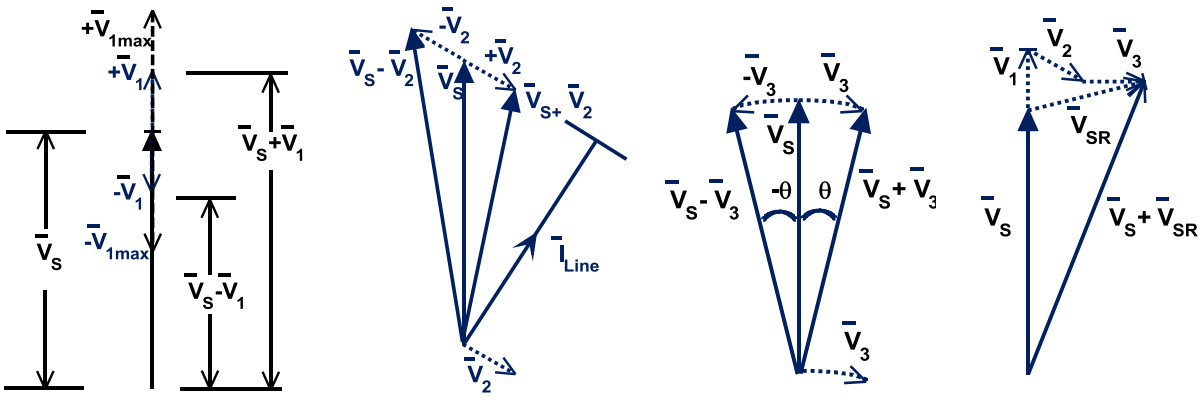

(a) (b) (c) (d)

Figure 2.6: **Phasor Diagrams**

Simultaneous control of terminal voltage, line impedance and phase angle allow the UPFC to perform multifunctional power flow control. The magnitude and the phase angle of the series injected voltage $\bar{V}_{SR} = \bar{V}_1 + \bar{V}_2 + \bar{V}_3$, shown in Figure 2.6 (d), are selected in such a way as to produce a line current that will result in the desired real and reactive power flow on the transmission line. Therefore, the UPFC series converter can be operated in four modes:

- direct voltage injection mode,
- line impedance compensation mode,
- phase angle regulation mode, and
- automatic power flow control mode.

D. Automatic power flow control mode

The automatic power control mode cannot be achieved with conventional compensators. In order to show how line power flow can be affected by the UPFC operated in the automatic power flow mode, UPFC is placed at the beginning of the transmission line connecting buses S and R as shown in Figure 2.7 [5]. Line conductance is neglected. UPFC is represented by two ideal voltage sources of controllable magnitude and phase

angle. Bus S and fictitious bus S_1 shown in Figure 2.7 represent UPFC sending and receiving buses respectively.

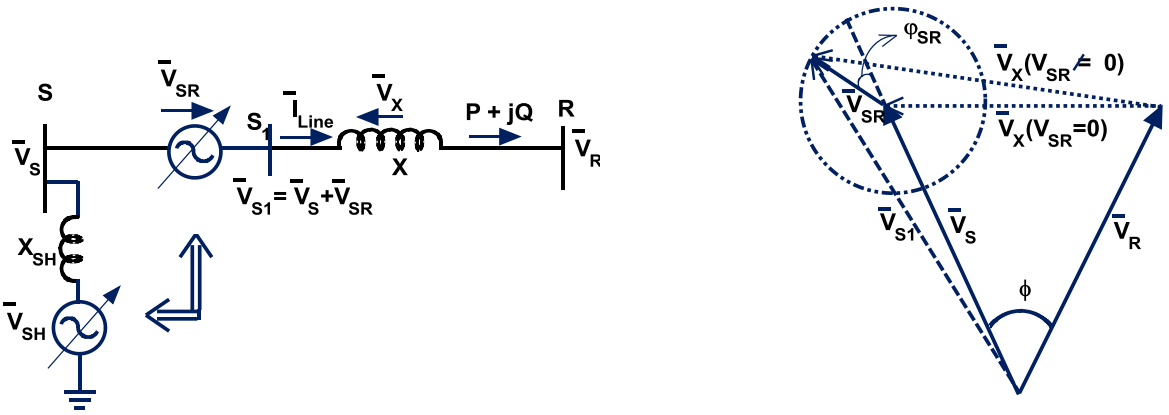

Figure 2.7: **Transmission line with UPFC**

In this case, the complex power received at the receiving end of the line is given by

$$S = \bar{V}_R \bar{I}^*_{Line} = \bar{V}_R \left(\frac{\bar{V}_S + \bar{V}_{SR} - \bar{V}_R}{jX}\right)^* \tag{2.14}$$

where $\bar{V}_{SR} = V_{SR}\angle(\phi_S - \varphi_{SE})$. The complex conjugate of this complex power is

$$S^*_S = P - jQ = \bar{V}^*_R \left(\frac{\bar{V}_S + \bar{V}_{SR} - \bar{V}_R}{jX}\right) \tag{2.15}$$

Performing simple mathematical manipulations and separating real and imaginary components of (2.15) the following expressions for real and the reactive powers received at the receiving end of the line are

$$\begin{cases} P = \dfrac{V_S V_R}{X}\sin\phi + \dfrac{V_{SR} V_R}{X}\sin(\phi - \varphi_{SR}) = P_0(\delta) + P_{SR}(\phi, \varphi_{SR}) \\ Q = -\dfrac{V_R^2}{X} + \dfrac{V_S V_R}{X}\cos(\phi) + \dfrac{V_{SR} V_R}{X}\cos(\phi - \varphi_{SR}) = Q_0(\delta) + Q_{SR}(\phi, \varphi_{SR}) \end{cases} \tag{2.16}$$

For $V_{SR} = 0$ the above equations (2.16) are identical to equation (2.12) and the second equation of (2.13), these equations represent the real and reactive powers of the uncompensated system. It was stated before that the UPFC series voltage magnitude can

be controlled between 0 and $V_{SR\max}$, and its phase angle can be controlled between 0 and 360 degrees at any power angle ϕ. It can be seen from (2.16) that the real and reactive power received at bus R for the system with the UPFC installed can be controlled between

$$\begin{cases} P_0(\phi) - \dfrac{V_{SR\max}V_R}{X} \le P \le P_0(\phi) + \dfrac{V_{SR\max}V_R}{X} \\ Q_0(\phi) - \dfrac{V_{SR\max}V_R}{X} \le Q \le Q_0(\phi) + \dfrac{V_{SR\max}V_R}{X} \end{cases} \tag{2.17}$$

Rotation of the series injected voltage phasor with RMS value of $V_{SR\max}$ from 0^0 to 360^0 allows the real and the reactive power flow to be controlled within the boundary circle with a radius of $\dfrac{V_{SR\max}V_R}{X}$ and a center at $(P_0(\phi), Q_0(\phi))$. This circle is defined by the following equation

$$(P_{SR}(\phi,\varphi_{SR}) - (P_0(\phi))^2 + (Q_{SR}(\phi,\varphi_{SR}) - Q_0(\phi))^2 = (\frac{V_{SR\max}V_R}{X})^2 \tag{2.18}$$

Consider Figure 2.8, which illustrates the case when the transmission angle is zero ($\phi = 0$). With $V_{SR} = 0$, P, Q_r, (and Q_s)are all zero, i.e., the system is at standstill at the origin of the Q_r, P coordinates. The circle around the origin of the $\{Q_r, P\}$ plane is the loci of the corresponding Q_r and P values, obtained as the voltage phasor $\mathbf{V}_{SR}$ is rotated a full revolution ($0 \le \varphi_{SR} \le 360$) with its maximum magnitude $V_{SR\max}$. The area within this circle defines all P and Q_r values obtainable by controlling the magnitude V_{SR} and φ_{SR} of the phasor $\mathbf{V}_{SR}$. In other words, the circle in the $\{Q_r, P\}$ defines all P and Q_r values attainable with the UPFC of a given rating.

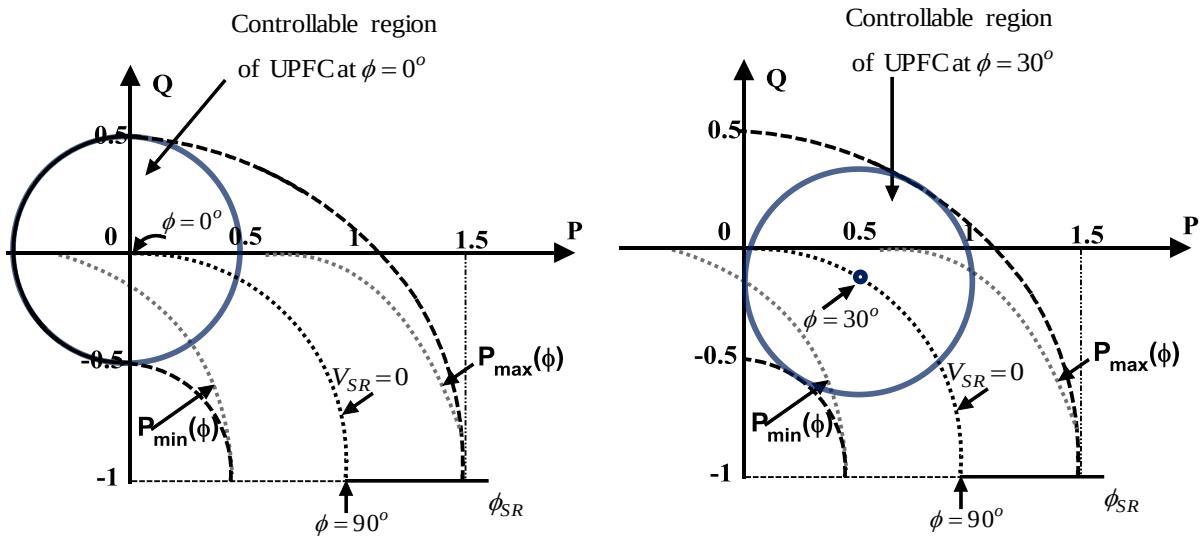

Figure 2.8: **P-Q relationship with a UPFC at $\phi = 0^0, 30^0$**

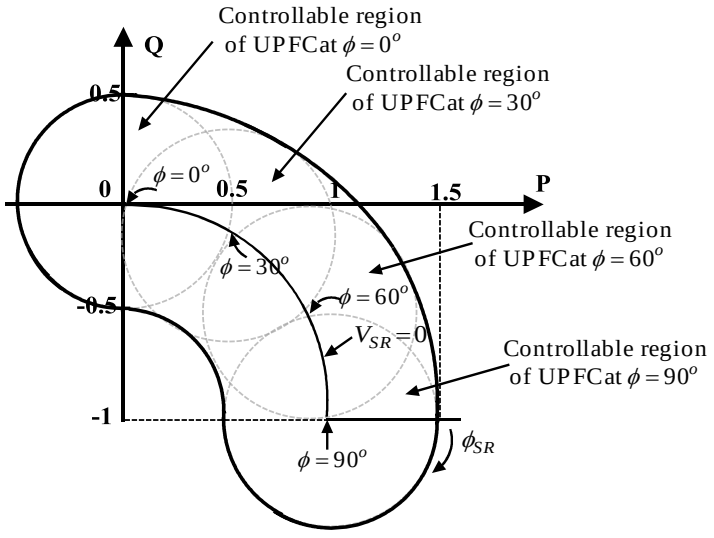

Figure 2.9: **P-Q relationship with a UPFC at $\phi = 0^0, 30^0, 60^0$ and 90^0**

Figure 2.9 shows plots of the reactive power Q demanded at the receiving bus versus the transmitted real power P as a function of the series voltage magnitude V_{SR} and phase angle φ_{SR} at four different power angles ϕ i.e. $\phi = 0^0, 30^0, 60^0$ and 90^0, with $V_S = V_R = V$

, $\frac{V^2}{X} = 1$ and $\frac{V_{SR\max} V_R}{X} = 0.5$ [5]. The capability of UPFC to independently control real and reactive power flow at any transmission angle is clearly illustrated in Figure 2.9.

2.3 Modeling of power system components

Studies of electrical power systems are based on the simulation of actual phenomena using models behaving exactly in the identical way as the elements in the physical system. Component modeling thus becomes very important. In research, it is necessary to have models permitting precise and detailed simulation. The different parameters must be accessible and the models are required to follow the physical process as closely and faithfully as possible. Then it is required to solve mathematical equations governing these phenomena. Modeling of active elements such as, generator is relatively difficult while that of passive elements such as transmission line, inductive VAR compensator, etc., is easier. Passive circuit elements are mostly modeled by their parameters in the equivalent circuits while the active power system components are modeled by their operation in steady, transient and sub-transient state. The overall power system representation includes models for the following individual components

- Synchronous generators, and the associated excitation systems
- Interconnecting transmission network
- static loads
- Other devices such as FACTS

The model used for each component should be appropriate for transient stability analysis, and the system equations must be organized in a form suitable for applying numerical methods. As we will see in what follows, the complete system model consists of a set of differential equations and algebraic equations. The transient stability analysis is thus a differential algebraic initial-value problem.

A. Synchronous machine modeling

Park's equations for a synchronous machine in which the effects of rotor damping are represented by two short-circuited damper windings may be expressed by [61]

$$\dot{\delta}_i = \omega_i - \omega_0 \tag{2.19}$$

$$\dot{\omega}_i = \frac{1}{M_i}(P_{mi} - P_{ei} - D_i(\omega_i - \omega_0)/\omega_0) \tag{2.20}$$

$$\dot{E}'_{qi} = \frac{1}{T'_{doi}}[E_{fdi} - (X_{di} - X'_{di})I_{di} - E'_{qi}] \tag{2.21}$$

$$\dot{E}''_{qi} = \frac{1}{T''_{doi}}[-E_{fdi} - (X'_{di} - X''_{di})I_{di} - E''_{qi} + E'_{qi}] + \dot{E}'_{qi} \tag{2.22}$$

$$\dot{E}''_{di} = \frac{1}{T''_{qoi}}[(X_{qi} - X''_{qi})I_{qi} - E''_{di}] \tag{2.23}$$

The algebraic equations are

$$E_d = -r_a I_d + \frac{\dot{E}''_{qi}}{\omega_0} + E''_d + X''_q I_q \tag{2.24}$$

$$E_q = -r_a I_q + \frac{\dot{E}''_{di}}{\omega_0} + E''_q + X''_d I_d \tag{2.25}$$

$$T_e = E''_d I_d + E''_q I_q + (X''_q - X''_d) I_d I_q \tag{2.26}$$

Following a disturbance, currents are induced in the machine rotor circuits. Some of these induced rotor currents decay more rapidly than others. Machine parameters that influence rapidly decaying components are called the sub-transient parameters while those influencing the slowly decaying components are called the transient parameters and those influencing sustained components are the synchronous parameters.

In most of the research articles the effect of rotor damper windings are neglected. In that case the differential equations (2.19)-(2.21) along with the algebraic equations (2.27)-(2.29) describe the synchronous machine. Throughout this thesis we follow the third order representation. The algebraic equation with this representation is given by

$$E_d = -r_a I_d + X_q I_q \tag{2.27}$$

$$E_q = -r_a I_q + E_q^{'} - X_d^{'} I_d \tag{2.28}$$

$$T_e = [E_q^{'} + (X_q - X_d^{'}) I_d] I_q \tag{2.29}$$

Power system exciter can be modeled as [55]

$$\dot{E}_{fdi} = \frac{1}{T_{Ai}}(-E_{fdi} + K_{Ai}(V_{refi} - V_{Ti})) \tag{2.30}$$

K_{Ai} and T_{Ai} are the exciter gain and time constant.

B. Load modeling

The power system loads, other than motors represented by equivalent circuits, can be treated in several ways during the transient period. The commonly used representations are static impedance or admittance to ground, constant currents at fixed power factor, constant real and reactive power, or a combination of these representations. The constant power load is either equal to the scheduled real and reactive bus load or is a percentage of the specified values in the case of a combined representation. The parameters associated with the static impedance and constant current representations are obtained from the scheduled bus loads and the bus voltages calculated from a load flow solution for the power system prior to a disturbance. The initial value of current for a constant current representation is obtained from

$$I_{Li0} = \frac{P_{Li} - jQ_{Li}}{V_{Ti}^{*}} \tag{2.31}$$

where P_{Li} and Q_{Li} are the scheduled bus loads, and V_{Ti} is the calculated bus voltage. The current I_{Li0} flows from bus i to ground, that is, to bus 0. The magnitude and power factor angle of I_{Li0} remain constant. The static admittance y_{i0} used to represent the load at bus i, can be obtained from

$$(V_{Ti} - V_0) y_{i0} = I_{Li0} \tag{2.32}$$

where V_{Ti} is the calculated bus voltage and V_0 is the ground voltage, equal to zero. Therefore,

$$y_{i0} = \frac{I_{Li0}}{V_{Ti}} \tag{2.33}$$

Multiplying both the dividend and divisor of above equation by V_{Ti}^* and separating the real and imaginary components,

$$g_{i0} = \frac{P_{Li}}{(V_{Ti})^2} \text{ and } b_{i0} = \frac{Q_{Li}}{(V_{Ti})^2} \quad \text{where} \quad y_{i0} = g_{i0} - jb_{i0}$$

C. Transmission network representation

In stability studies it has been found adequate to represent the net work as a collection of lumped resistances, inductances, and capacitances and to neglect the short-lived electrical transients in the transmission system [62]. As a consequence of this fact, the terminal constraints imposed by the network appear as a set of algebraic equations which may be conveniently solved by matrix methods. The network admittance matrix may be written in partitioned form as

$$Y = \begin{bmatrix} y_1 & y_{12} \\ y_{21} & y_2 \end{bmatrix} \tag{2.34}$$

In the portioned matrix, the subscript 1 is associated with nodes to which controlled sources are connected and subscript 2 refers to those not connected to controlled sources. For the analysis no information about nodes associated with subscript 2 is necessary, and for this

reason they are eliminated by a series of single row and column reductions in accordance with

$$Y_R = y_1 - y_{12} y_2^{-1} y_{21} \tag{2.35}$$

The resultant network equations in terms of the reduced admittance matrix are

$$I = Y_R V \tag{2.36}$$

These may be written in expanded form as

$$\begin{bmatrix} I_N \\ I_M \end{bmatrix} = \begin{bmatrix} Y_{NN} & Y_{NM} \\ Y_{MN} & Y_{MM} \end{bmatrix} \begin{bmatrix} V_N \\ V_M \end{bmatrix} \tag{2.37}$$

where the subscripts denote

N nodes connected to synchronous machines represented in detail by Park's equations

M nodes behind transient reactance of machines represented by fixed voltages.

D. Axis transformation

Equations (2.19)-(2.21) describe an individual machine with respect to its own reference frame. In general the reference frame of each machine is different from that of any other machine as well as from the common reference frame rotating at synchronous speed. Consequently, it is necessary to perform axis transformation at each connection node in order to relate the components of voltages and currents expressed in the d, q reference axis of each machine to the synchronously rotating reference axis D, Q of the network [62]. Phasor relations between the two reference frames are shown in Figure 2.10. On its basis, the transformation of e_d, e_q to e_D, e_Q and of i_d, i_q to i_D, i_Q may be stated as

$$\begin{bmatrix} e_d \\ e_q \end{bmatrix} = \begin{bmatrix} \cos\alpha & \sin\alpha \\ -\sin\alpha & \cos\alpha \end{bmatrix} \begin{bmatrix} e_D \\ e_Q \end{bmatrix}; \qquad \begin{bmatrix} i_D \\ i_Q \end{bmatrix} = \begin{bmatrix} \cos\alpha & -\sin\alpha \\ \sin\alpha & \cos\alpha \end{bmatrix} \begin{bmatrix} i_d \\ i_q \end{bmatrix} \tag{2.38}$$

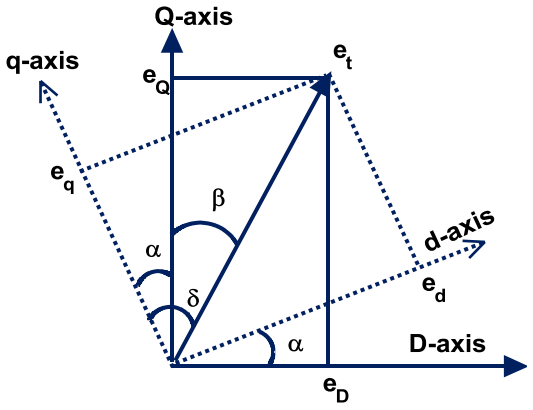

Figure 2.10: **Axis-Transformation Phasor diagram**

E. UPFC modeling

In order to simulate a power system that contains a UPFC, the UPFC needs to be modeled for steady-state and dynamic operations. The UPFC model needs to be interfaced with the power system model. Hence, in this section modeling and interfacing of the UPFC with the power network are described.

UPFC steady state model

Neglecting UPFC losses, during steady-state operation it neither absorbs nor injects real power with respect to the system. For steady-state operation, the DC link voltage remains constant at its pre-specified value. In the case of a lossless DC link, the real power supplied to the shunt converter $P_{SH} = R_e(\bar{V}_{SH}\bar{I}^*_{SH})$ satisfies the real power demanded by the series converter $P_{SR} = R_e(\bar{V}_{SR}\bar{I}^*_{Line})$

$$P_{SH} = P_{SR} \tag{2.39}$$

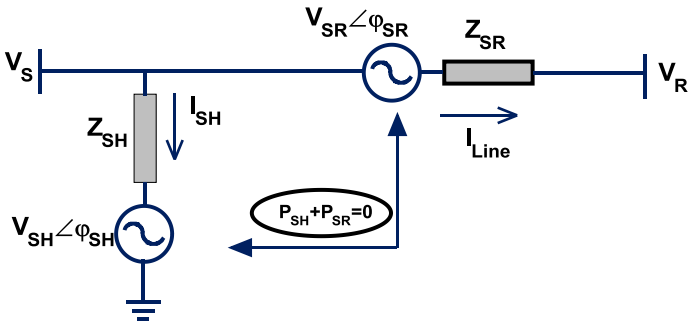

Figure 2.11: **UPFC single line diagram**

$$I_{SH} * Z_{SH} = V_S - V_{SH} \tag{2.40}$$

$$I_{Line} * Z_{SR} = V_S + V_{SR} - V_R \tag{2.41}$$

where

$$Z_{SH} = R_{SH} + j\omega L_{SH},\ Z_{SR} = R_{SR} + j\omega L_{SR},\ V_{SH} = (\frac{m_{SH} V_{dc}}{2\sqrt{2}})\angle\varphi_{SH} \text{ and } V_{SR} = (\frac{m_{SR} V_{dc}}{2\sqrt{2}})\angle\varphi_{SR}$$

Based on the above equation, the UPFC single-line diagram under a steady state condition is given by figure below

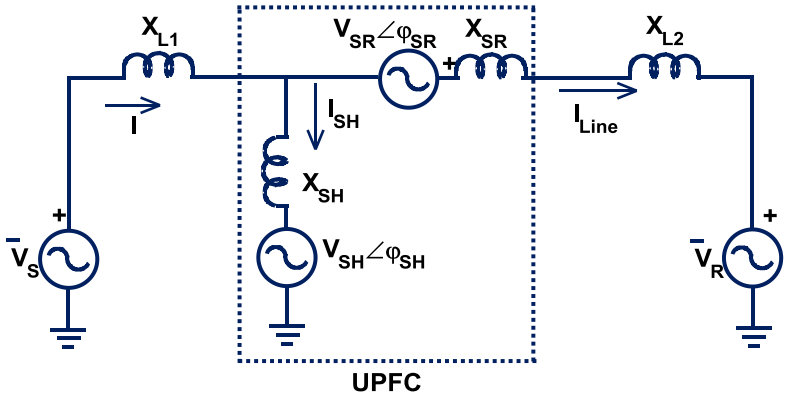

Figure 2.12: **Steady-state diagram of two machine system**

The constraint $P_{SH} + P_{SR} = 0$ in figure implies that:

- No real power is exchanged between the UPFC and the system, thus the DC link voltage remains constant, and
- The two sources are mutually dependent.

Depending upon the UPFC control strategy and function, its various power flow models can be deduced from the above equation and figure as follows.

UPFC load flow model

The load flow model discussed here assumes that the UPFC is operated to keep (i) real and reactive power flows at the receiving bus and (ii) sending bus voltage magnitude at their pre-specified values [58]. In this case UPFC can be replaced by an "equivalent generator" at the sending bus (PV-type bus using load flow terminology) and a "load" at the receiving bus (PQ-type bus) as shown in Figure 2.13. Neglecting UPFC losses, $P_{SH} = P_{SR} =$ pre-specified value. φ_{SR} and m_{SR} determine P_{SR} (as well as P_{SH}) and V_R respectively. Further, φ_{SH} and m_{SH} determine Q_{SH} and V_{dc} respectively. To calculate the UPFC control variable for the given power flow condition, a power flow analysis is performed where the UPFC is modeled as given in Figure 2.13 (b). Then, the power flow analysis results are used to solve the UPFC steady-state equations to determine $\varphi_{SR}, \varphi_{SH}$, m_{SR} and m_{SH}.

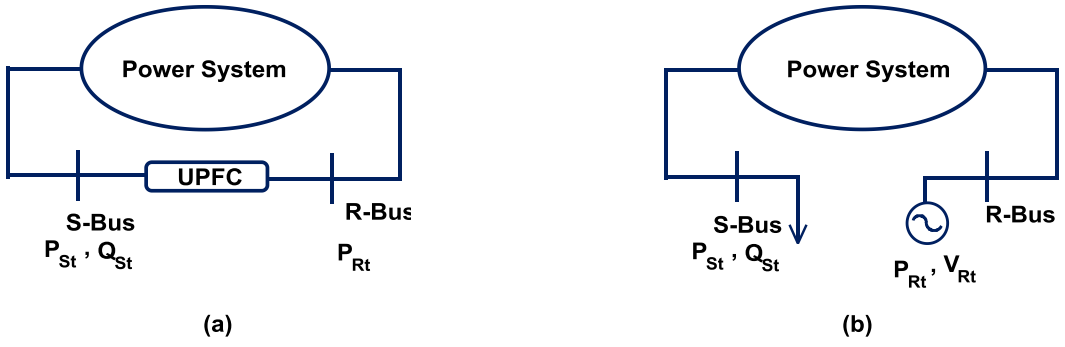

Figure 2.13: **UPFC power flow model**

$$\begin{cases} \dfrac{V_S * V_R}{X_{SR}} \sin(\phi_1 - \phi_2) + \dfrac{V_S * V_{SH}}{X_{SH}} \sin(\phi_1 - \varphi_{SH}) - \dfrac{V_S * V_{SR}}{X_{SR}} \sin(\phi_1 - \varphi_{SR}) - P_S = 0 \\ \dfrac{V_R * V_S}{X_{SR}} \sin(\phi_2 - \phi_1) + \dfrac{V_R * V_{SR}}{X_{SR}} \sin(\phi_2 - \varphi_{SR}) - P_R = 0 \\ \dfrac{V_S^2}{X_{SH}} + \dfrac{V_S^2}{X_{SR}} - \dfrac{V_S * V_R}{X_{SR}} \cos(\phi_1 - \phi_2) - \dfrac{V_S * V_{SH}}{X_{SH}} \cos(\phi_1 - \varphi_{SH}) + \dfrac{V_S * V_{SR}}{X_{SR}} \cos(\phi_1 - \varphi_{SR}) - Q_S = 0 \\ \dfrac{V_R^2}{X_{SR}} + \dfrac{V_R * V_S}{X_{SR}} \cos(\phi_2 - \phi_1) + \dfrac{V_R * V_{SR}}{X_{SR}} \cos(\phi_2 - \varphi_{SR}) - Q_R = 0 \end{cases} \tag{2.42}$$

The above equation is nonlinear and it can be written as

$$F - S = 0 \tag{2.43}$$

where $F = [\, f_1(P_S),\, f_2(P_R),\, f_3(Q_S),\, f_4(Q_R)]^T$ and $S = [P_S, P_R, Q_S, Q_R]^T$

To obtain the load flow solution for the power network with the UPFC an iterative procedure is needed. Power demanded at the receiving bus is set to the desired real and reactive powers at that bus. Its solution is best obtained by an iterative numerical approach as

$$u^{k+1} = u^k + (j - 1)\Delta S \tag{2.44}$$

where $u = [\varphi_{SH}, m_{SH}, \varphi_{SR}, m_{SR}]^T$, $\Delta S = F - S$ and j is the jacobian matrix.

UPFC power injection model

In this section, a general power injection model is derived for series-shunt connected FACTS devices (UPFC). This model, which is referred to as the injection model, is valid for load flow and angle stability analysis, UPFC inject a voltage in series with a line through a series transformer. The active power involved in the series injection is taken from the line through a shunt transformer. UPFC generates or absorbs the needed reactive power locally by the switching operation of its converters. Figure 2.14 shows a general equivalent diagram of a series-shunt-connected device UPFC.

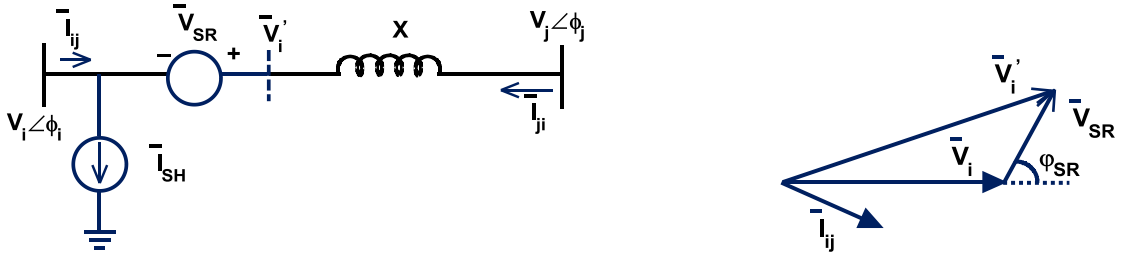

Figure 2.14: **Equivalent circuit and Phasor diagram of UPFC**

In Figure 2.14, X is the effective reactance seen from the line side of the series transformer. For UPFC $X = X_{SR}$, here X_{SR} is the reactance of series transformer. X_{SH} represents the reactance of shunt transformer [52]. Further, $\bar{V}_{SR}$ is the induced series voltage, and $\bar{I}_{SH}$ represents a current source. $\bar{V}_i'$ is a fictitious voltage behind the series reactance. Figure 2.14 also shows the phasor diagram of the equivalent circuit diagram. The magnitude of $\bar{V}_{SR}$ is controllable by UPFC. The angle φ_{SR} is controllable by UPFC from 0 to 2π. It is shown in [52] and [67] that the equivalent circuit diagram of Figure 2.14 can be modeled as the dependent loads injected at nodes i and j. This model is called injection model and the general configuration is shown in Figure 2.15:

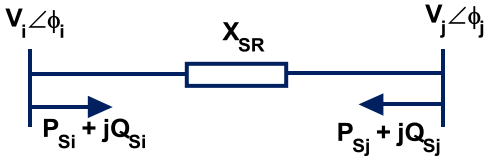

Figure 2.15: **Injection model for UPFC**

The expressions for P_{Si}, Q_{Si}, P_{Sj}, Q_{Sj} are given below[67]

$$\begin{cases} P_{S\,i} = B_{i\,j} V_{SR} V_j \sin((\phi_i + \varphi_{SR}) - \phi_j) \\ P_{S\,j} = -B_{i\,j} V_{SR} V_j \sin((\phi_i + \varphi_{SR}) - \phi_j) \\ Q_{S\,i} = B_{i\,j} V_{SR} V_i \cos(\varphi_{SR}) \\ Q_{S\,j} = -B_{i\,j} V_{SR} V_j \cos((\phi_i + \varphi_{SR}) - \phi_j) \end{cases} \tag{2.46}$$

It is seen that $P_{S\,i} = -P_{S\,j}$ which is expected, since UPFC does not generate or absorb active power when losses are ignored

UPFC dynamic model

Figure 2.16 shows a schematic diagram for UPFC, where X_{SH} and X_{SR} are the reactance of the shunt and series transformers respectively. All the variables used in UPFC model are denoted in Figure 2.16. Per unit system and MKS units are jointly used in modeling. The AC system uses per unit system with its variables calculated based on the system-side S_B and V_B (base value), while the DC variables are expressed in MKS units. We first consider the UPFC DC link capacitor charging dynamics. The DC currents I_{d1}, I_{d2} (see Figure 2.16) and the capacitor voltage and current have the following relation with harmonics neglected:

$$\begin{cases} I_{dc} = C \dfrac{dV_{dc}}{dt} \\ I_{dc} = I_{d1} + I_{d2} \end{cases} \tag{2.47}$$

If we assume the inverters are ideal, the real power exchange with the AC system is

(P_{SH} and P_{SR} are in pu):

$$\begin{cases} P_{SH} = V_{dc} I_{d1} / S_B \\ P_{SR} = V_{dc} I_{d2} / S_B \end{cases} \tag{2.48}$$

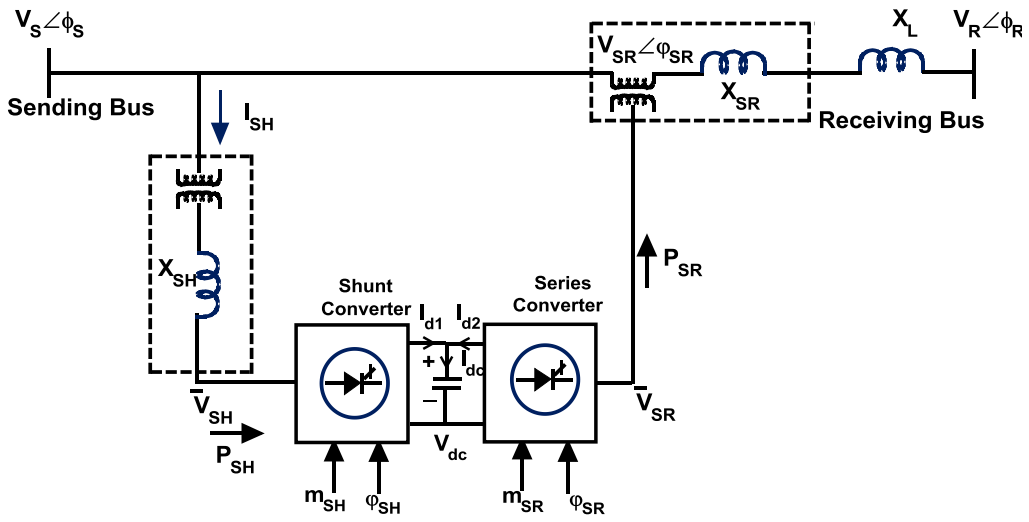

Figure 2.16: **Transmission line with UPFC**

From equations (2.47) and (2.48), we have:

$$CV_{dc}\frac{dV_{dc}}{dt} = (P_{SH} - P_{SR})S_B \tag{2.49}$$

From AC system, we know that P_{SH} and P_{SR} can be calculated by (see Figure 2.16):

$$\begin{cases} P_{SH} = R_e(\bar{V}_{SH}\bar{I}_{SH}^*) = R_e(\bar{V}_{SH}(\dfrac{\bar{V}_S - \bar{V}_{SH}}{jX_{SH}})^*) \\ P_2 = R_e(\bar{V}_{SR}\bar{I}_L^*) = R_e(\bar{V}_{SR}(\dfrac{\bar{V}_S + \bar{V}_{SR} - \bar{V}_R}{j(X_{SR} + X_L)})^*) \end{cases} \tag{2.50}$$

Applying modern PWM control technique [63] to the two-voltage source converters, the relations between the inverter DC- and AC-side voltages can be expressed by:

$$\begin{cases} V_{SH} = \dfrac{m_{SH}V_{dc}}{2\sqrt{2}\ V_B} \\ V_{SR} = \dfrac{m_{SR}V_{dc}}{2\sqrt{2}\ V_B} \end{cases} \tag{2.51}$$

where coefficients m_{SH} and m_{SR} represent the PWM control effects in order to maintain desired inverter AC-side voltages V_{SH} and V_{SR} respectively. The desired m_{SH} and m_{SR} are UPFC main control outputs. V_{SH} and V_{SR} are in pu and V_B is the AC system base voltage. The phase angles of $\bar{V}_{SH}$ and $\bar{V}_{SR}$ are denoted as φ_{SH} and φ_{SR} respectively. Finally, taking the series transformer ratio as 1:1, and rewriting equations (2.47)- (2.51), the UPFC power frequency model used in dynamic study is:

$$CV_{dc}\frac{dV_{dc}}{dt} = (P_{SH} - P_{SR})S_B \tag{2.52}$$

where $P_{SH} = R_e(\bar{V}_{SH}(\frac{\bar{V}_S - \bar{V}_{SH}}{jX_{SH}})^*)$, $P_{SR} = R_e(\bar{V}_{SR}(\frac{\bar{V}_S + \bar{V}_{SR} - \bar{V}_R}{j(X_{SR} + X_L)})^*)$, $\bar{V}_{SH} = (m_{SH}V_{dc}/V_B)\angle(\phi_S - \varphi_{SH})$,

$\bar{V}_{SR} = (m_{SR}V_{dc}/V_B)\angle(\phi_S - \varphi_{SR})$.

Here there are two network interface (complex) equations. The desired m_{SH}, m_{SR}, φ_{SH} and φ_{SR} can be obtained from UPFC main control system. Therefore, based on equation (2.52) together with UPFC control system equations and AC network interface equations we can analyze UPFC dynamics without difficulty. The first three equations (2.47)-(2.49) are for state variable V_{dc} calculation and the latter 2 equations (2.50)-(2.51) are for network interface calculation. It is clear that the UPFC power frequency model derived above can fit various control strategies and multi-machine power system stability analysis.

2.4 Interfacing UPFC with power network

The interface of the UPFC with the power network is shown in Figure 2.17 [60]. In order to get the network solution (bus voltages and the currents) an iterative approach is used. The UPFC sending and receiving bus voltages $\bar{V}_S$ and $\bar{V}_R$ can be expressed as a function of generator internal voltages $\bar{E}_G$ and the UPFC injection voltages $\bar{V}_{SH}$ and $\bar{V}_{SR}$. Control output and (2.59) determine the UPFC injection voltage magnitudes V_{SH} and V_{SR}.

However, the phase angles of the injected voltages, φ_{SH} and φ_{SR}, are unknown since they depend on the phase angle of the sending bus voltage, ϕ_S, which is the result of the network solution. Necessary computations are shown below.

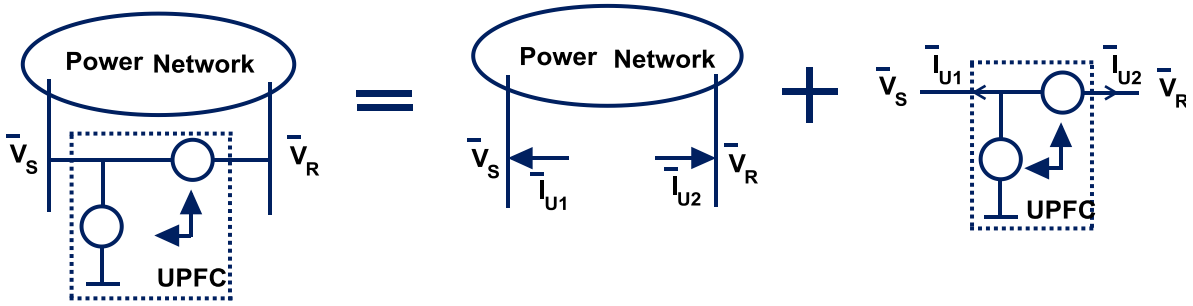

Figure 2.17: **Interface of UPFC with power network**

Reducing the bus admittance matrix to generator internal buses and UPFC terminal buses, the following equation can be written

$$\begin{bmatrix} Y_{GG} & Y_{GU} \\ Y_{UG} & Y_{UU} \end{bmatrix} \begin{bmatrix} \bar{E}_G \\ \bar{V}_U \end{bmatrix} = \begin{bmatrix} \bar{I}_G \\ \bar{I}_U \end{bmatrix} \tag{2.53}$$

where:

Y_{GG} - reduced admittance matrix connecting the generator current injection to the internal generator voltages,

Y_{GU} - admittance matrix component which gives the generator currents due to the voltages at UPFC buses

Y_{UG} - admittance matrix component which gives UPFC currents in terms of the generator internal voltages

Y_{UU} - admittance matrix connecting UPFC currents to the voltages at UPFC buses

$\bar{E}_G$ - vector of generator internal bus voltages

$\bar{V}_U$ - vector of UPFC AC bus voltages

$\bar{I}_G$ - vector of generator current injections

$\bar{I}_U$ - vector of UPFC currents injected to the power network.

The second equation of (2.53) is of the form

$$\bar{I}_U = Y_{UG}\bar{E}_G + Y_{UU}\bar{V}_U \tag{2.54}$$

Neglecting series and shunt transformer resistances, the following equations can be written for the UPFC currents injected into the power network (see Figure 2.17)

$$\bar{I}_{U1} = -\bar{I}_{SH} - \bar{I}_{Line} \tag{2.55}$$

$$\bar{I}_{U2} = \bar{I}_{Line} \tag{2.56}$$

$$\bar{I}_{SH} = \frac{\bar{V}_S - \bar{V}_{SH}}{jX_{SH}}; \qquad \bar{I}_{Line} = \frac{\bar{V}_{SR} + \bar{V}_S - \bar{V}_R}{j(X_{SR} + X_L)}; \tag{2.57}$$

Combining the above equations the following equation can be obtained

$$\bar{I}_U = W_U\bar{V}_U + W_C\bar{V}_C \tag{2.58}$$

where

$$W_U = \begin{bmatrix} -j\left(\frac{1}{X_{SH}} + \frac{1}{(X_{SR}+X_L)}\right) & \frac{1}{j(X_{SR}+X_L)} \\ \frac{1}{j(X_{SR}+X_L)} & -\frac{1}{j(X_{SR}+X_L)} \end{bmatrix}; \qquad W_C = \begin{bmatrix} \frac{1}{jX_{SH}} & -\frac{1}{j(X_{SR}+X_L)} \\ 0 & \frac{1}{j(X_{SR}+X_L)} \end{bmatrix}$$

$$\bar{I}_U = \begin{bmatrix} \bar{I}_{U1} \\ \bar{I}_{U2} \end{bmatrix}; \qquad \bar{V}_U = \begin{bmatrix} \bar{V}_S \\ \bar{V}_R \end{bmatrix}; \qquad \bar{V}_C = \begin{bmatrix} \bar{V}_{SH} \\ \bar{V}_{SR} \end{bmatrix}$$

Equating (2.54) with (2.58) the following equation can be written

$$\bar{V}_U = (W_U - Y_{UU})^{-1}Y_{UG}\bar{E}_G - (W_U - Y_{UU})^{-1}W_C\bar{V}_C = L_G\bar{E}_G + L_C\bar{V}_C \tag{2.59}$$

Substitution of (2.59) into (2.53) gives

$$\begin{cases} \bar{I}_G = M_G \bar{E}_G + M_C \bar{V}_C \\ \bar{I}_U = M_{G1} \bar{E}_G + M_{C1} \bar{V}_C \end{cases} \tag{2.60}$$

where

$$L_G = (W_U - Y_{UU})^{-1} Y_{UG}\,;\, L_C = -(W_U - Y_{UU})^{-1} W_C\,;\, M_G = Y_{GG} + Y_{GU} L_G\,;\; M_{G1} = Y_{UG} + Y_{UU} L_G$$

$$M_C = Y_{GU} L_C\,;\; M_{C1} = Y_{UU} L_C$$

By defining

$$\bar{I} = \begin{bmatrix} \bar{I}_G \\ \bar{I}_U \end{bmatrix};\; \bar{V} = \begin{bmatrix} \bar{E}_G \\ \bar{V}_C \end{bmatrix};\; M = \begin{bmatrix} M_G & M_C \\ M_{G1} & M_{C1} \end{bmatrix}$$

The above equation becomes

$$\bar{I} = M\bar{V} \tag{2.61}$$

And by applying d-q transformation [1] to equation (2.61) the following equation is obtained

$$\bar{I}_{dq} = M_{dq} \bar{V}_{dq} \tag{2.62}$$

UPFC DC link equation (2.52) can now be written in d-q frame as

$$CV_{dc} \frac{dV_{dc}}{dt} = (V_{SHd} I_{SHd} + V_{SHq} I_{SHq} - V_{SRd} I_{Lined} - V_{SRq} I_{Lineq}) S_B \tag{2.63}$$

or

$$CV_{dc} \frac{dV_{dc}}{dt} = (-V_{SHd} I_{U1d} - (V_{SHd} + V_{SRd}) I_{U2d} - V_{SHq} I_{U1q} - (V_{SHq} + V_{SRq}) I_{U2q}) S_B \tag{2.64}$$

where

$$V_{SHd} = \frac{m_{SH} V_{dc}}{2\sqrt{2} V_B} \sin(\varphi_{SH})\,;\; V_{SHq} = \frac{m_{SH} V_{dc}}{2\sqrt{2} V_B} \cos(\varphi_{SH})$$

$$V_{SRd} = \frac{m_{SR} V_{dc}}{2\sqrt{2} V_B} \sin(\varphi_{SR}) \; ; \; V_{SRq} = \frac{m_{SR} V_{dc}}{2\sqrt{2} V_B} \cos(\varphi_{SR})$$

2.5 Conclusion

In the first part, brief description of UPFC is provided. PWM techniques used for VSCs are explained in the next section. The basic knowledge of these methods is essential for controller development in the subsequent chapters.

In the modeling part, mathematical representation of different power system components are provided. It contains the model of synchronous generator with excitation system and load models. An overview of network model is provided as it enables key system elements to be connected. The power injection model as well as dynamic model for UPFC is also provided.

In next chapter, a multi-machine test system is described. The overall differential and algebraic equations describing models of different power system components developed in this chapter are first combined, and then linearized around an operating point. Conventional control techniques are then used on the linearized system.

Chapter 3

Lead-Lag Control Design for Multi-Machine Power System with UPFC

Chapter 3

Lead-Lag Control Design for Multi-Machine Power System with UPFC

3.1 Introduction

Chapter 2 provided a general introduction to the power system components, including a discussion of the basic concepts, modeling and interfacing with the power network. In this chapter, the various control strategies applied to electromechanical oscillation damping is considered in detail beginning with a Lead-Lag controller. Knowledge of the characteristics and modeling of individual system components as presented in Chapter 2 is helpful in this regard. Describing the small signal performance of a multi-machine power system by a set of differential equations of the form $[\dot{x}]=[A][x]+[B][u]$ allows standard control theory to be used in dynamic stability studies.

3.2 Linearization

The linearized model of the power system including UPFC is derived in this section. This model can be used for small signal analysis and damping controller design. The model derived following the approach described in [6] is explained here.

The behavior of a dynamic system, such as a power system, may be described by a set of n first order nonlinear ordinary differential equations of the following form:

$$\dot{x}_i = f_i(x_1, x_2, ...x_n; u_1, u_2, ...u_r; t) \qquad i = 1, 2, ...n \tag{3.1}$$

where n is the order of the system and r is the number of inputs. This can be written in the following form by using vector-matrix notation:

$$\dot{x} = f(x, u, t) \tag{3.2}$$

where

$$x = [x_1 \quad x_2 \quad .... \quad x_n]^T, \qquad u = [u_1 \quad u_2 \quad .... \quad u_n]^T, \qquad f = [f_1 \quad f_2 \quad .... \quad f_n]^T$$

The column vector x is referred to as the state vector, and its entries x_i as state variables. The column vector u is the vector of inputs to the system. These are the external signals that influence the performance of the system. Time is denoted by t, and the derivative of a state variable x with respect to time is denoted by $\dot{x}$. If the derivatives of the state variables are not explicit functions of time, the system is said to be autonomous. In this case, the above equation simplifies to

$$\dot{x} = f(x,u). \tag{3.3}$$

We are often interested in output variables which can be observed on the system. These may be expressed in terms of the state variables and the input variables in the following form:

$$y = g(x,u) \tag{3.4}$$

where

$$y = [y_1 \quad y_2 \quad .... \quad y_n]^T,$$

$$g = [g_1 \quad g_2 \quad .... \quad g_n]^T$$

The column vector y is the vector of outputs, and g is a vector of nonlinear functions relating state and input variables to output variables.

We now describe the procedure for linearizing equation (3.3). Let x_0 be the initial state vector and u_0 the input vector corresponding to the equilibrium point about which the small signal performance is to be investigated. Since x_0 and u_0 satisfy equation (3.3), we have

$$\dot{x}_0 = f(x_0,u_0) = 0 \tag{3.5}$$

Let us perturb the system from the above state, by letting

$x = x_0 + \Delta x, \quad u = u_0 + \Delta u$

where the prefix Δ denotes a small deviation. The new state must satisfy equation (3.5). Hence

$$\dot{x} = \dot{x}_0 + \dot{\Delta x} = f[(x_0 + \Delta x), (u_0 + \Delta u)] \tag{3.6}$$

As the perturbations are assumed to be small, the linear functions $f(x,u)$ can be expressed in terms of Taylor's series expansion. With terms involving second and higher order powers of Δx and Δu neglected, we may write

$$\dot{x}_i = \dot{x}_{i0} + \dot{\Delta x}_i = f_i[(x_0 + \Delta x), (u_0 + \Delta u)]$$

$$= f_i(x_0, u_0) + \frac{\partial f_i}{\partial x_1}\Delta x_1 + ...\frac{\partial f_i}{\partial x_n}\Delta x_n + \frac{\partial f_i}{\partial u_1}\Delta u_1 + ...\frac{\partial f_i}{\partial u_r}\Delta u_r \tag{3.7}$$

Since $\dot{x}_{i0} = f_i(x_0, u_0)$, we obtain

$$\dot{\Delta x}_i = \frac{\partial f_i}{\partial x_1}\Delta x_1 + ...\frac{\partial f_i}{\partial x_n}\Delta x_n + \frac{\partial f_i}{\partial u_1}\Delta u_1 + ...\frac{\partial f_i}{\partial u_r}\Delta u_r \qquad i = 1, 2, ...n. \tag{3.8}$$

In a similar manner from equation (3.4), we have

$$\Delta y_i = \frac{\partial g_j}{\partial x_1}\Delta x_1 + ...\frac{\partial g_j}{\partial x_n}\Delta x_n + \frac{\partial g_j}{\partial u_1}\Delta u_1 + ...\frac{\partial g_j}{\partial u_r}\Delta u_r \qquad j = 1, 2, ...m. \tag{3.9}$$

Therefore, the linearized forms of equations (3.3) and (3.4) are

$$\Delta \dot{x} = A\Delta x + B\Delta u \qquad \Delta y = C\Delta x + D\Delta u \tag{3.10}$$

where $A = \begin{bmatrix} \frac{\partial f_1}{\partial x_1} & .... & \frac{\partial f_1}{\partial x_n} \\ .... & .... & .... \\ \frac{\partial f_n}{\partial x_1} & .... & \frac{\partial f_n}{\partial x_n} \end{bmatrix} \quad B = \begin{bmatrix} \frac{\partial f_1}{\partial u_1} & .... & \frac{\partial f_1}{\partial u_r} \\ .... & .... & .... \\ \frac{\partial f_n}{\partial u_1} & .... & \frac{\partial f_n}{\partial u_r} \end{bmatrix} \quad C = \begin{bmatrix} \frac{\partial g_1}{\partial x_1} & .... & \frac{\partial g_1}{\partial x_n} \\ .... & .... & .... \\ \frac{\partial g_m}{\partial x_1} & .... & \frac{\partial g_m}{\partial x_n} \end{bmatrix}$

$$D = \begin{bmatrix} \frac{\partial g_1}{\partial u_1} & .... & \frac{\partial g_1}{\partial u_r} \\ .... & .... & .... \\ \frac{\partial g_m}{\partial u_1} & .... & \frac{\partial g_m}{\partial u_r} \end{bmatrix}$$

The above partial derivatives are evaluated at the equilibrium point about which the small perturbation is being analyzed.

In equation (3.10),

- Δx is the state vector of dimension n
- Δy is the output vector of dimension m
- Δu is the input vector of dimension r
- A is the $n \times n$ plant matrix
- B is the $n \times r$ input matrix
- C is the $m \times n$ output matrix
- D is the $m \times r$ feed forward matrix

Eigen-values of the matrix A, $\lambda_i = \sigma_i \pm j\omega_{ni}$, where $i = 1....n$, are the roots of the characteristic polynomial

$$p(\lambda) = |\ \lambda I - A| \tag{3.11}$$

where: I is an $n \times n$ identity matrix. Complex eigen-values always appear in pairs of complex conjugate numbers.

Lyapunov's stability criteria:

The *stability in the small* of a nonlinear system is given by the roots of the characteristic equation of the system of first approximations, i.e, by the eigen values of A:

(1) When the eigen values have negative real parts, the original system is asymptotically stable.

(2) When at least one of the eigen values has a positive real part, the original system is unstable.

(3) When the eigen values have real parts equal to zero, it is not possible on the basis of the first approximation to say anything in general.

The *stability in large* can find out using Lyapunov second method. The second method attempts to determine stability directly by using suitable functions which are defined in the state space. The sign of the Lyapunov function and the sign of its time derivative with respect to the system state equation are considered.

The equilibrium of equation (3.3) is stable if there exists a positive definite function $V(x_1, x_2, ..., x_n)$ such that its total derivative $\dot{V}$ with respect to equation (3.3) is not positive.

The equilibrium of equation (3.3) is asymptotically stable if there is a positive definite function $V(x_1, x_2, ..., x_n)$ such that its total derivative $\dot{V}$ with respect to equation (3.3) is negative definite.

The system is stable in that region in which $\dot{V}$ is negative semi definite, and asymptotically stable if $\dot{V}$ is negative definite.

The stability in the large of power systems is the subject of the fifth and sixth chapters. This chapter is concerned with the stability in the small of power systems, and this is given by the eigen values of A.

Table 3.1: **Stability criteria for a linear system [64]**

Unstable	If $\sigma_i > 0$ for any simple root or if $\sigma_i \geq 0$ for any repeated root
Stable i.s. Lyapunov	If $\sigma_i \leq 0$ for all simple roots and if $\sigma_i < 0$ for all repeated root
Asymptotically stable	If $\sigma_i < 0$ for all roots

3.3 Linearized model for a two-machine power system

The linearized model of the power network including UPFC, as shown in Figure 3.1, is derived in this section. This model can be used for small signal analysis and damping controller design. The operating points at which the equations are linearized are given in Table 3.2. These steady state values are obtained after conducting load flow analysis using Newton-Raphson method.

Consider n-machine power system. Using two axis model generator differential equations can be written as follows

$$\dot{\delta}_i = \omega_i - \omega_0 \tag{3.12}$$

$$\dot{\omega}_i = \frac{1}{2H_i}(P_{mi} - P_{ei} - D_i(\omega_i - \omega_0)/\omega_0) \tag{3.13}$$

$$\dot{E}'_{qi} = \frac{1}{T'_{doi}}[E_{fdi} - (X_{di} - X'_{di})I_{di} - E'_{qi}] \tag{3.14}$$

$$\dot{E}_{fdi} = \frac{1}{T_{Ai}}(-E_{fdi} + K_{Ai}(V_{refi} - V_{Ti})) \tag{3.15}$$

$$\dot{V}_{dc} = \frac{(P_{SH} - P_{SR})S_B}{CV_{dc}} \tag{3.16}$$

Where P_{SH} is real power supplied to the shunt converter and P_{SR} is the real power demanded by the series converter

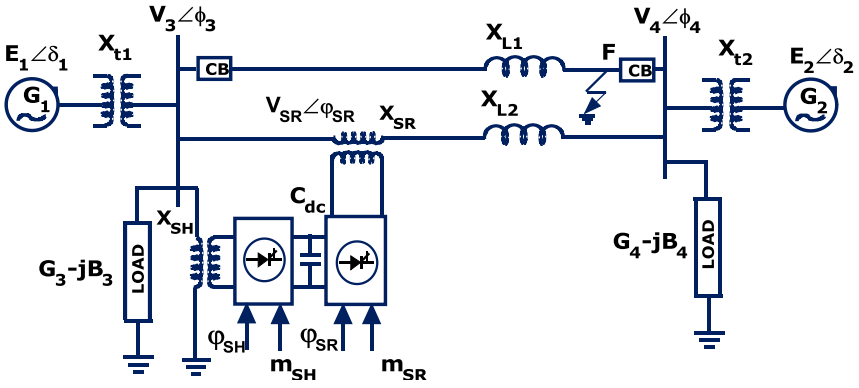

Figure 3.1: **Sample power system with UPFC**

The algebraic equations are

$$V_{di} = X_{qi}I_{qi} \tag{3.17}$$

$$V_{qi} = E'_{qi} - X'_{di}I_{di} \tag{3.18}$$

$$T_{ei} = V_{di}I_{di} + V_{qi}I_{qi} \qquad i = 1...n \tag{3.19}$$

From network interfacing we get

$$\bar{I}_{dq} = M_{dq}\bar{V}_{dq} \tag{3.20}$$

Linearizing (3.20) around the operating point and separating d and q components, the following expressions for generator and UPFC currents can be obtained

$$\begin{cases} \Delta I_d = A_1\Delta\delta + A_3\Delta E_q^{'} + A_4\Delta V_{dc} + A_6 m_{SH} + A_7\varphi_{SH} + A_8 m_{SR} + A_9\varphi_{SR} \\ \Delta I_q = Q_1\Delta\delta + Q_3\Delta E_q^{'} + Q_4\Delta V_{dc} + Q_6 m_{SH} + Q_7\varphi_{SH} + Q_8 m_{SR} + Q_9\varphi_{SR} \\ \Delta I_{Ud} = D_1\Delta\delta + D_3\Delta E_q^{'} + D_4\Delta V_{dc} + D_6 m_{SH} + D_7\varphi_{SH} + D_8 m_{SR} + D_9\varphi_{SR} \\ \Delta I_{Uq} = R_1\Delta\delta + R_3\Delta E_q^{'} + R_4\Delta V_{dc} + R_6 m_{SH} + R_7\varphi_{SH} + R_8 m_{SR} + R_9\varphi_{SR} \end{cases} \quad (3.21)$$

Table 3.2: **System parameters and initial conditions**

$P_1 = 0.5pu$	$Q_1 = 0.3pu$	$X_{L1} = 0.33pu$	$X_{L2} = 0.33pu$	$X_{SR} = 0.1pu$
$B_3 = 0.2pu$	$G_4 = 1.0pu$	$B_4 = 0.4pu$	$\delta_1 = 0.341rad$	$\delta_2 = 0.086rad$
$\phi_4 = 0.0$	$V_3 = 1.018pu$	$V_4 = 1.0pu$	$X_d^{'} = 0.11pu$	$M_1 = 10MJ/MVA$
$D_1 = 0.0$	$X_d = 1.2pu$	$X_{SH} = 0.1pu$	$P_2 = 0.8pu$	$M_2 = 10MJ/MVA$
$G_3 = 0.3pu$	$\phi_3 = 0.037rad$	$X_{t1} = 0.1pu$	$X_{t2} = 0.1pu$	$K_A = 4.0$
$T_A = 0.01s$	$X_q = 0.8pu$	$f = 60HZ$	$T_{do}^{'} = 5.044S$	

where

$$\begin{cases} A_1 = \frac{\partial I_d}{\partial\delta}; A_3 = \frac{\partial I_d}{\partial E_q^{'}}; A_4 = \frac{\partial I_d}{\partial V_{dc}}; A_6 = \frac{\partial I_d}{\partial m_{SH}}; A_7 = \frac{\partial I_d}{\partial\varphi_{SH}}; A_8 = \frac{\partial I_d}{\partial m_{SR}}; A_9 = \frac{\partial I_d}{\partial\varphi_{SR}} \\ Q_1 = \frac{\partial I_q}{\partial\delta}; Q_3 = \frac{\partial I_q}{\partial E_q^{'}}; Q_4 = \frac{\partial I_q}{\partial V_{dc}}; Q_6 = \frac{\partial I_q}{\partial m_{SH}}; Q_7 = \frac{\partial I_q}{\partial\varphi_{SH}}; Q_8 = \frac{\partial I_q}{\partial m_{SR}}; Q_9 = \frac{\partial I_q}{\partial\varphi_{SR}} \\ D_1 = \frac{\partial I_{Ud}}{\partial\delta}; D_3 = \frac{\partial I_{Ud}}{\partial E_q^{'}}; D_4 = \frac{\partial I_{Ud}}{\partial V_{dc}}; D_6 = \frac{\partial I_{Ud}}{\partial m_{SH}}; D_7 = \frac{\partial I_{Ud}}{\partial\varphi_{SH}}; D_8 = \frac{\partial I_{Ud}}{\partial m_{SR}}; D_9 = \frac{\partial I_{Ud}}{\partial\varphi_{SR}} \\ R_1 = \frac{\partial I_{Uq}}{\partial\delta}; R_3 = \frac{\partial I_{Uq}}{\partial E_q^{'}}; R_4 = \frac{\partial I_{Uq}}{\partial V_{dc}}; R_6 = \frac{\partial I_{Uq}}{\partial m_{SH}}; R_7 = \frac{\partial I_{Uq}}{\partial\varphi_{SH}}; R_8 = \frac{\partial I_{Uq}}{\partial m_{SR}}; R_9 = \frac{\partial I_{Uq}}{\partial\varphi_{SR}} \end{cases}$$

Linearizing $\dot{V}_{dc}$ (3.16) and substituting UPFC injected currents d and q components given by (3.21) the following equation can be written

$$\Delta\dot{V}_{dc} = L_1\Delta\delta + L_3\Delta E_q^{'} + L_4\Delta V_{dc} + L_6 m_{SH} + L_7\varphi_{SH} + L_8 m_{SR} + L_9\varphi_{SR} \quad (3.22)$$

where

$$\begin{cases} L_1 = K_{11}R_1 + K_{22}D_1; L_3 = K_{11}R_3 + K_{22}D_3; L_4 = K_{11}R_4 + K_{22}D_4; L_6 = K_{11}R_6 + K_{22}D_6 + K_6 \\ L_7 = K_{11}R_7 + K_{22}D_7 + K_7; L_8 = K_{11}R_8 + K_{22}D_8 + K_8; L_9 = K_{11}R_9 + K_{22}D_9 + K_9 \\ K_{11} = \dfrac{\partial V_{dc}}{\partial I_{Ud}}; K_{22} = \dfrac{\partial V_{dc}}{\partial I_{Uq}}; K_6 = \dfrac{\partial V_{dc}}{\partial m_{SH}}; K_7 = \dfrac{\partial V_{dc}}{\partial \varphi_{SH}}; K_8 = \dfrac{\partial V_{dc}}{\partial m_{SR}}; K_9 = \dfrac{\partial V_{dc}}{\partial \varphi_{SR}} \end{cases}$$

AVR is represented by simplified first order transfer function. The function of governors are neglected ($P_{mi} = 0$). Linearizing (3.12) to (3.15) the following equations can be obtained

$$\begin{cases} \Delta \dot{\omega} = W_1\Delta\delta + W_2\Delta\omega + W_3\Delta E_q^{'} + W_4\Delta V_{dc} + W_6\Delta m_{SH} + W_7\Delta\varphi_{SH} + W_8\Delta m_{SR} + W_9\Delta\varphi_{SR} \\ \Delta \dot{E}_q^{'} = N_1\Delta\delta + N_3\Delta E_q^{'} + N_4\Delta V_{dc} + N_5\Delta E_{fd} + N_6\Delta m_{SH} + N_7\Delta\varphi_{SH} + N_8\Delta m_{SR} + N_9\Delta\varphi_{SR} \\ \Delta \dot{E}_{fd} = S_1\Delta\delta + S_3\Delta E_q^{'} + S_4\Delta V_{dc} + S_5\Delta E_{fd} + S_6\Delta m_{SH} + S_7\Delta\varphi_{SH} + S_8\Delta m_{SR} + S_9\Delta\varphi_{SR} \end{cases} \quad (3.23)$$

$$\Delta V_T = P_1\Delta V_d + P_2\Delta V_q$$

$$= M_1\Delta\delta + M_3\Delta E_q^{'} + M_4\Delta V_{dc} + M_6\Delta m_{SH} + M_7\Delta\varphi_{SH} + M_8\Delta m_{SR} + M_9\Delta\varphi_{SR} \quad (3.24)$$

where

$W_1 = -(U_1Q_1 + U_2A_1)$; $W_2 = -(D_{damp})$; $W_3 = -(I_{q0} + U_1Q_3 + U_2A_3)$; $W_4 = -(U_1Q_4 + U_2A_4)$;

$W_6 = -(U_1Q_6 + U_2A_6)$; $W_7 = -(U_1Q_7 + U_2A_7)$; $W_8 = -(U_1Q_8 + U_2A_8)$;

$W_9 = -(U_1Q_9 + U_2A_9)$; $U_1 = (I_{d0}X_d^{'} + V_{q0})$; $U_2 = (-I_{q0}X_d^{'} + V_{d0})$

I_{d0}, I_{q0}, V_{d0} and V_{q0} are all steady state values and can be calculated using load flow analysis

$N_1 = -(X_d - X_d^{'})A_1$; $N_3 = -I - (X_d - X_d^{'})A_3$; $N_4 = -(X_d - X_d^{'})A_4$; $N_5 = 1$;

$N_6 = -(X_d - X_d^{'})A_6$; $N_7 = -(X_d - X_d^{'})A_7$; $N_8 = -(X_d - X_d^{'})A_8$; $N_9 = -(X_d - X_d^{'})A_9$

$P_1 = \dfrac{V_{q0i}}{V_{T0i}}$; $P_2 = \dfrac{V_{d0i}}{V_{T0i}}$; $M_1 = P_1X_d^{'}Q_1 - P_2X_d^{'}A_1$; $M_3 = P_1X_d^{'}Q_3 + P_2(I - X_d^{'}A_3)$;

$M_4 = P_1X_d^{'}Q_4 - P_2X_d^{'}A_4$; $M_6 = P_1X_d^{'}Q_6 - P_2X_d^{'}A_6$; $M_7 = P_1X_d^{'}Q_7 - P_2X_d^{'}A_5$;

$$M_8 = P_1 X_d^{'} Q_8 - P_2 X_d^{'} A_8; \qquad M_9 = P_1 X_d^{'} Q_9 - P_2 X_d^{'} A_9$$

$$S_1 = -K_A M_1; \quad S_3 = -K_A M_3; \quad S_4 = -K_A M_4; \quad S_5 = -1; \quad S_6 = -K_A M_6;$$

$$S_7 = -K_A M_7; \quad S_8 = -K_A M_8; \quad S_9 = -K_A M_9$$

$$\begin{bmatrix} \Delta\dot{\delta} \\ M\Delta\dot{\omega} \\ T_{do}^{'}\Delta\dot{E}_q^{'} \\ \Delta\dot{V}_{dc} \\ T_A\Delta\dot{E}_{fd} \end{bmatrix} = \begin{bmatrix} 0 & \omega_0 I & 0 & 0 & 0 \\ W_1 & W_2 & W_3 & W_4 & 0 \\ N_1 & 0 & N_3 & N_4 & N_5 \\ L_1 & 0 & L_3 & L_4 & 0 \\ S_1 & 0 & S_3 & S_4 & S_5 \end{bmatrix} \begin{bmatrix} \Delta\delta \\ \Delta\omega \\ \Delta E_q^{'} \\ \Delta V_{dc} \\ \Delta E_{fd} \end{bmatrix} + \begin{bmatrix} 0 & 0 & 0 & 0 \\ W_6 & W_7 & W_8 & W_9 \\ N_6 & N_7 & N_8 & N_9 \\ L_6 & L_7 & L_8 & L_9 \\ S_6 & S_7 & S_8 & S_9 \end{bmatrix} \begin{bmatrix} \Delta m_{SH} \\ \Delta\varphi_{SH} \\ \Delta m_{SR} \\ \Delta\varphi_{SR} \end{bmatrix} \tag{3.25}$$

The eigen-values for the simple two-machine/UPFC power system are given in Table 3.3.

Table 3.3: **System states and eigen-values**

States	Eigen Values
δ_{12}	-0.5878 ± j 7.3234
ω_1	-3.504
ω_2	-3.0043
E'_{q1}	-0.00002
E'_{q2}	-0.4156 ± j 0.0634
V_{dc}	-0.3097
E_{fd1}	
E_{fd2}	

The UPFC is treated as an external controller installed in the network and its effect is included in the network current-voltage equation. Here the dynamics of the UPFC,

mainly the DC capacitor, are included by expressing line current explicitly. Thus the final form of the linearized model is obtained.

3.4 Participation factor

Right eigen Vectors

For any eigen value λ_i, the n-column vector γ_i which satisfies $A\gamma = \lambda\gamma$ is called the right eigen vector of 'A' associated with the eigen value λ_i

$$[A]\begin{bmatrix}\gamma_{1i}\\ \gamma_{2i}\\ .\\ \gamma_{ni}\end{bmatrix} = \lambda_i\begin{bmatrix}\gamma_{1i}\\ \gamma_{2i}\\ .\\ \gamma_{ni}\end{bmatrix} \tag{3.26}$$

Left eigen Vectors

For any eigen value λ_i, the 'n' row vector w_i which satisfies $w_i A = \lambda_i w_i$ is called the left eigen vector of A associated with the eigen value λ_i

$$\begin{bmatrix}w_{i1} & w_{i2} & ... & w_{in}\end{bmatrix}[A] = \lambda_i\begin{bmatrix}w_{i1} & w_{i2} & ... & w_{in}\end{bmatrix}$$

Participation factor corresponding to eigen value λ_i is given by

$$P_1 = \begin{bmatrix}P_{1i}\\ P_{2i}\\ .\\ P_{ni}\end{bmatrix} = \begin{bmatrix}\gamma_{1i}w_{i1}\\ \gamma_{2i}w_{i2}\\ .\\ \gamma_{ni}w_{in}\end{bmatrix} \tag{3.27}$$

The element $P_{ki} = \gamma_{ki}w_{ik}$ is termed the participation factor. It is a measure of the relative participation of the K^{th} state variable in the i^{th} mode. The eigen value corresponding to electromechanical mode of oscillation is -0.5878± j 7.3234. This is achieved using the above-mentioned participation factor method.

3.5 Controllability index

Equation (3.25) can be arranged into the following form

$$\begin{bmatrix} \Delta\dot{\delta}_j \\ \Delta\dot{\omega}_j \\ \dot{X} \end{bmatrix} = \begin{bmatrix} 0 & \omega_0 & 0 \\ -W_j & -D_j & \mathbf{A}_{23} \\ \mathbf{A}_{31} & \mathbf{A}_{32} & \mathbf{A}_{33} \end{bmatrix} \begin{bmatrix} \Delta\delta_j \\ \Delta\omega_j \\ X \end{bmatrix} + \begin{bmatrix} 0 \\ \mathbf{B}_{2k} \\ \mathbf{B}_{3k} \end{bmatrix} \Delta u_k = A \begin{bmatrix} \Delta\delta_j \\ \Delta\omega_j \\ X \end{bmatrix} + B_K \Delta u_k \tag{3.28}$$

Then any control function of the UPFC is

$$\Delta u_k = T_C(s)\Delta y_C \qquad \Delta y_C = C^T \begin{bmatrix} \Delta\delta_j \\ \Delta\omega_j \\ X \end{bmatrix} \tag{3.29}$$

which can be power flow control, voltage control, transient stability control or damping control. Therefore, the impact of these control functions of the UPFC upon system oscillation stability can be studied by computing system oscillation modes from the linearized model.

Another application of the linearized model derived above is the selection of the most efficient input control signal of the UPFC from Δm_{SH}, Δm_{SR}, $\Delta\varphi_{SH}$ and $\Delta\varphi_{SR}$ to apply a damping control function. Once it is decided that a damping controller is added as one of the secondary control functions of the UPFC, there are four candidates, namely, Δm_{SH}, Δm_{SR}, $\Delta\varphi_{SH}$ and $\Delta\varphi_{SR}$ to be considered to superimpose damping control. The signal which can achieve effective damping control at minimum control cost is most efficient. Since this selection is made at open-loop condition before the installation of the damping controller and only the input control signal changes, the following controllability index $b_i(\lambda_i) = W_i^T B_K$ can be used [59], where W_i is the left eigenvector of the state matrix 'A' corresponding to the oscillation mode λ_i. In [59], it has been proved that

$$b_i(\lambda_i) = K_{bki}(\lambda_i) w_{i2} = \left[B_{2k} + A_{23}(\lambda_i I - A_{33})^{-1} B_{3k} \right] w_{i2} \tag{3.30}$$

where w_{i2} is second element of W_i and its module does not change with the different selection of the input control signal of the UPFC. Hence, $|K_{bki}(\lambda_i)|$ can replace $|b_i(\lambda_i)|$ to be used as the controllability index. In the case that the frequency of power system oscillations is known to be $\omega_{Ni} \approx \lambda_i$ [39], [59], $|K_{bki}(\omega_{Ni})|$ can be used as the approximation of $|K_{bki}(\lambda_i)|$ so that eigen solution of the system state matrix is avoided in the selection. To demonstrate these applications of a UPFC integrated into a two-area power system is presented below.

Table 3.4 shows that the controllability index of φ_{SR} is zero, hence φ_{SR} cannot be used for damping control purpose. Out of the balance three control signals, m_{SR} shows the highest controllability index. Here onwards, in this thesis m_{SR} is selected as the control signal of UPFC for stability enhancement.

Table 3.4: **Computational results to select the best input control signal**

u_k	$\|K_{bki}\|$
m_{SH}	0.0214
m_{SR}	0.1386
φ_{SH}	0.0163
φ_{SR}	0.0000

To tackle the inter-area oscillation, we have to introduce a damping controller into UPFC. Table 3. presents the results of computing $|K_{bki}|$ which show that the most efficient input control signal is $u_k = m_{SR}$. Hence the damping controller is chosen to be

$$m_{SR} = \frac{sT_w}{1+sT_w}\frac{K_I}{1+sT_D}\frac{(1+sT_2)}{(1+sT_1)}\frac{(1+sT_4)}{(1+sT_3)}y_C \tag{3.31}$$

The speed deviation signal Δω is used as an input to the damping controller. The transfer-function block diagram of the damping controller is shown in Figure 3.2. The optimum parameters for the damping controllers are determined using genetic algorithm.

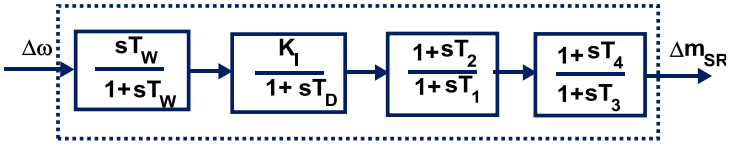

Figure 3.2: **Block diagram of damping controller**

3.6 Genetic algorithm

Genetic algorithms are probabilistic search approaches which are founded on the idea of evolutionary processes. They are global search algorithms based on the concept of natural genetics and the Darwinian survival-of-the-fittest code [65]. Each individual has an associated fitness measure, typically representing an objective value. The fittest individuals in a population will produce fitter offspring which is then implemented in order to generate the next population. Then selected individuals are chosen for reproduction or crossover at each generation, with an appropriate mutation factor to randomly modify the genes of an individual, in order to develop the new population. The result is a set of individuals based on the original subjects leading to subsequent populations with better individual fitness. In this work, GA is used for optimizing the control variables of (3.31).

In an optimization process to find the optimal parameter values, which results in a maximum or minimum of a function, is called an objective function. Objective function is a mathematical expression describing a relationship of the optimization parameters that uses the optimization parameters as inputs. In this chapter, an eigen value based objective function is considered. The main objective is to damp the power system oscillations. This can be achieved by maximizing the damping ratio (ζ) of the

electromechanical mode of oscillation. For i^{th} eigen value $\lambda_i = \sigma_i \pm j\omega_{ni}$, the damping ratio (ζ) is given by

$$\zeta_i = \frac{-\sigma_i}{\sqrt{\sigma_i^2 + \omega_{ni}^2}} \tag{3.32}$$

Hence the objective function 'J' is given by

$$J = \max(\zeta_i) \tag{3.33}$$

So the objective is to maximize 'J' such that to satisfy the following eight inequality constraints.

$K_I^{\min} \le K_I \le K_I^{\max}$; $T_w^{\min} \le T_w \le T_w^{\max}$; $T_1^{\min} \le T_1 \le T_1^{\max}$; $T_2^{\min} \le T_2 \le T_2^{\max}$; $T_3^{\min} \le T_3 \le T_3^{\max}$; $T_4^{\min} \le T_4 \le T_4^{\max}$; $T_D^{\min} \le T_D \le T_D^{\max}$

Details of the GA parameters are given in Table 3.. The genetic operators used in this work are extracted from standard GA procedure which includes selection using roulette wheel, crossovers and mutation [65]. In this work, the rates for crossovers and mutation are chosen as 80% and 1% respectively. This was chosen through experimentation as it provides sufficient solution diversity. The population size and maximum generations are limited to 100 to avoid more complexity.

Table 3.5: **Parameters used in Genetic Algorithm**

Parameters	**Value/Type**
Population size	100
Maximum generations	100
Selection operator	Roulette wheel
Crossover probability	0.8
Mutation probability	0.01
Termination method	Maximum generations

The parameters obtained after optimization are

$K_I = 15.1$; $T_D = 0.01s$; $T_w = 10.0s$; $T_1 = 0.39$; $T_2 = 0.12s$; $T_3 = 0.9s$; $T_4 = 0.11s$.

The eigen-values corresponding to electromechanical mode of oscillation after implementing the Lead-Lag damping controller is given in Table 3.:

Table 3.6: **Eigen-values for the electromechanical modes**

	Eigen value	Damping ratio	Frequency (Hz)
Without Lead-Lag control	-0.5878±j7.323	0.08	1.221
With Lead-Lag control	-1.103±j7.67	0.142	1.22

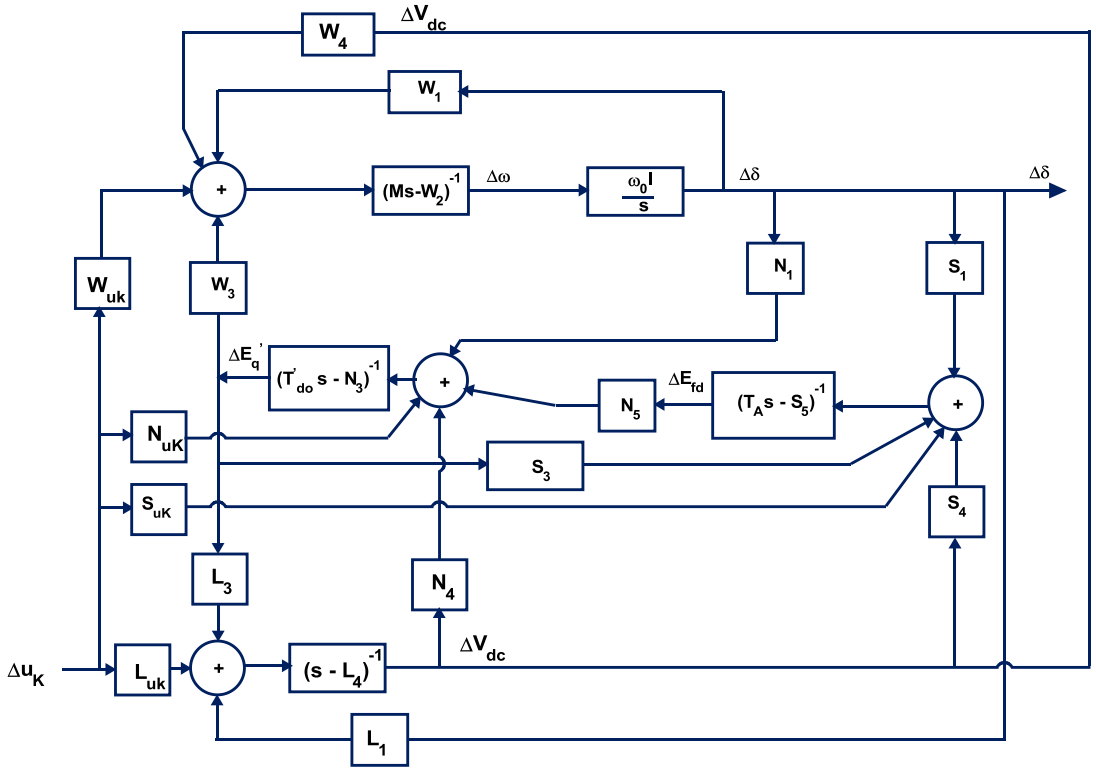

Figure 3.3: **Linearized Phillips-Heffron model of power system with UPFC**

3.7 Phillips-Heffron model

Pictorial representation of the linearized dynamic model of (3.25) can be shown by Figure 3.3. Here only one input control signal is demonstrated. Δu_k could be Δm_{SH}, Δm_{SR}, $\Delta \varphi_{SH}$ or $\Delta \varphi_{SR}$, the linearization of the input control signals of the UPFC. Details of this model are given in Appendix A.

3.8 Results and discussion

For control validation, the two-area power system shown in Figure 3.1 is used, where three phase to ground fault is injected close to bus 4 at point F at time t = 0.5s. Fault is removed after 0.15s by disconnecting the circuit breakers at both the ends. The UPFC placed at bus 3 is activated after fault clearance. The software program to simulate the power system and the controller has been written in FORTRAN in house and graphs are plotted using MATLAB software. RK4 numerical integration method is used to solve the differential equations with an integration step of 0.001 second. Performance analysis with and without damping controller are shown in the following figures.

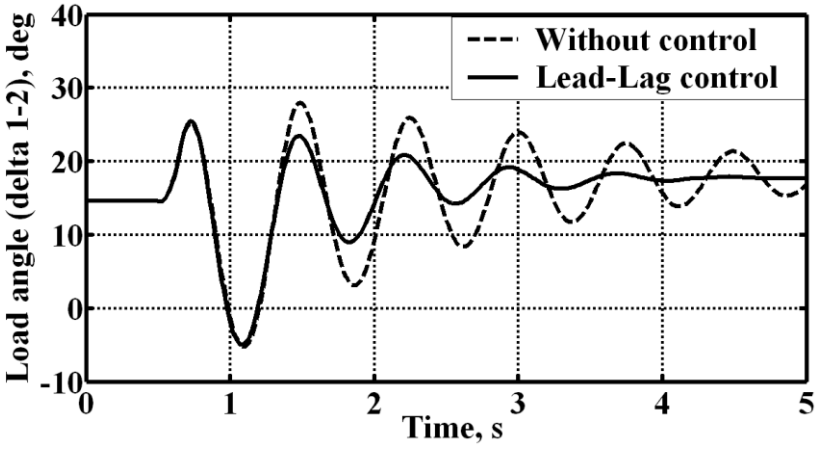

Figure 3.4: **Load angle variation**

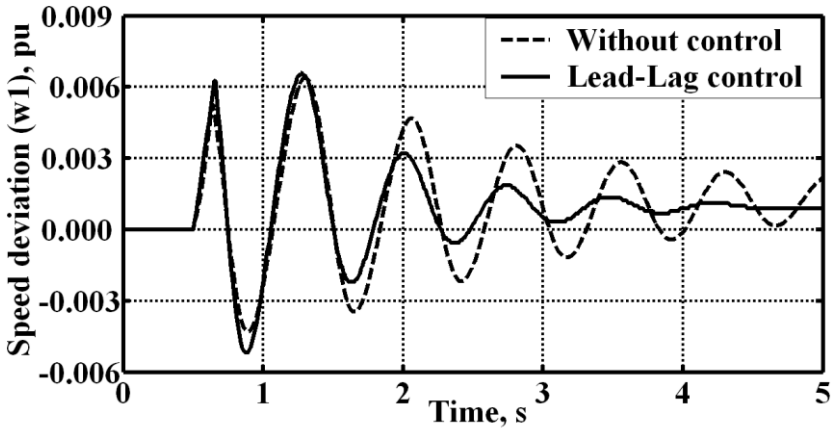

Figure 3.5: **Angular speed variation**

Figure 3.4 shows the load angle variation between generator-1 and 2, i.e., $(\delta_1 - \delta_2)$. Figure 3.5 shows the angular speed variation of the generator-1. Both show a considerable improvement in the electromechanical oscillation damping with the proposed Lead-Lag controller.

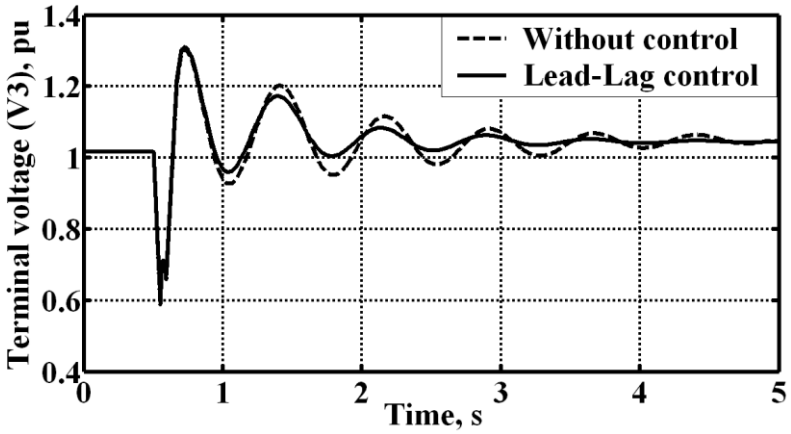

Figure 3.6: **Terminal voltage variation**

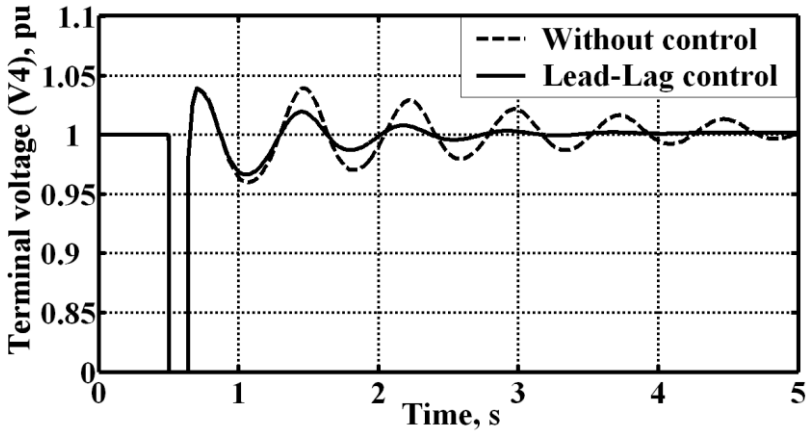

Figure 3.7: **Terminal voltage variation**

Terminal voltage variation of the bus 3 is shown in Figure 3.6, terminal voltage variation of bus 4 is shown Figure 3.7 and the injected UPFC real power is shown in Figure 3.8.

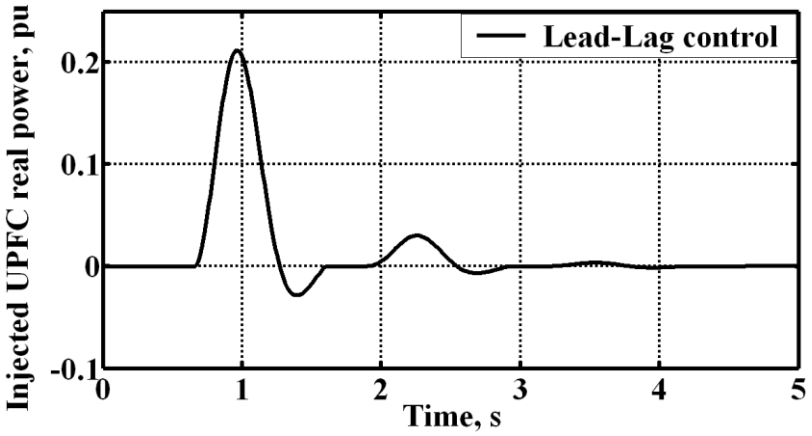

Figure 3.8: **Injected UPFC real power variation**

From Figure 3.4 to Figure 3.8 we can see that the suggested Lead-Lag controller behaves very well in improving transient stability when the system is subject to a large disturbance. The Lead-Lag controller can damp angle swings much more quickly than

without any control. As exhibited in figure, the injected UPFC power during fault is 21% of the steady state power flow value. This is slightly more than the acceptable limit.

The experiment is repeated for different operating points with Lag / Lead power factors. The operating points are $P_1 = 1.0,\ 0.8,\ 0.2\,pu$. The results are shown below

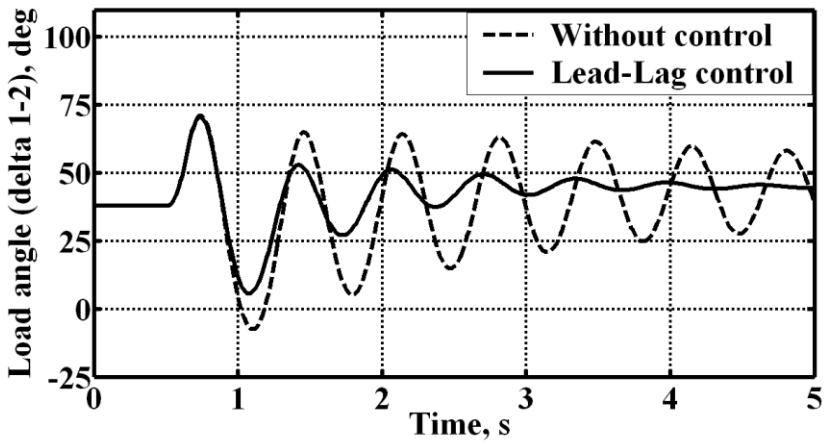

Figure 3.9: **Load angle variation at** $P_1 = 1.0,\ \ Q_1 = 0.3$

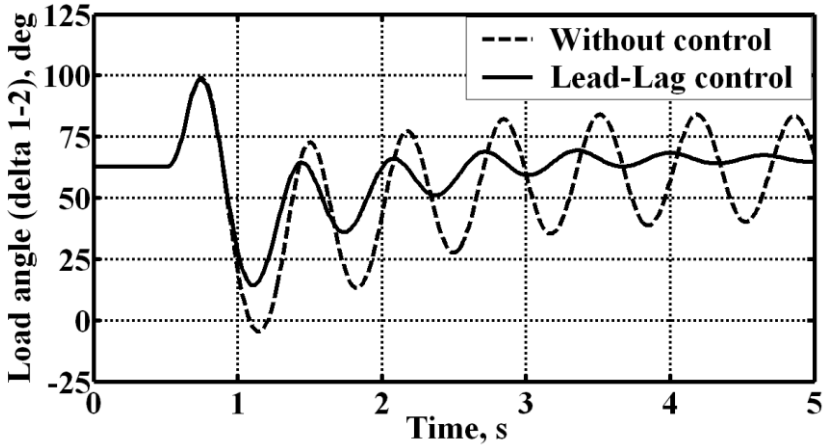

Figure 3.10: **Load angle variation at** $P_1 = 1.0,\ \ Q_1 = -0.3$

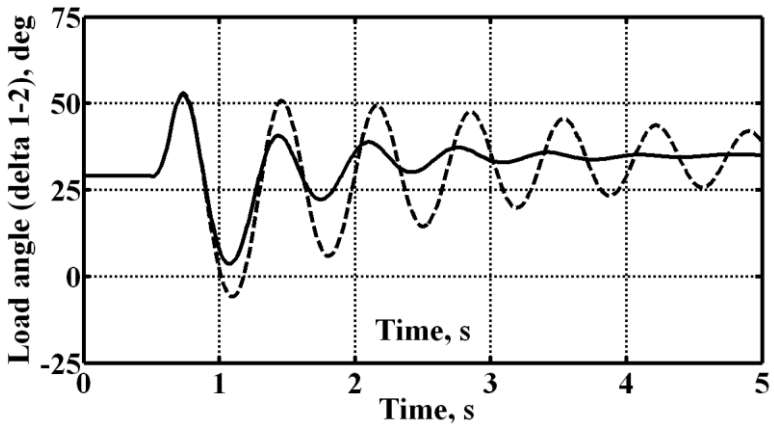

Figure 3.11: **Load angle variation at** $P_1 = 0.8,\ \ Q_1 = 0.3$

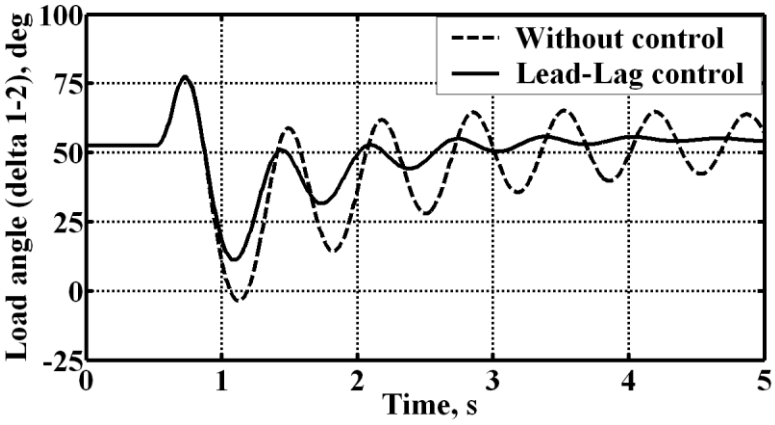

Figure 3.12: **Load angle variation at** $P_1 = 0.8,\ \ Q_1 = -0.3$

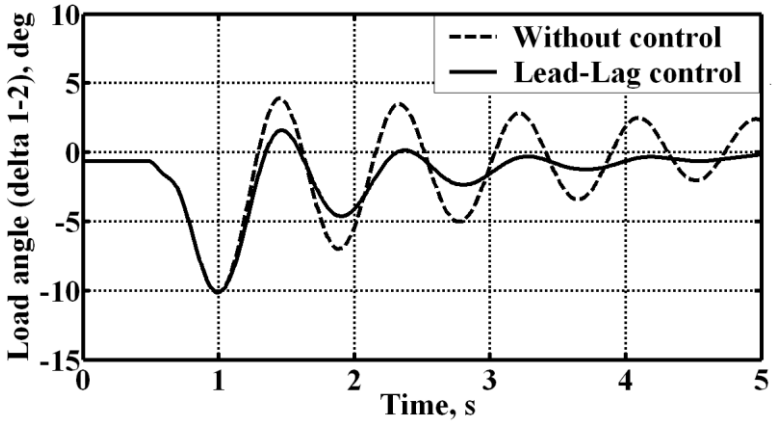

Figure 3.13: **Load angle variation at** $P_1 = 0.2,\ \ Q_1 = 0.3$

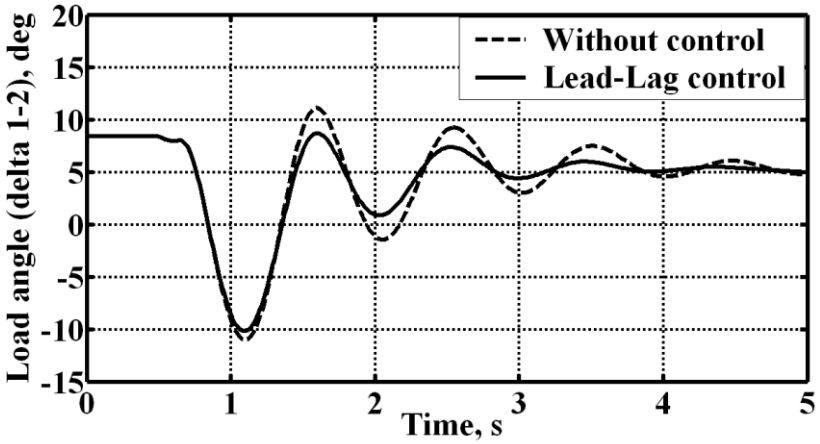

Figure 3.14: **Load angle variation at** $P_1 = 0.2,\ \ Q_1 = -0.3$

The generator with leading power factor can absorb reactive power; causing an increase in the load angle difference between the two generators. Leading power factor reduce generator terminal voltage. Even though leading power factor operation is effective and economic means for descending the higher voltage at low load it reduces the stability of the generator considerably.

We have considered modulation index of series converter, m_{SR} as the input control signal in the above discussions. The examining of variation of load angle with other control signals m_{SH} and φ_{SH} is also done. The signal φ_{SR} is not considered as the oscillation mode is not controllable with it. The results are shown in Figure 3.15. Analysis of figure shows the correctness of the selection of the input control signal m_{SR} as it provides the smoothest damping to the load angle variation.

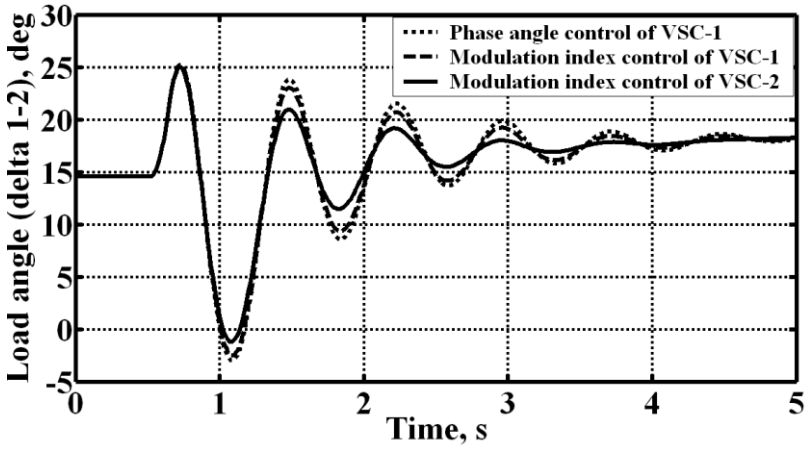

Figure 3.15: **Load angle variation with** φ_{SH} , m_{SH} , m_{SR}

The experiment is repeated for open circuit study. In the open circuit study, one of the transmission lines is disconnected after 0.5s without any fault. The load angle variation for this case is shown in Figure 3.16. Experiments for input mechanical power excursions are also conducted. Figure 3.17 and Figure 3.18 shows the variation of load angles corresponding to 10% and 20% reduction in the input mechanical power. Figure 3.19 shows the load angle variation when the loads at bus bar 3 are disconnected suddenly after 0.5s of the simulation.

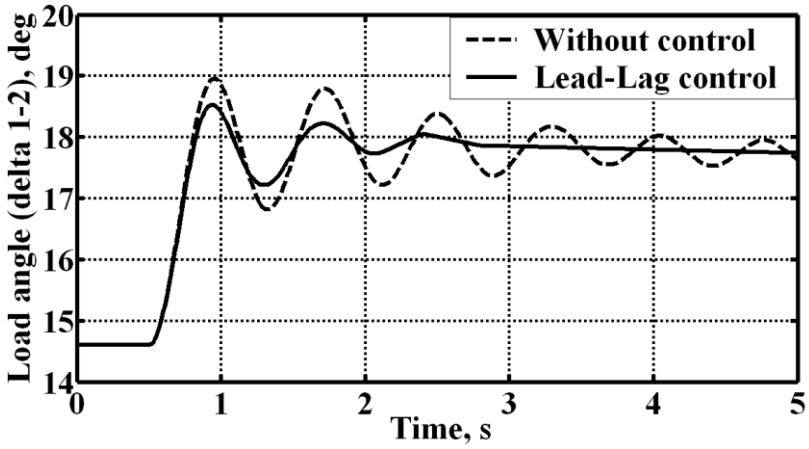

Figure 3.16: **Load angle variation with one line open after 0.5s**

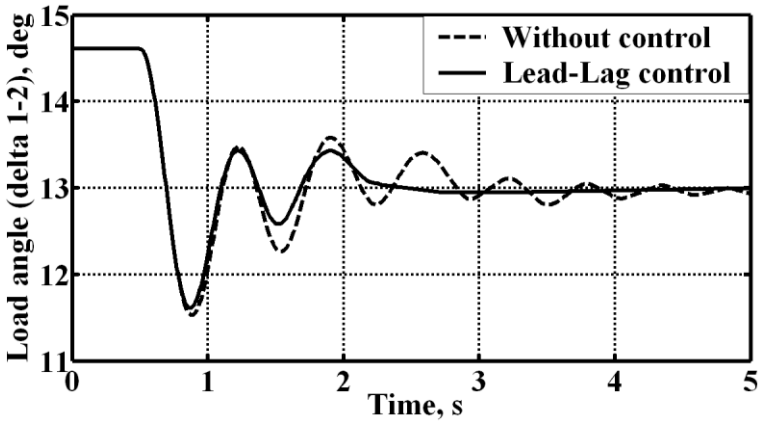

Figure 3.17: **Load angle variation with 10% reduction in input mechanical power**

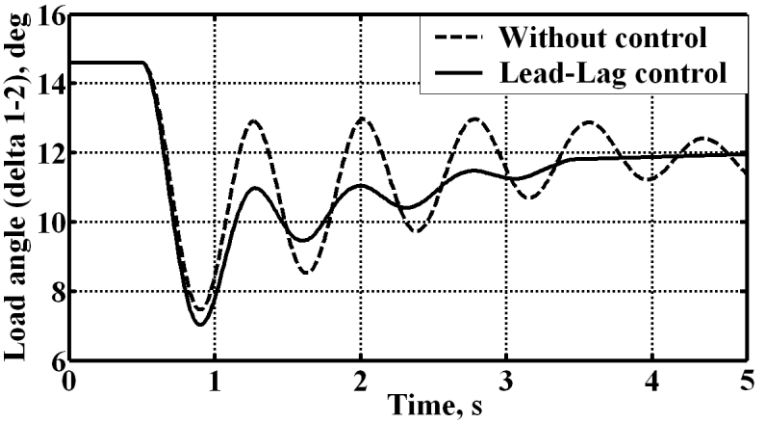

Figure 3.18: **Load angle variation with 20% reduction in input mechanical power**

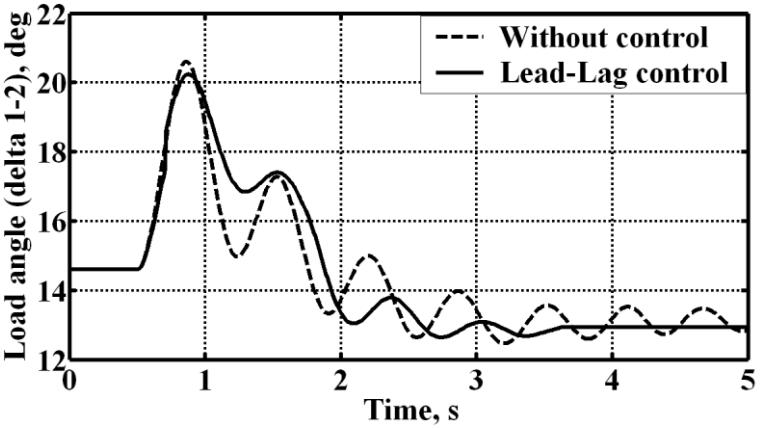

Figure 3.19: **Load angle variation with loads at bus bar 3 is disconnected at 0.5s**

3.9 Conclusion

This chapter has presented the development of a mathematical model of the small-signal dynamic performance of a two-area power system. Electromechanical mode of oscillation is identified using participation factor method. The most suitable control signal of the UPFC for oscillation damping is identified using controllability index method. The parameters of the developed Lead-Lag damping controller are optimized using genetic algorithm. Simulation results illustrate the effectiveness of the suggested method.

Chapter 4

Dynamic Modeling and Adaptive Control of Single Machine Infinite Bus System with UPFC

Chapter 4

Dynamic Modeling and Adaptive Control of Single Machine-Infinite Bus System with UPFC

4.1 Introduction

Chapter 3 has proposed to linearize the differential-algebraic equation network and eliminate the algebraic equations through step-by-step procedure. Then, linear control method is applied to the linearized power system. This approach, however, tacitly assumes that the network variables remain in the neighbourhood of the desired operating point. This is not true. Continuous load change would be experienced by the generators in a power system in their daily operation and when there is a fault in the power system, drastic changes can occur. As the system conditions shift from the operating point at which the controller was optimized, the developed Lead-Lag controller shows poor performance.

Hence, we include developing a nonlinear dynamic approximation of the power network, using UPFC as a controller, augmenting UPFC with nonlinear adaptive control based on back stepping for oscillation damping, and using an adaptive control law to approximate uncertain parameters that contribute significantly to the stability of the power system. To introduce the design concept, we initially design a controller for a single generator power system with UPFC using the standard back-stepping design method. The feasibility of the proposed technique is validated using simulation on a single machine to infinite bus system. This approach is extended to multiple generators in the next two chapters.

4.2 Power system modeling

Representation of power system with UPFC

Figure 4.1 shows the schematic diagram of a single-machine infinite bus system connected with UPFC. The main constituents are converters, transformers and a DC link capacitor. General pulse width modulation technique is adopted for the VSC. A third order nonlinear mathematical model describes the generator as explained in section 2.3.1. While deriving the algebraic equations, resistance of transformer, transmission lines, convertor and generator, etc., are neglected. The transients of the transmission lines are also ignored.

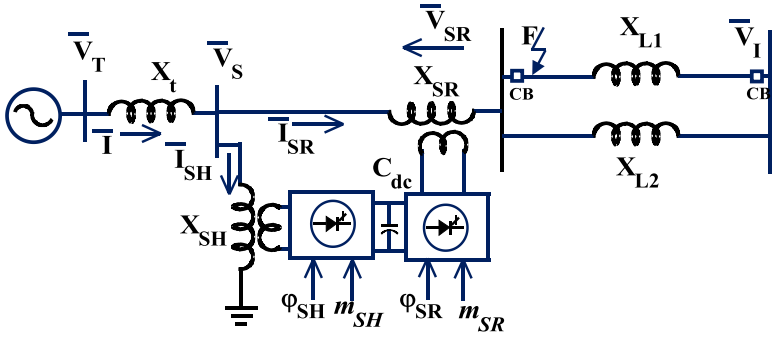

Figure 4.1: **Single machine infinite bus power system**

In Figure 4.1, $\hat{\mathbf{V}}_{\mathbf{T}}$ and $\hat{\mathbf{V}}_{I}$ are the generator terminal and infinite-bus voltages respectively. The algebraic equations are

$$P_e = V_{Td}\, I_d + V_{Tq}\, I_q \tag{4.1}$$

where $V_{Td} = X_q\, I_q$; $V_{Tq} = E_q^{'} - X_d^{'}\, I_d$; $E_q^{'} = E_q - (X_d - X_d^{'})\, I_d$

$I_d = I_{SHd} + I_{SRd}$; $I_q = I_{SHq} + I_{SRq}$; $V_T = \sqrt{(V_{Td})^2 + (V_{Tq})^2}$

where E_q and $E_q^{'}$ are the voltage back of q-axis synchronous reactance and q-axis component of voltage back of transient reactance of the generator respectively; I_{SHd}, I_{SHq}, I_{SRd} and I_{SRq} are the d-q components of the shunt ($\hat{\mathbf{I}}_{\mathbf{SH}}$) and series ($\hat{\mathbf{I}}_{\mathbf{SR}}$) currents of the UPFC respectively; I_d and I_q represent the d-q components of the generator terminal current $\hat{\mathbf{I}}$.

$$\hat{\mathbf{V}}_{\mathbf{T}} = j\, X_t\, \hat{\mathbf{I}} + \hat{\mathbf{V}}_{\mathbf{S}} \tag{4.2}$$

$$\hat{\mathbf{V}}_{\mathbf{SH}} = \hat{\mathbf{V}}_{\mathbf{S}} = \hat{\mathbf{V}}_{\mathbf{SR}} + j\, X_L\, \hat{\mathbf{I}}_{\mathbf{SR}} + \hat{\mathbf{V}}_{\mathbf{I}} \tag{4.3}$$

Here $X_L = (\frac{X_{L1}X_{L2}}{X_{L1}+X_{L2}})$ i.e. the equivalent reactance of the parallel combination of the transmission lines X_{L1} and X_{L2}. V_{SHd}, V_{SHq} are the d-q components of the voltage injected by the shunt ($\hat{\mathbf{V}}_{\mathbf{SH}}$) and series ($\hat{\mathbf{V}}_{\mathbf{SR}}$) converters of the UPFC respectively. According to [55],

$$\begin{pmatrix} V_{SHd} \\ V_{SHq} \\ V_{SRd} \\ V_{SRq} \end{pmatrix} = \begin{pmatrix} 0 & -X_{SH} & 0 & 0 \\ X_{SH} & 0 & 0 & 0 \\ 0 & 0 & 0 & -X_{SR} \\ 0 & 0 & X_{SR} & 0 \end{pmatrix} \begin{pmatrix} I_{SHd} \\ I_{SHq} \\ I_{SRd} \\ I_{SRq} \end{pmatrix} + \begin{pmatrix} m_{SH}V_{dc}\cos(\varphi_{SH})\ /2 \\ m_{SH}V_{dc}\sin(\varphi_{SH})\ /2 \\ m_{SR}V_{dc}\cos(\varphi_{SR})\ /2 \\ m_{SR}V_{dc}\sin(\varphi_{SR})\ /2 \end{pmatrix} \tag{4.4}$$

Subsequent manipulation besides rearrangement gives

$$I_{SHd} = \frac{X_{SRL}E_q^{'}}{X_{DT}} - \frac{X_{SRLTd}}{X_{DT}}\frac{m_{SH}V_{dc}\sin(\varphi_{SH})}{2} + \frac{X_{Td}}{X_{DT}}V_I\cos(\delta) + \frac{X_{Td}}{X_{DT}}\frac{m_{SR}V_{dc}\sin(\varphi_{SR})}{2} \tag{4.5}$$

$$I_{SHq} = \frac{X_{SRLTq}}{X_{QT}}\frac{m_{SH}V_{dc}\cos(\varphi_{SH})}{2} - \frac{X_{Tq}}{X_{QT}}V_I\sin(\delta) - \frac{X_{Tq}}{X_{QT}}\frac{m_{SR}V_{dc}\cos(\varphi_{SR})}{2} \tag{4.6}$$

$$I_{SRd} = \frac{X_{SH}E_q^{'}}{X_{DT}} + \frac{X_{Td}}{X_{DT}}\frac{m_{SH}V_{dc}\sin(\varphi_{SH})}{2} - \frac{X_{TSHd}}{X_{DT}}V_I\cos(\delta) - \frac{X_{TSHd}}{X_{DT}}\frac{m_{SR}V_{dc}\sin(\varphi_{SR})}{2} \tag{4.7}$$

$$I_{SRq} = \frac{X_{TSHq}}{X_{QT}}\frac{m_{SR}V_{dc}\cos(\varphi_{SR})}{2} + \frac{X_{TSHq}}{X_{QT}}V_I\sin(\delta) - \frac{X_{Tq}}{X_{QT}}\frac{m_{SH}V_{dc}\cos(\varphi_{SH})}{2} \tag{4.8}$$

Equations (4.9)-(4.11) give the non-linear dynamic representation of the generator [1], [66]. Equation (4.12) shows the dynamic model of the UPFC [55]. The nominal loading condition and system parameters are mentioned in the Table 4.1. The initial values are calculated by conducting load-flow analysis using Newton – Raphson method.

$$\dot{\delta} = \omega - \omega_0 \tag{4.9}$$

$$\dot{\omega} = \frac{\omega_0}{2H}[P_m - P_e - D(\frac{\omega - \omega_0}{\omega_0})] \tag{4.10}$$

$$\dot{E}_q^{'} = \frac{1}{T_{do}^{'}}[E_{fd} - (X_d - X_d^{'})I_d - E_q^{'}] \tag{4.11}$$

$$\dot{V}_{dc} = \frac{3m_{SH}}{4C_{dc}}[\cos(\varphi_{SH})I_{SHd} + \sin(\varphi_{SH})I_{SHq}] + \frac{3m_{SR}}{4C_{dc}}[\cos(\varphi_{SR})I_{SRd} + \sin(\varphi_{SR})I_{SRq}] \tag{4.12}$$

In this equivalent D, X_d and $X_d^{'}$ are understood as uncertain parameters because the damping coefficient exists hard to be precisely evaluated and the reactance X_d and $X_d^{'}$ will vary slowly on account of the saturation issue.

Table 4.1: **System parameters and initial conditions**

$P_1 = 1.2\,pu$	$V_T = 1.0\,pu$	$V_I = 1.0\,pu$	$X_d^{'} = 0.3\,pu$	$f = 60HZ$
$X_d = 1.0\,pu$	$X_q = 0.6\,pu$	$T_{do}^{'} = 5.044S$	$D_1 = 0.0$	$M = 8MJ/MVA$
$X_t = 0.1pu$	$X_{L1} = 0.3pu$	$X_{L2} = 0.3pu$	$X_{SR} = 0.1pu$	$X_{SH} = 0.1pu$
$V_{dc} = 10.0\,pu$	$C_{dc} = 2.0\,pu$	$m_{SR} = 0.0$	$\varphi_{SR} = 131.5^0$	$m_{SH} = 0.1935\,pu$
$\varphi_{SH} = 52.76^0$				

New dynamic representation of power network

Equations (4.1)-(4.8) contain algebraic equations while (4.9)-(4.12) has the differential

equations. Together they form an approximate representation of power system. But it is difficult to achieve a controller design in this environment. Therefore, it is better to use an appropriate set to replace the set of algebraic equations. Taking derivatives [67] of the generator terminal current equations $I_d = I_{SHd} + I_{SRd}$ and $I_q = I_{SHq} + I_{SRq}$ for obtaining $\dot{I}_d$ and $\dot{I}_q$ terms is a method to have a dynamical representation of the network. Thus we have

$$\frac{\partial I_d}{\partial t} = \frac{\partial I_d}{\partial \delta}\dot{\delta} + \frac{\partial I_d}{\partial E_q^{'}}\dot{E}_q^{'} + \frac{\partial I_d}{\partial V_{dc}}\dot{V}_{dc} + \frac{\partial I_d}{\partial m_{SH}}\dot{m}_{SH} + \frac{\partial I_d}{\partial \varphi_{SH}}\dot{\varphi}_{SH} + \frac{\partial I_d}{\partial m_{SR}}\dot{m}_{SR} + \frac{\partial I_d}{\partial \varphi_{SR}}\dot{\varphi}_{SR} \tag{4.13}$$

$$\frac{\partial I_q}{\partial t} = \frac{\partial I_q}{\partial \delta}\dot{\delta} + \frac{\partial I_q}{\partial E_q^{'}}\dot{E}_q^{'} + \frac{\partial I_q}{\partial V_{dc}}\dot{V}_{dc} + \frac{\partial I_q}{\partial m_{SH}}\dot{m}_{SH} + \frac{\partial I_q}{\partial \varphi_{SH}}\dot{\varphi}_{SH} + \frac{\partial I_q}{\partial m_{SR}}\dot{m}_{SR} + \frac{\partial I_q}{\partial \varphi_{SR}}\dot{\varphi}_{SR} \tag{4.14}$$

Solving equations (4.13) and (4.14) we obtain a new set of dynamic equations as

$$\begin{pmatrix} \dot{I}_d \\ \dot{I}_q \end{pmatrix} = \begin{pmatrix} a_{11} & a_{12} & a_{13} \\ a_{21} & a_{22} & a_{23} \end{pmatrix} \begin{pmatrix} \dot{\delta} \\ \dot{E}_q^{'} \\ \dot{V}_{dc} \end{pmatrix} + \begin{pmatrix} b_{11} & b_{12} & b_{13} & b_{14} \\ b_{21} & b_{22} & b_{23} & b_{24} \end{pmatrix} \begin{pmatrix} \dot{m}_{SH} \\ \dot{\varphi}_{SH} \\ \dot{m}_{SR} \\ \dot{\varphi}_{SR} \end{pmatrix} \tag{4.15}$$

Parameters $a_{11}.....b_{24}$ are shown in the Appendix B. The expression for $\dot{I}_d$ and $\dot{I}_q$ thus obtained is a nonlinear dynamic system in continuous time with control inputs $\dot{m}_{SH}$, $\dot{\varphi}_{SH}$, $\dot{m}_{SR}$ and $\dot{\varphi}_{SR}$. The formation of these equations not only avoid the need for solving difficult nonlinear algebraic equations but also help us to convert the nonlinear system described by equations (4.9)-(4.11) into standard parametric feed-back form without losing the nonlinear characteristics of the power system. Once the control inputs are defined, the UPFC control parameters m_{SH}, φ_{SH}, m_{SR} and φ_{SR} can be obtained by integrating

the control inputs. By substituting the values of $\dot{\delta}$, $\dot{E}_q'$ and $\dot{V}_{dc}$ from equations (4.9)-(4.12) into (4.15) we obtain

$$\begin{pmatrix} \dot{I}_d \\ \dot{I}_q \end{pmatrix} = \begin{pmatrix} C_1(x) \\ C_2(x) \end{pmatrix} + \begin{pmatrix} b_{11} & b_{12} & b_{13} & b_{14} \\ b_{21} & b_{22} & b_{23} & b_{24} \end{pmatrix} \begin{pmatrix} u_1 \\ u_2 \\ u_3 \\ u_4 \end{pmatrix} \tag{4.16}$$

According to equation (4.16) there are four choices of input control signals which can be used to superimpose on the damping function of the UPFC. Since converter 2 does the main function of UPFC by injecting a voltage V_{SR} with a controllable magnitude and phase angle, the control signals m_{SH} and φ_{SH} of the shunt controller are not important. Again unlike conventional controller, where magnitude of the injected series voltage will remain constant with a variable phase angle, here the authors are interested for a constant phase angle with a variable voltage magnitude for controller design. Therefore, the above equation becomes

$$\begin{cases} \dot{I}_d = C_1(x) + b_{13}u_3 \\ \dot{I}_q = C_2(x) + b_{23}u_3 \end{cases} \tag{4.17}$$

4.3 Controller design

The UPFC is designed with an aim to control two quantities of the generator, the load angle δ and speed ω, to a reference value δ_0 and ω_0, the pre-fault power angle and speed of the generator respectively. The controller needs to be adaptive to uncertain parameters throughout the simulation such that these parameters will not influence the efficiency of the controller. First step needed to undertake for the controller design is the following coordinate transformation for equation (4.9)-(4.11)

$$x = [\delta - \delta_0,\ \ \omega - \omega_0,\ \ \omega_0(P_m - P_e)/2H] \tag{4.18}$$

With $P_e = E_q^{'} I_q$ [66], the new coordinate will satisfy

$$\begin{cases} \dot{x}_1 = x_2 \\ \dot{x}_2 = x_3 + \psi_2 x_2 \\ \dot{x}_3 = C_{T1} + g u_3 + \Gamma \psi_3 \end{cases} \tag{4.19}$$

where $\psi_2 = -\dfrac{D}{2H}$, and $\psi_3 = X_d - X_d^{'}$ are the uncertain parameters.

$$C_{T1} = \frac{\omega_0}{2H}\left[\frac{I_q E_{fd}}{T_{do}^{'}} - \frac{I_q E_q^{'}}{T_{do}^{'}} - E_q^{'} C_2(x)\right]; \qquad g = -\frac{\omega_0 E_q^{'} b_{2i}}{2H}; \qquad \Gamma = \frac{\omega_0 I_d I_q}{2HT_{do}^{'}}$$

With the introduction of the following functions

$f_1(x_1) = 0;\ \ \eta_1(x_1) = 1;\ \ \mu_1(x_1) = 0;\ \ f_2(x_1, x_2) = 0;\ \ \eta_2(x_1, x_2) = 1;\ \ \mu_2(x_1, x_2) = x_2$

$f_3(x_1, x_2, x_3) = C_{T1};\ \eta_3(x_1, x_2, x_3) = g;\ \mu_3(x_1, x_2, x_3) = \Gamma.$

The standard parametric feedback form [68] as shown in (4.20) can be obtained from equation (4.19)

$$\dot{x}_i = f_i(x_1, .., x_i) + \eta_i(x_1, .., x_i) x_{i+1} + \mu_i^T(x_1, .., x_i)\psi_i \qquad (1 \le i \le n) \tag{4.20}$$

Here n represents the order of the system which equals to three for our case; and $x_{n+1} = u_3$.

In power systems, the system dynamics may have been well known at the beginning but experience unpredictable parameter variations as the control operation goes on. These unknown variations in plant parameters are defined as the uncertain parameters. Damping ratio, transient and sub-transient reactance etc are the examples of such uncertain parameters of power system study. Without continuous "redesign" of the controller, the initially appropriate controller design may not be able to control the changing plant well. Generally, the basic objective of adaptive control is to maintain consistent performance of a system in the presence of uncertainty or unknown variation

in plant parameters. Since such parameter uncertainty or variation occurs in many practical problems, adaptive control is useful in many industrial contexts.

Adaptive law for uncertain parameters

We look to attain an adaptive law for the uncertain parameters ψ_i in this part. Let us define ε_i as the error between the uncertain parameters ψ_i and its estimated value $\hat{\psi}_i$. Therefore it can be represented as

$$\varepsilon_i = \hat{\psi}_i - \psi_i + \beta_i(x_1,...,x_i) \qquad (i = 1,2,...n) \tag{4.21}$$

where $\beta_i(x_1,...,x_i) = \mu_i(x_1,...,x_i)x_i$.

Equation (4.22) represents the error dynamic for ψ_i

$$\dot{\varepsilon}_i = \dot{\hat{\psi}}_i + \dot{\beta}_i(x_1,...,x_i) \tag{4.22}$$

Using partial differentiation, $\dot{\beta}_i(x_1,...,x_i)$ can be expressed as

$$\dot{\beta}_i(x_1,..x_i) = \frac{\partial \beta_i}{\partial x_1}\dot{x}_1 + \frac{\partial \beta_i}{\partial x_2}\dot{x}_2 + .. + \frac{\partial \beta_i}{\partial x_i}\dot{x}_i \tag{4.23}$$

Substituting (4.23) in (4.22) and using (4.20) and (4.21), error dynamic can be written as

$$\dot{\varepsilon}_i = \dot{\hat{\psi}}_i + \sum_{k=1}^{i}\frac{\partial \beta_i}{\partial x_k}[\, f_k(x_1,..,x_k) + \eta_k(x_1,..,x_k)x_{k+1}$$

$$+\mu_k^T(x_1,..,x_k)(\hat{\psi}_k + \beta_k(x_1,...,x_k) - \varepsilon_k)] + \frac{\partial \mu_i}{\partial t}x_i \tag{4.24}$$

Now by selecting the update laws $\dot{\hat{\psi}}_i$ to cancel all known quantities [69], gives

a) the adaptive law for uncertain parameter as

$$\dot{\hat{\psi}}_i = -\sum_{k=1}^{i}\frac{\partial \beta_i}{\partial x_k}[\, f_k(x_1,..,x_k) + \eta_k(x_1,..,x_k)x_{k+1}$$

$$+\mu_i^T(x_1,..,x_k)(\widehat{\psi}_i+\beta_i(x_1,...,x_i))]-\frac{\partial\mu_i}{\partial t}x_i \tag{4.25}$$

b) error dynamics as

$$\dot{\varepsilon}_i=-\sum_{k=1}^{i}\frac{\partial\beta_i}{\partial x_k}\mu_k^T(x_1,..,x_k)\varepsilon_k \tag{4.26}$$

thus an influential inequality can be derived as

$$\frac{d}{dt}\left(\sum_{i=1}^{n}\tau_i\varepsilon_i^T\varepsilon_i\right)\le-\sum_{i=1}^{n}[\mu_i^T(x_1,..,x_i)\varepsilon_i]^2 \tag{4.27}$$

here τ_i is a positive constant. Further, the proof of the inequality is given in [69].

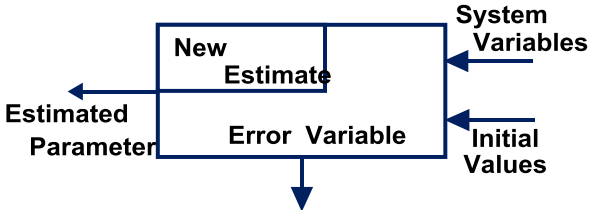

Figure 4.2: **Structure of parameter estimator**

The structure of the uncertain parameter is shown in Figure 4.2. In each step, estimator generates an error variable and a new estimate. This value of the parameter is used for next iteration of the power system.

Adaptive law for control inputs

The objective of our suggested controller is to design the control input $x_{n+1}=u_3$ such that the system states x_i can be driven to the small neighbourhood of a given equilibrium point, say δ_0 and ω_0, where δ_0 and ω_0 are the pre-fault stable operating points of the generator. The control law can be defined in such a way that all the system states will be forced to advance to its steady state value with this input. This steady state value is taken as the reference and represented as x_i^*. This can be achieved using the following back

stepping formation. We first examine controlling x_1 to a constant reference x_1^*.

$$\tilde{x}_1 = x_1 - x_1^* \tag{4.28}$$

The dynamics of $\tilde{x}_1$ are given by $\dot{\tilde{x}}_1 = \dot{x}_1 - 0$ and using (4.20)

$$\dot{\tilde{x}}_1 = f_1(x_1) + \eta_1(x_1)x_2 + \mu_1^T(x_1)\psi_1 \tag{4.29}$$

Now taking x_2 as a "virtual" control input, we can describe the error as

$$\tilde{x}_2 = x_2 - \xi_2(x_1, \psi_1) \tag{4.30}$$

where $\xi_2(x_1, \psi_1) = x_2^*$ is derived from (4.29) as $\xi_2 = \frac{1}{\eta_1(x_1)}\left[-\alpha_1(x_1, \psi_1) - f_1(x_1) - \mu_1^T(x_1)\psi_1\right]$ for some function $\alpha_1(\cdot)$ is still to be defined. The dynamics of $\tilde{x}_2$ are given by

$$\dot{\tilde{x}}_2 = \dot{x}_2 - \frac{\partial \xi_2}{\partial x_1}\dot{x}_1 - \frac{\partial \xi_2}{\partial \psi_1}\dot{\psi}_1 = f_2(x_1, x_2) + \eta_2(x_1, x_2)x_3 + \mu_2^T(x_1, x_2)\psi_2$$

$$- \frac{\partial \xi_2}{\partial x_1}(f_1(x_1) + \eta_1(x_1)x_2 + \mu_1^T(x_1)\psi_1) - \frac{\partial \xi_2}{\partial \psi_1}\dot{\psi}_1 \tag{4.31}$$

This is obtained by substituting values of $\dot{x}_2$ and $\dot{x}_1$ using (4.20) where now the virtual control input is x_3, and hence we define the error as

$$\tilde{x}_3 = x_3 - \xi_3(x_1, x_2, \psi_1, \psi_2) \tag{4.32}$$

where $\xi_3 = \frac{1}{\eta_2(x_1, x_2)}\{-\alpha_2(x_1, x_2, \psi_1, \psi_2) - f_2(x_1, x_2) -$

$$- \frac{\partial \xi_2}{\partial x_1}(f_1(x_1) + \eta_1(x_1)x_2 + \mu_1^T(x_1)\psi_1) - \frac{\partial \xi_2}{\partial \psi_1}\dot{\psi}_1\}$$

The dynamics of $\tilde{x}_3$ are given by

$$\dot{\tilde{x}}_3 = \dot{x}_3 - \frac{\partial \xi_3}{\partial x_1}\dot{x}_1 - \frac{\partial \xi_3}{\partial x_2}\dot{x}_2 - \frac{\partial \xi_3}{\partial \psi_1}\dot{\psi}_1 - \frac{\partial \xi_3}{\partial \psi_2}\dot{\psi}_2 \tag{4.33}$$

$$\dot{\tilde{x}}_3 = f_3(x_1, x_2, x_3) + \eta_3(x_1, x_2, x_3)x_4 + \mu_3^T(x_1, x_2, x_3)\psi_3 \; - \frac{\partial \xi_3}{\partial x_1}[f_1(x_1) + \eta_1(x_1)x_2 + \mu_1^T(x_1)\psi_1]$$

$$- \frac{\partial \xi_3}{\partial x_2}[f_2(x_1, x_2) + \eta_2(x_1, x_2)x_3 + \mu_2^T(x_1, x_2)\psi_2] \; - \frac{\partial \xi_3}{\partial \psi_1}\dot{\psi}_1 - \frac{\partial \xi_3}{\partial \psi_2}\dot{\psi}_2 \qquad (4.34)$$

where $x_4 = u_3$, suppose that $\eta_i(x_1,.,x_i) \neq 0$ holds for all $i = 1,2,..,n$ then we can define the control input as [69]

$$u_3 = \frac{1}{\eta_3(x_1,.,x_3)}\{-\alpha_3(x_1,.,x_3,\psi_1,.,\psi_3) - f_3(x_1,.,x_3) - \mu_3^T(x_1,.,x_3)\psi_3 - \sum_{k=1}^{3-1}\frac{\partial \xi_3}{\partial \psi_k}\dot{\psi}_k -$$

$$\sum_{k=1}^{3-1}\frac{\partial \xi_3}{\partial x_k}[f_k(x_1,.,x_k) + \eta_k(x_1,.,x_k)x_{k+1} + \mu_k^T(x_1,.,x_k)\psi_k]\} \qquad (4.35)$$

The functions $\alpha_i(\cdot)$ selected are given in the Appendix B. The block diagram representation of the proposed controller is shown in Figure 4.3. With the control input defined as in (4.35) and adaptive law in (4.25) the system (4.20) is globally asymptotic stable at $\tilde{x}_i = 0$. In other words x_i converges to x_i^* and all the closed-loop signals like system states and estimation errors (ε_i) will be bounded. The proof for the same is given in [69]. Further, we can see that all the variables and system states can be defined independently.

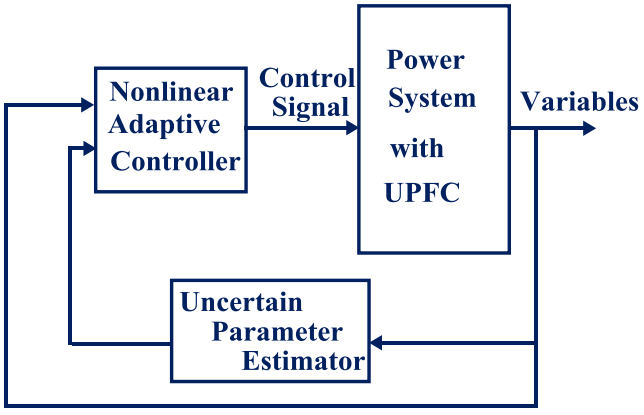

Figure 4.3: **Block diagram representation of nonlinear adaptive control**

4.4 Results and discussion

The advantage of the designed controller is proved by performing the computer verification on a single-machine infinite bus system. The aim of the controller is the damping of the generator oscillations after the fault is cleared. For comparing, the generator is first fitted with conventional controller. The details are given in [55]. Figure 4.4 displays the block diagram image of the conventional controller where the input to the damping controller is the deviations in generator speed.

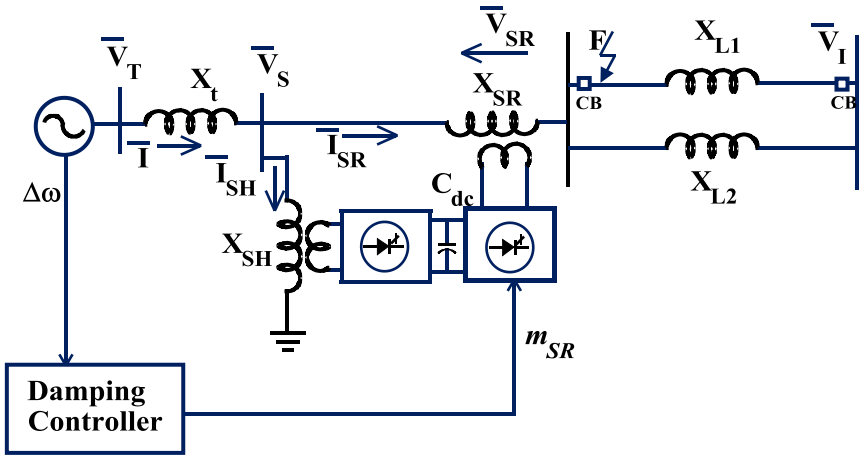

Figure 4.4: **Conventional controller**

The damping controller for Figure 4.4 is made using the equation 3.31. The reference setting of the power flow controller is modulated by its output. Therefore, an increased electric power output is secured in phase with the speed variation. The parameters of this controller have been optimized using Genetic Algorithm for better operation. The details of the Genetic Algorithm have been explained in section 3.6. The main objective is to damp the power oscillations by maximizing the damping ratio of the electromechanical mode of oscillation.

The parameters obtained after optimization are

$K_D = 7.1; \quad T_D = 0.01s; \quad T_w = 9.5s; \quad T_1 = 0.9s; \quad T_2 = 0.73s; \quad T_3 = 0.9s; \quad T_4 = 0.6s.$

Secondly, the above-mentioned controller is changed by the suggested adaptive control whose parameters are determined by trial and error method. In both these examples, the generator is modeled by the third-order approximation with δ, ω and $E_q^{'}$ as state variables. The loads are represented by constant impedance model. The fault studied in the simulation is that the system runs without any fault for 0.2 seconds. Next a three-phase to ground fault occurs on one of the transmission lines at mark F as shown in Figure 4.1 and persists for 0.15 seconds. Finally, the fault is cleared by disconnecting the faulted line by opening the circuit breakers at both ends. Simulation results are shown in Figure 4.5 to Figure 4.12. RK4 numerical integration method is used to solve the differential equations with an integration step of 0.001 second.

Figure 4.5 shows the variation of rotor angle and Figure 4.6 variation of speed of the generator at an operating condition P_e = 1.2 pu With the proposed adaptive controller, the generator load angle increases from an initial value of 56.69^0 to a maximum value of 84.58^0 and then returns back to initial value.

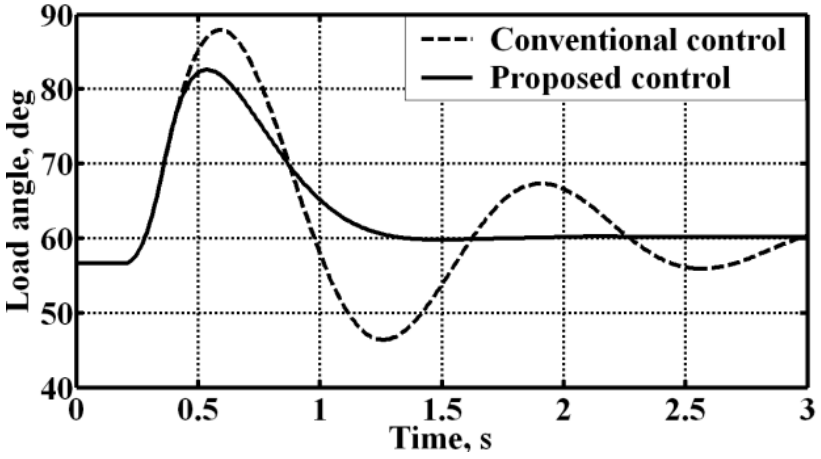

Figure 4.5: **Load angle variation of generator at P_e = 1.2, Q_e=0.4 pu**

Here the system gets stabilized within 1.25 seconds and thus the proposed controller gains an advantage over the conventional controller. The maximum angle, number of major oscillations and settling time, all have a smaller value in the presence of new controller. The suggested controller can damp angle swings and angular speed variations faster than the conventional controller due to its adaptive characteristics.

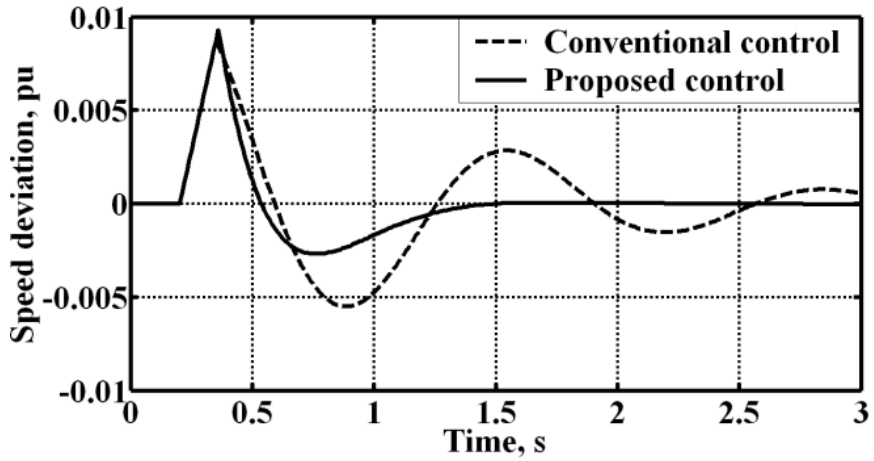

Figure 4.6: **Speed variation of generator at P_e=1.2, Q_e=0.4 pu**

Figure 4.7 shows the changes in the generator terminal voltage for a period of three seconds. The quick convergence of the terminal voltage of the generator to an acceptable range can be seen. The acceptable range is ±10% of its steady state reading. The active power flow on the tie line between generator and infinite bus is shown in Figure 4.8. Apparently, the proposed controller damps the power oscillations quickly and efficiently by reducing the time of oscillation. Hence, there is an improvement in the dynamic stability of power system.

Figure 4.9 and Figure 4.10 display injected real power and voltage of the UPFC with proposed controller. As exhibited in figure, the injected power during fault is less than 10 % of the steady state power flow value.

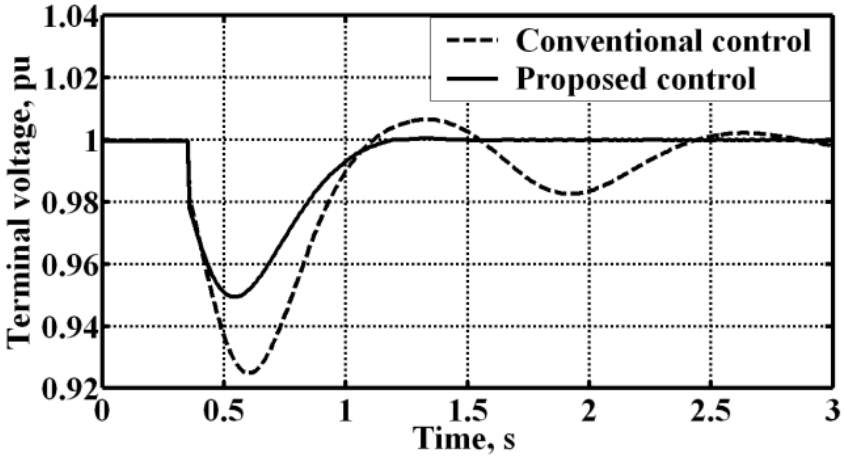

Figure 4.7: T**erminal voltage variation of V_S at P_e=1.2, Q_e=0.4 pu**

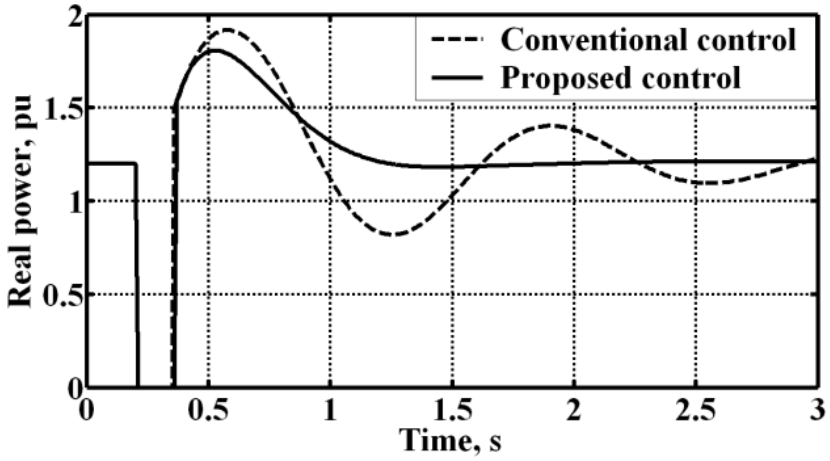

Figure 4.8: **Variation of real power transfer from generator at P_e=1.2, Q_e=0.4 pu**

Similarly, injected voltage is also getting reduced considerably. Consequently, the required rating of the transformers and converters gets significantly minimized as compared to that of conventional controller. Note that in case of UPFC, shunt and series active powers are related to each other. Since a UPFC with no loss does not generate or absorb active power, P_{shunt} and P_{series} will be equal in magnitude and opposite in polarity.

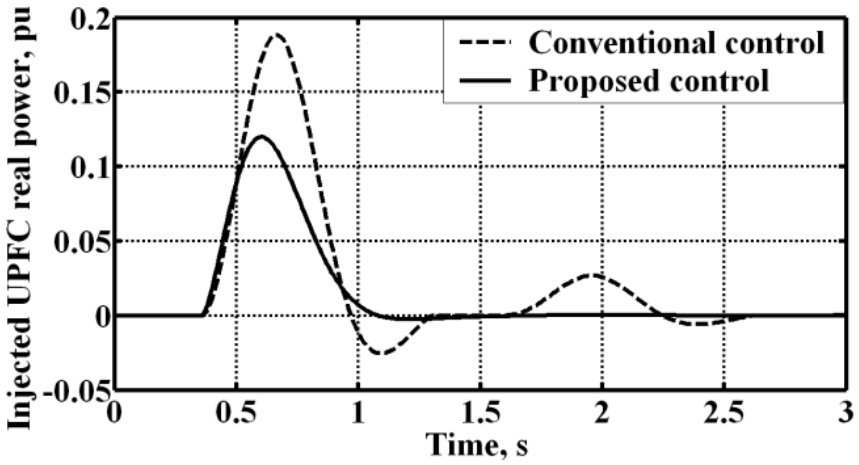

Figure 4.9: **Injected UPFC real power at P_e=1.2, Q_e=0.4 pu**

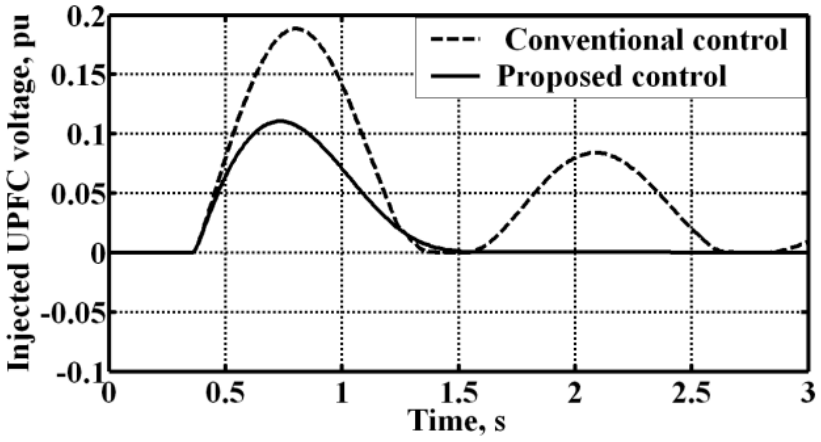

Figure 4.10: **Injected UPFC voltage at P_e=1.2, Q_e=0.4 pu**

Figure 4.11 and Figure 4.12 show the evaluation results of the uncertain parameters of the generator. Initial value is taken as zero for these two uncertain parameters. From the figure, it can be observed that the suggested estimator converges very quickly and finally becomes constant.

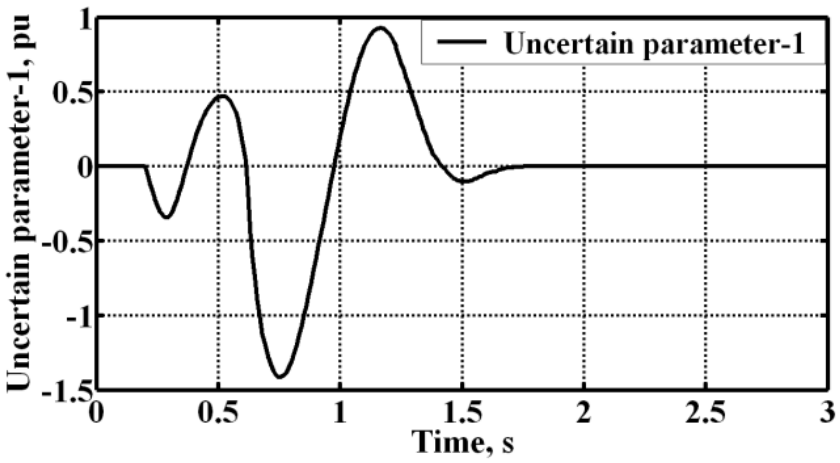

Figure 4.11: **Variation of uncertain parameter ψ_2 at P_e=1.2, Q_e=0.4 pu**

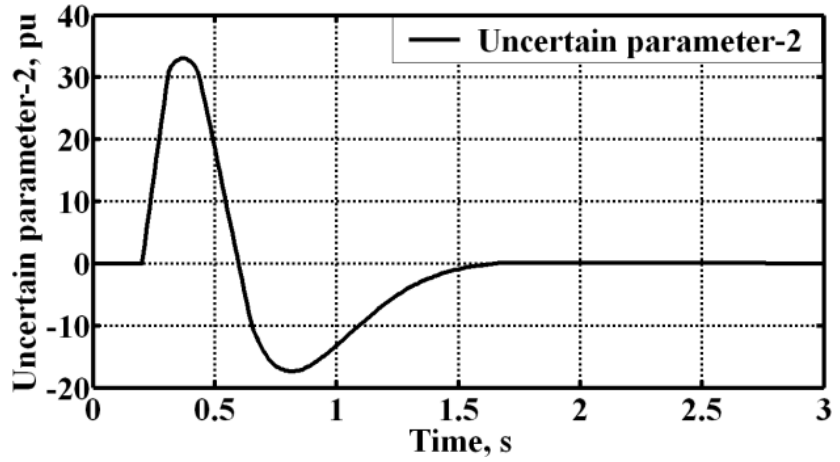

Figure 4.12: **Variation of uncertain parameter ψ_3 at P_e=1.2, Q_e=0.4 pu**

The designed controller with same initial parameters is now subjected to a new operating condition to show that the proposed controller is independent of any particular operating point. Here with P_e = 0.1 pu, the dynamic performance is shown in Figure 4.13 and Figure 4.14. The results show that the proposed controller behaves satisfactorily in damping rotor oscillations. Secondly, no appreciable difference in controller performance between the two cases (P_e = 0.1and P_e = 1.2) are observed when using

proposed controller. This proves that the proposed controller works well over a wide range of operating condition.

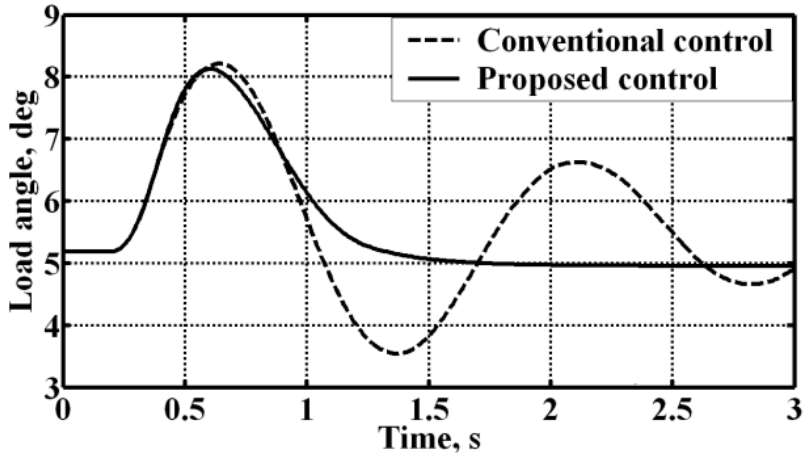

Figure 4.13: **Load angle variation of the generator at P_e =0.1 pu**

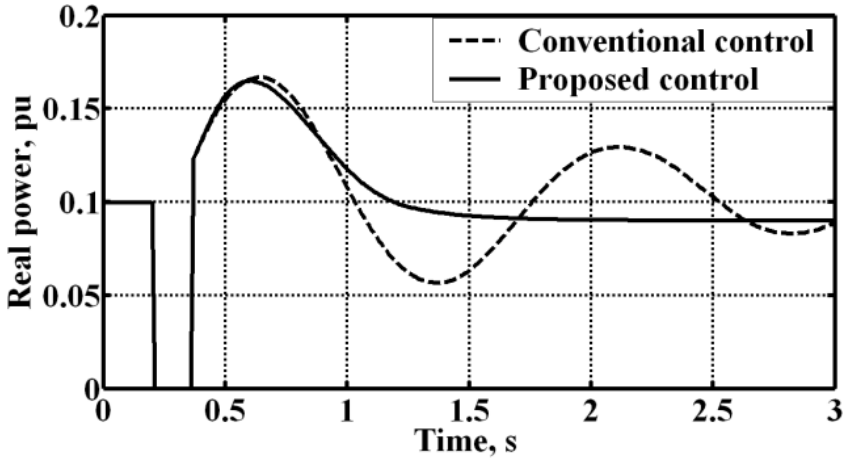

Figure 4.14: **Real power variation of the generator at P_e =0.1 pu**

A third case experimented here is the performance of the proposed controller with two topologies: one by disconnecting the faulted line and the other with original topology.

When we implement the proposed controller, it reveals that there is not much difference between these two topologies. This comparison between the two cases for the generator load angle is shown in Figure 4.15.

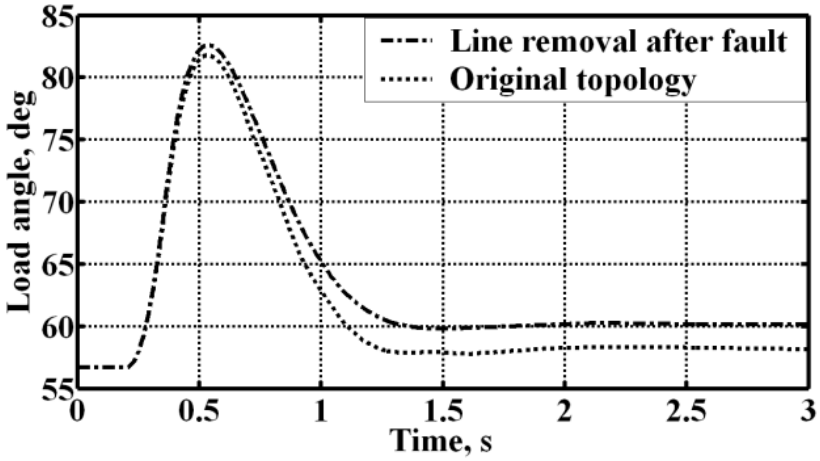

Figure 4.15: **Load angle variation with different topologies at P_e=1.2, Q_e=0.4 pu**

To show the effectiveness of the proposed controller, several studies with different loading conditions and various fault locations were performed and all results show similar trends. However, due to space limitations, only one set of result is given here. Figure 4.16 shows the load angle variation of the generator for a fault at the middle of the transmission line. The fault is cleared after four cycles without changing the original topology. Simulation results show the robustness of our approach.

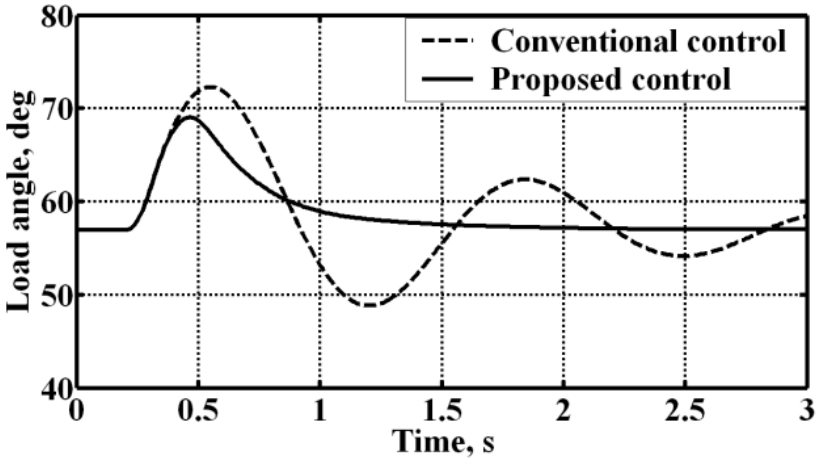

Figure 4.16: **Load angle variation at different fault location with P_e=1.2, Q_e=0.4 pu**

We have considered modulation index of series converter, m_{SR} as the input control signal in the above discussions. The examining of variation of load angle with other control signals m_{SH} and φ_{SH} is also done. The signal φ_{SR} is not considered as the oscillation mode is not controllable with it. The results are shown in Figure 4.17. Analysis of figure shows the correctness of the selection of the input control signal m_{SR} as it provides the smoothest damping to the load angle variation.

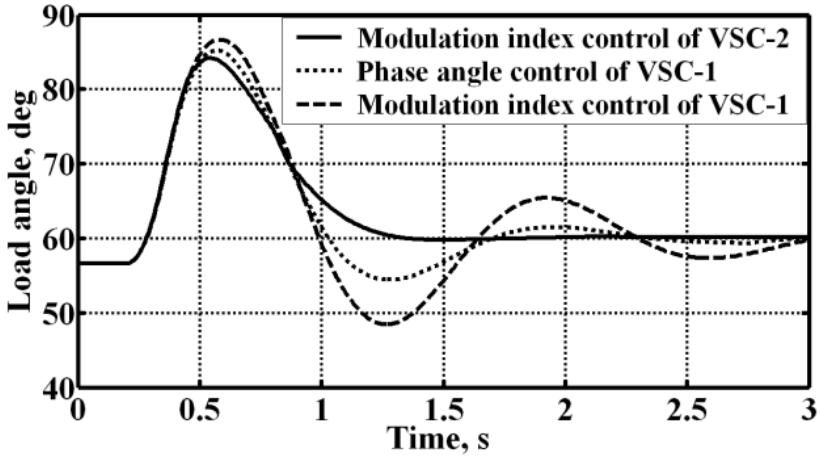

Figure 4.17: **Load angle variation with m_{SR}, φ_{SH}, m_{SH} at P_e=1.2,Q_e=0.4pu**

4.5 Conclusion

The major contributions of this chapter are:

- A new dynamic representation of the power network has been introduced with the identification of the generator as a third order model and UPFC as the stabilizing device.
- The conversion of nonlinear equations into standard parametric feedback form is explained in a simple way.
- After obtaining the standard form, a new recursive method is explained for the design of a nonlinear robust adaptive controller to mitigate generator oscillation.
- An adaptive control law for uncertain parameters is introduced to avoid the deterioration of the controller performance.
- For a given UPFC lower injected real power and voltage can be achieved with the proposed controller. Hence, only a comparatively lower rating UPFC is required.

The effectiveness of the approach can be seen in the simulation results.

Chapter 5

Dynamic Modeling and Nonlinear Control of Multi-Machine Power System with UPFC

Chapter 5

Dynamic Modeling and Nonlinear Control of Multi-Machine Power System with UPFC

5.1 Introduction

In Chapter 4, a single-machine infinite bus model is used to apply nonlinear adaptive control schemes. However, the infinite bus assumption required for this approach is not valid for large multi-machine systems when fault affects the power system. The over parameterization problem that usually appears in the adaptive method will be more predominant with multi-machine power systems.

To overcome the above-mentioned challenges, this chapter attempts a nonlinear control procedure based on back stepping method for stability enhancement of a two-machine power system. A dynamic modeling approach involving only differential equation is due presented. The proposed modeling is a complementary scheme of solving the differential-algebraic equations; for which achieving the control design has always been a challenge. A relevant Lyapunov function is defined in the proposed technique to derive the control signal. The control signal for the UPFC is derived with an aim to mitigate the generator oscillations developing from perturbations. Simulation results on multi-machine power systems illustrate the effectiveness of the suggested method.

5.2 Nonlinear dynamic representation

Power system without UPFC

The system analyzed is shown in Figure 5.1. It has one low frequency inter-area mode. Generators are represented as classical model with internal voltages behind transient reactance assumed constant. This representation is adequate for the control formulation

since only the generator speed variations are of concern. While deriving the equations, resistance of power system components are ignored. Mechanical input power and loads are assumed to be constants. Power system's differential equations are given below:

$$\begin{cases} \dot{\delta}_i = \omega_i - \omega_0 \\ \dot{\omega}_i = \dfrac{1}{M_i}(P_{mi} - B_{i,i+n}E_iV_{i+n}\sin(\delta_i - \phi_{i+n})) \end{cases} \qquad i = 1,..n \tag{5.1}$$

Here n is the number of generators (n = 2). In the above equation V_{i+n} and ϕ_{i+n} are the bus voltage and phase angle, respectively. $B_{i,i+n}$ represents the reactance of the admittance matrix. E_i is the i^{th} machine internal voltage.

The bus voltages and phase angles of all the power system buses are constrained by the following set of algebraic power balance equations

$$\begin{cases} P_{L3} + \sum_{j=1}^{N+n} B_{3j}V_3V_j\sin(\phi_3 - \phi_j) = 0 \\ P_{L4} + \sum_{j=1}^{N+n} B_{4j}V_4V_j\sin(\phi_4 - \phi_j) = 0 \\ -Q_{L3} + \sum_{j=1}^{N+n} B_{3j}V_3V_j\cos(\phi_3 - \phi_j) = 0 \\ -Q_{L4} + \sum_{j=1}^{N+n} B_{4j}V_4V_j\cos(\phi_4 - \phi_j) = 0 \end{cases} \tag{5.2}$$

$V_j = E_j$; $\phi_j = \delta_j$ for $1 \le j \le n$. In addition, N is the number of non-generator buses in the power system.

UPFC power injection model

In the proposed approach UPFC is selected as the FACTS device which behaves as a controller to damp system oscillations. According to the power injection theory, the effect of UPFC is that it injects real and reactive power to the connecting buses. As shown in Figure 5.1, the shunt portion of the UPFC is connected to the bus 3 and series portion is connected between buses 3 and 4.

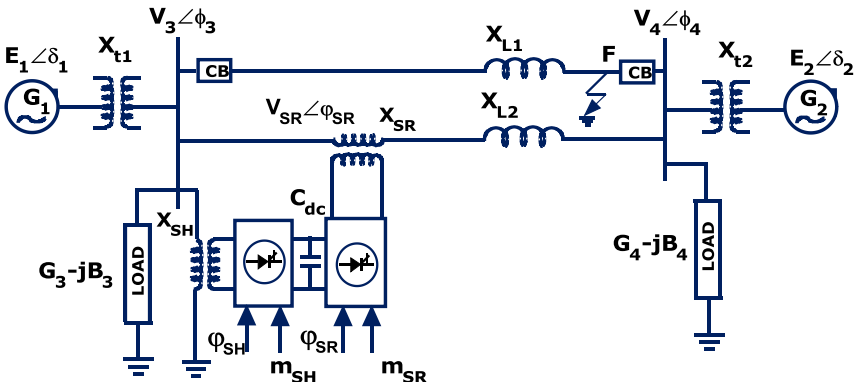

Figure 5.1: **Sample two area power system**

The injected real and reactive powers at buses 3 and 4, as explained in section 2.3.5 (2.46), are given by [67]

$$\begin{cases} P_{3inj} = B_{34}V_{SR}V_4 \sin((\phi_3 + \varphi_{SR}) - \phi_4) \\ P_{4inj} = -B_{34}V_{SR}V_4 \sin((\phi_3 + \varphi_{SR}) - \phi_4) \\ Q_{3inj} = B_{34}V_{SR}V_3 \cos(\varphi_{SR}) \\ Q_{4inj} = -B_{34}V_{SR}V_4 \cos((\phi_3 + \varphi_{SR}) - \phi_4) \end{cases} \tag{5.3}$$

where $V_{SR}\angle(\phi_3 + \varphi_{SR})$ is the output voltage from the series transformer of UPFC. The above equations can be written as

$$\begin{cases} P_{3inj} = B_{34}u_1V_4 \sin(\phi_3 - \phi_4) + B_{34}u_2V_4 \cos(\phi_3 - \phi_4) \\ P_{4inj} = -B_{34}u_1V_4 \sin(\phi_3 - \phi_4) - B_{34}u_2V_4 \cos(\phi_3 - \phi_4) \\ Q_{3inj} = B_{34}u_1V_3 \\ Q_{4inj} = B_{34}u_1V_4 \cos(\phi_3 - \phi_4) - B_{34}u_2V_4 \sin(\phi_3 - \phi_4) \end{cases} \tag{5.4}$$

where $u_1 = V_{SR}\cos(\varphi_{SR})$ and $u_2 = V_{SR}\sin(\varphi_{SR})$ are the control signals to the UPFC.

Power system with UPFC

Power injection model neglects the dynamics of UPFC. Hence, power system's differential equations are same as (5.1). The algebraic power balance equation at buses 3 and 4 are now modified. The new equations including injected powers of UPFC are

$$\begin{cases} P_{L3} + \sum_{j=1}^{N+n} B_{3j} V_3 V_j \sin(\phi_3 - \phi_j) + V_4 B_{34} \{u_1 \sin(\phi_3 - \phi_4) + u_2 \cos(\phi_3 - \phi_4)\} = 0 \\ P_{L4} + \sum_{j=1}^{N+n} B_{4j} V_4 V_j \sin(\phi_4 - \phi_j) - B_{34} V_4 \{u_1 \sin(\phi_3 - \phi_4) + u_2 \cos(\phi_3 - \phi_4)\} = 0 \\ -Q_{L3} + \sum_{j=1}^{N+n} B_{3j} V_3 V_j \cos(\phi_3 - \phi_j) - B_{34} u_1 V_3 = 0 \\ -Q_{L4} + \sum_{j=1}^{N+n} B_{4j} V_4 V_j \cos(\phi_4 - \phi_j) + B_{34} V_4 [u_1 \cos(\phi_3 - \phi_4) - u_2 \sin(\phi_3 - \phi_4)] = 0 \end{cases} \quad (5.5)$$

Dynamic representation

For the given power system, (5.1) and (5.5) form the set of algebraic-differential equations. For the advanced control design, it is desirable to substitute the set of algebraic equations with a more appropriate set of differential equations. We employ network power balance equations to derive the nonlinear dynamical model of the power system. The benefit of this approach is that the same method can be applied to other FACTS devices too. We can achieve this, by taking the derivative of (5.5) as explained by (5.6)

$$\begin{cases} \frac{\partial P_i}{\partial t} = \frac{\partial P_i}{\partial V_3} * \dot{V}_3 + \frac{\partial P_i}{\partial V_4} * \dot{V}_4 + \frac{\partial P_i}{\partial \phi_3} * \dot{\phi}_3 + \frac{\partial P_i}{\partial \phi_4} * \dot{\phi}_4 + \frac{\partial P_i}{\partial \delta_1} * \dot{\delta}_1 + \frac{\partial P_i}{\partial \delta_2} * \dot{\delta}_2 + \frac{\partial P_i}{\partial u_1} * \dot{u}_1 + \frac{\partial P_i}{\partial u_2} * \dot{u}_2 = 0 \\ \frac{\partial Q_i}{\partial t} = \frac{\partial Q_i}{\partial V_3} * \dot{V}_3 + \frac{\partial Q_i}{\partial V_4} * \dot{V}_4 + \frac{\partial Q_i}{\partial \phi_3} * \dot{\phi}_3 + \frac{\partial Q_i}{\partial \phi_4} * \dot{\phi}_4 + \frac{\partial Q_i}{\partial \delta_1} * \dot{\delta}_1 + \frac{\partial Q_i}{\partial \delta_2} * \dot{\delta}_2 + \frac{\partial Q_i}{\partial u_1} * \dot{u}_1 + \frac{\partial Q_i}{\partial u_2} * \dot{u}_2 = 0 \end{cases} \quad (5.6)$$

where i = 3,4; Solving (5.5), we can get the new set of differential equation as

$$\begin{bmatrix} a_{11} & a_{12} & a_{13} & a_{14} \\ a_{21} & a_{22} & a_{23} & a_{24} \\ a_{31} & a_{32} & a_{33} & a_{33} \\ a_{41} & a_{42} & a_{43} & a_{44} \end{bmatrix} \begin{bmatrix} \dot{V}_3 \\ \dot{V}_4 \\ \dot{\phi}_3 \\ \dot{\phi}_4 \end{bmatrix} = - \begin{bmatrix} b_{11} & b_{12} \\ b_{21} & b_{22} \\ b_{31} & b_{32} \\ b_{41} & b_{42} \end{bmatrix} \begin{bmatrix} \dot{\delta}_1 \\ \dot{\delta}_2 \end{bmatrix} - \begin{bmatrix} g_{11} & g_{12} \\ g_{21} & g_{22} \\ g_{31} & g_{32} \\ g_{41} & g_{42} \end{bmatrix} \begin{bmatrix} \dot{u}_1 \\ \dot{u}_2 \end{bmatrix} \quad (5.7a)$$

Parameters $a_{11}.....a_{44}$, $b_{11}.....b_{42}$ and $g_{11}.....g_{42}$ are shown in the Appendix C. In (5.7a) $\dot{u}_1$ as well as $\dot{u}_2$ are the control inputs. Our next aim is to define the control inputs. Once

the control inputs are defined, the UPFC parameters u_1 and u_2 can be obtained by integrating the control inputs. Equation (5.7a) can be written in the simplified form as

$$[A]\left[\dot{x}\right] = -[B][\dot{\delta}] - [G]\left[\dot{u}\right] \tag{5.7b}$$

from this we can get $-[A]^{-1}[B] = [C]$ and $-[A]^{-1}[G] = [K]$ where C and K are 4 × 2 matrices. By defining $r_1 = \dot{u}_1$, $r_2 = \dot{u}_2$ and using equation (5.1) and (5.7) we get the new nonlinear dynamic representation as

$$\begin{cases} \dot{\delta}_i = \omega_i - \omega_0 \\ \dot{\omega}_i = \dfrac{1}{M_i}(P_{mi} - B_{i,i+n}E_{gi}V_{i+n}\sin(\delta_i - \phi_{i+n})) \\ \dot{V}_3 = C_{11}(\omega_1 - \omega_0) + C_{12}(\omega_2 - \omega_0) + K_{11}r_1 + K_{12}r_2 \\ \dot{V}_4 = C_{21}(\omega_1 - \omega_0) + C_{22}(\omega_2 - \omega_0) + K_{21}r_1 + K_{22}r_2 \\ \dot{\phi}_3 = C_{31}(\omega_1 - \omega_0) + C_{32}(\omega_2 - \omega_0) + K_{31}r_1 + K_{32}r_2 \\ \dot{\phi}_4 = C_{41}(\omega_1 - \omega_0) + C_{42}(\omega_2 - \omega_0) + K_{41}r_1 + K_{42}r_2 \\ \dot{u}_1 = r_1 \\ \dot{u}_2 = r_2 \end{cases} \tag{5.8}$$

5.3 Nonlinear control design

In the two-area network, generator-1 is the machine being analyzed in detail. Therefore, a swing equation of generator-1 is important for the electromechanical oscillation damping. Firstly, we introduce the following coordinate transformation

$$\begin{cases} x_1 = \delta_1 - \delta_0 \\ x_2 = \omega_1 - \omega_0 \\ x_3 = V_3\sin(\delta_1 - \phi_3) \end{cases} \tag{5.9}$$

where δ_0 and ω_0 are the pre-fault load angle and speed of generator-1. The choice of x_3 renders the generator dynamic equation (5.1) in back stepping forms as will be explained later. Derivative of x_3 is

$$\dot{x}_3 = \dot{V}_3 \sin(\delta_1 - \phi_3) + V_3 \cos(\delta_1 - \phi_3)(\dot{\delta}_1 - \dot{\phi}_3) \tag{5.10a}$$

Substitute values of $\dot{V}_3$, $\dot{\phi}_3$ and $\dot{\delta}_1$ from equation (5.8). We have

$$\dot{x}_3 = f_{T1} + g_{T1} r_1 + g_{T2} r_2 \tag{5.10b}$$

where $g_{T1} = K_{11} \sin(\delta_1 - \phi_3) - K_{31} V_3 \cos(\delta_1 - \phi_3)$; $g_{T2} = K_{12} \sin(\delta_1 - \phi_3) - K_{32} V_3 \cos(\delta_1 - \phi_3)$

and $f_{T1} = (\omega_1 - \omega_0)\{C_{11} \sin(\delta_1 - \phi_3) + V_3 \cos(\delta_1 - \phi_3)(1 - C_{31})\} +$

$$(\omega_2 - \omega_0)(C_{12} \sin(\delta_1 - \phi_3) - C_{32} V_3 \cos(\delta_1 - \phi_3))$$

Assumption: Constant phase angle control

Control of UPFC injected power is essential for oscillation damping. One way of achieving this is by varying V_{SR} under constant phase angle φ_{SR}. Then for φ_{SR} around ± 90^0, maximum active power is injected for a given V_{SR}. This requires that $u_1 = V_{SR} \cos(\varphi_{SR}) = 0$ and thus $\dot{u}_1 = 0$. With this assumption let us start the design considering $\dot{u}_1 = r_1 = 0$ thereby decreasing the number of inputs required in (5.10b).

By using equations (5.1), (5.9) and (5.10), a new set of state equation can be constructed as

$$\begin{cases} \dot{x}_1 = x_2 \\ \dot{x}_2 = \dfrac{P_{m1}}{M_1} - \dfrac{(B_{13} E_1)}{M_1} x_3 \\ \dot{x}_3 = f_{T1} + (g_{T2}) r_2 \end{cases} \tag{5.11}$$

where $r_2 = \dot{u}_2$ is the control input, P_{m1}/M_1 and $(B_{13}E_1)/M_1$ are constants instead of functions of states. Our next aim is define the control input r_2. This can be achieved by defining an appropriate Lyapunov function. In equation (5.11) the control gain g_{T2} is bounded away from zero. Without loss of generality it will be assumed that $g_{T2} > 0$. The controller design is explained as follows.

Introducing K_δ as design constants, we introduce $z_1 = x_2 + K_\delta x_1$ and $z_2 = (x_3 - x_{3s})$, which results in

$$\dot{x}_1 = x_2 = z_1 - K_\delta x_1 \tag{5.12}$$

Differentiate z_1 we get, $\dot{z}_1 = \dot{x}_2 + K_\delta \dot{x}_1$ now substitute the value of $\dot{x}_1$ and $\dot{x}_2$ from (5.11)

$$\dot{z}_1 = \frac{P_{m1}}{M_1} + K_\delta x_2 - \frac{(B_{13}E_1)z_2}{M_1} - \frac{(B_{13}E_1)}{M_1} x_{3s} \tag{5.13}$$

similarly

$$\dot{z}_2 = f_{T1} + (g_{T2})r_2 - \dot{x}_{3s} \tag{5.14}$$

Now choose a Lyapunov function $L_f = \frac{x_1^2}{2} + \frac{z_1^2}{2} + \frac{z_2^2}{2}$

$$\frac{d}{dt}(L_f) = x_1 \dot{x}_1 + z_1 \dot{z}_1 + z_2 \dot{z}_2 \tag{5.15}$$

Substituting the values $\dot{x}_1$ and $\dot{z}_1$, then by rearranging we get

$$\frac{d}{dt}(L_f) = -K_\delta x_1^2 + z_1[x_1 + \frac{P_{m1}}{M_1} + K_\delta x_2 - \frac{(B_{13}E_1)}{M_1} x_{3s}] + z_2[\dot{z}_2 - \frac{(B_{13}E_1)}{M_1} z_1] \tag{5.16}$$

The system will be asymptotically stable if RHS of the equation (5.16) is negative. This can be achieved by assuming

$$x_{3s} = \frac{M_1}{(B_{13}E_1)}[x_1 + \frac{P_{m1}}{M_1} + K_\delta x_2 + K_T z_1] \tag{5.17}$$

$$\dot{z_2} = \frac{(B_{13}E_1)}{M_1} z_1 - K_S z_2 \tag{5.18}$$

with this the equation (5.16) become

$$\frac{d}{dt}(L_f) = -K_\delta x_1^2 - K_T z_1^2 - K_S z_2^2 < 0$$

We have to select the design constants (K_δ, K_T, K_S) in such a way that the eigen-values of the linear system have negative real parts.

Now by equating (5.14) and (5.18) we have

$$r_2 = \frac{1}{g_{T2}}[\frac{(B_{13}E_1)}{M_1} z_1 - K_s z_2 - f_{T1} + \dot{x_{3s}}] \tag{5.19}$$

By differentiating equation (5.17), and using (5.12), (5.13) and the relation $z_2 = (x_3 - x_{3s})$, we can get

$$\dot{x_{3s}} = \frac{M_1}{(B_{13}E_1)}[x_2(1 + K_\delta K_T) + (\frac{P_{m1}}{M_1} + \frac{(B_{13}E_1)}{M_1} x_3)(K_T + K_\delta)] \tag{5.20}$$

5.4 Results and discussion

For control substantiation, the system in Figure 5.1 is chosen where three phase to ground fault is injected close to bus 4 (as shown by the point F in Figure 5.1) at t = 0.5s. Fault is removed after 4 cycles (0.0667s) without changing the topology. The UPFC placed at bus 3 is activated after fault clearance. The design constants selected are $K_\delta = 0.1$; $K_T = 0.2$ and $K_S = 90$. Simulation results are compared with the Lead-Lag controller explained in Chapter 3. System parameters and initial conditions are same as given in Table 3.2.

Figure 5.2 shows the variation of rotor angle of the generator-1 with respect to generator 2 (δ_{12}). With the proposed controller, the generator load angle increases from an initial value of 14.6^0 (0.255rad) to a maximum value of 19.8^0 (0.345rad) and then returns back to initial value. Here the system gets stabilized within two seconds and thus the proposed controller gains an advantage over the conventional controller where it takes four seconds for the same. Angular speed variation of generator-1 is shown in Figure 5.3.

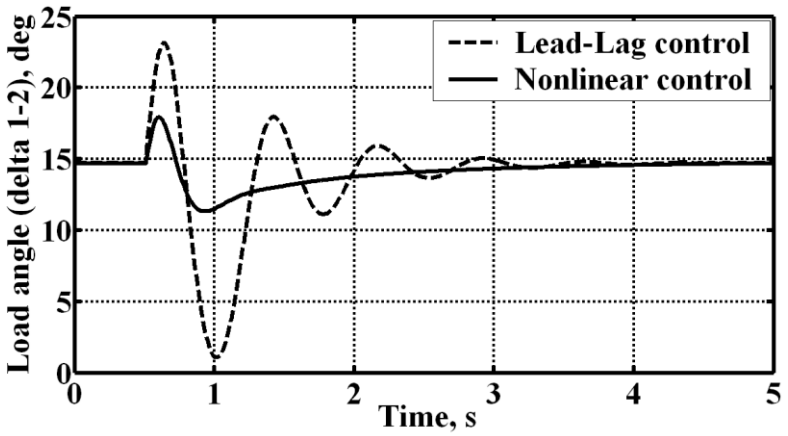

Figure 5.2: **Load angle variation of generator-1 at P_e=0.5, Q_e=0.3pu**

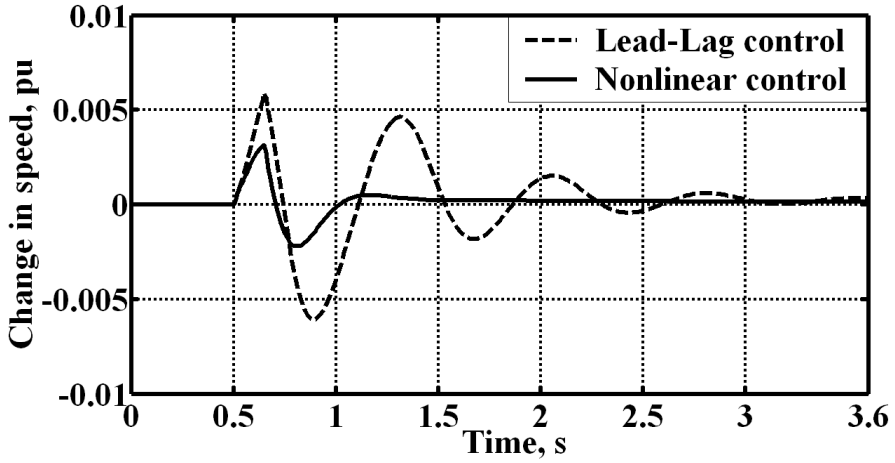

Figure 5.3: **Speed Variation of generator-1 at P_e=0.5, Q_e=0.3pu**

Figure 5.4 shows the active power variation of generator-1 over a time period of 3.6s. The number of major oscillations and settling time has a smaller value in the presence of new controller. The terminal voltage variation of generator is shown in Figure 5.5. On employing the proposed nonlinear control, it is confirmed that there is no unnecessary side effect on the generator terminal voltage.

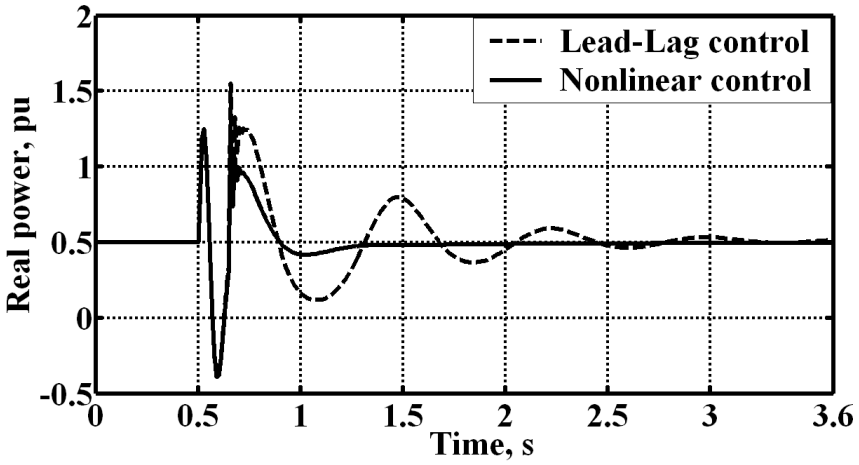

Figure 5.4: **Active power Variation of generator-1 at P_e=0.5, Q_e=0.3pu**

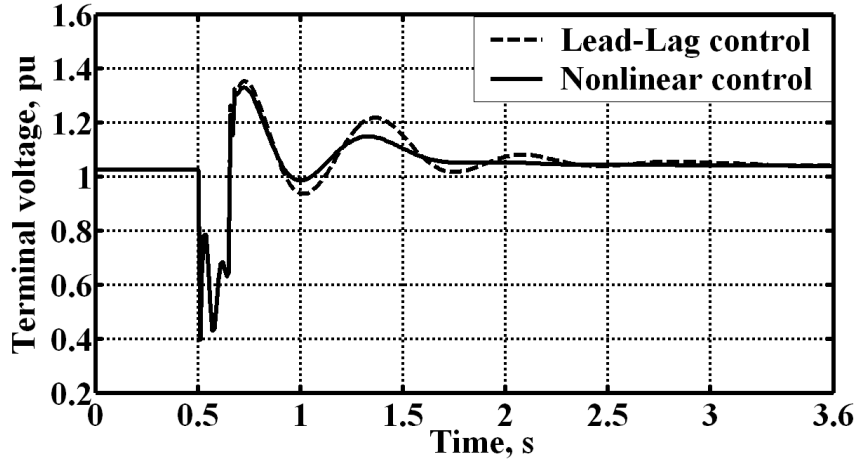

Figure 5.5: **Terminal voltage variation of generator-1 at P_e=0.5, Q_e=0.3pu**

5.5 Conclusion

In this chapter, a nonlinear dynamic representation for a two-area power system with UPFC as stabilizing controller was proposed. The proposed model is free from algebraic equations. This representation is necessary for converting the nonlinear power system equations into standard parametric feedback form. A nonlinear control scheme is proposed for the UPFC which is faster in damping inter-area oscillation. The simulation results support the analytical approach and prove effective of the designed controller.

Chapter 6

Integrated Linear-Nonlinear Control of Multi-Machine Power System with UPFC

Chapter 6

Integrated Linear-Nonlinear Control of Multi-Machine Power System with UPFC

6.1 Introduction

In Chapter 5, the dynamics of UPFC is neglected. The power injection model neglects the dynamics of UPFC. However, when a power system is in its dynamic state, the energy stored in the DC capacitor of a UPFC changes. Hence, the active power absorbed by the shunt part is not equal to the active power converted back to the system by its series part. Therefore, when we describe the dynamics of a power system with a UPFC installed, the dynamics of the DC-link capacitor could not be neglected [60].

Secondly, A UPFC is a multifunctional device. AC voltage control, DC voltage control and damping control are the main functions of the UPFC. In Chapter 5, we explored only one degree of freedom of UPFC, i.e., damping control. The full utilization of the UPFC has not been achieved in Chapter 5.

Motivated by the above observation, a new integrated linear-nonlinear (Hybrid) control procedure for a multi-machine power system is presented in this chapter. AC voltage control and DC voltage control have been achieved using a single multivariable, proportional–integral (PI) controller. This multi-input multi-output controller avoids the negative interaction between AC and DC voltage regulators. The nonlinear control signal for oscillation damping is derived using a relevant Lyapunov function as explained in Chapter 5. Finally, the adaptive law derived in Chapter 4 is used to adapt uncertain parameters of the generator. The block diagram representation of the proposed control scheme is shown in Figure 6.1. It consists of an uncertain parameter estimator and an integrated control signal generation portion. With the control input and adaptive law as shown in section 6.2-D, the system is globally asymptotically stable. In other words, all

the closed-loop signals like system states will be bounded. Simulation results on multi-area power systems illustrate the effectiveness of the suggested method.

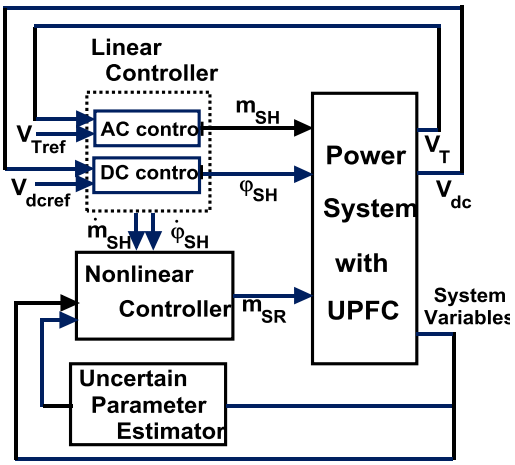

Figure 6.1: **Proposed hybrid controller**

6.2 System under study

The system analyzed is shown in Figure 6.2. Here, the generators are represented by a third-order model [66]. In the proposed approach UPFC behaves as a controller for AC voltage regulation, DC voltage regulation and to damp system oscillations. Mechanical input power and loads are assumed to be constants.

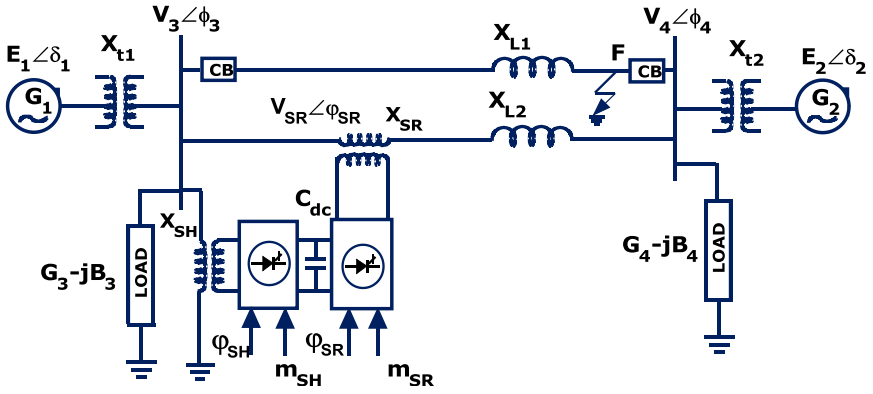

Figure 6.2: **Sample two generator power system**

A. Power system model

Power system's differential equations are given below [1], [66].

$$\begin{cases} \dot{\delta}_i = \omega_i - \omega_0 \\ \dot{\omega}_i = \dfrac{1}{M_i}(P_{mi} - P_{ei} - D_i(\omega_i - \omega_0)/\omega_0) \\ \dot{E}_q^{'} = \dfrac{1}{T_{do}^{'}}[E_{fd} - (X_d - X_d^{'})I_d - E_q^{'}] \end{cases} \qquad i = 1,..n \tag{6.1}$$

Here n is the number of generators. In the above equation $P_{ei} = B_{i,i+n}E_iV_{i+n}\sin(\delta_i - \phi_{i+n})$, where V_{i+n} and ϕ_{i+n} are the bus voltage and phase angle, respectively. B_{ij} represents the reactance of the admittance matrix. E_i is the i^{th} machine internal voltage.

The dynamic model of UPFC is [60]

$$C_{dc}V_{dc}\frac{dV_{dc}}{dt} = (P_{Shunt} - P_{Series}) \tag{6.2}$$

$$P_{Shunt} = Re(\bar{V}_{\mathbf{SH}}(\frac{\bar{V}_{\mathbf{3}} - \bar{V}_{\mathbf{SH}}}{jX_{SH}})^*); \qquad P_{Series} = Re(\bar{V}_{\mathbf{SR}}(\frac{\bar{V}_{\mathbf{3}} + \bar{V}_{\mathbf{SR}} - \bar{V}_{\mathbf{4}}}{j(X_{SR} + X_{L2})})^*)$$

where $\bar{V}_{\mathbf{SH}} = V_{SH}\angle\varphi_{SH}$ and $\bar{V}_{\mathbf{SR}} = V_{SR}\angle\varphi_{SR}$ are the output voltage from the shunt and series transformer of UPFC respectively. $V_{SH} = m_{SH}V_{dc}/2$; $V_{SR} = m_{SR}V_{dc}/2$. In this V_{dc} is the voltage across the DC- link capacitor, m_{SH}, m_{SR} and φ_{SH}, φ_{SR} are the amplitude modulation ratios and phase angles of the control signal of each VSC, respectively, which are the input control signals to the UPFC. From (6.2) we can derive that

$$\dot{V}_{dc} = \frac{1}{C_{dc}V_{dc}}\{B_{SH}V_3V_{SH}\sin(\phi_3 - \varphi_{SH}) + B_{SR}V_{SR}[V_4\sin(\phi_4 - \varphi_{SR}) - V_3\sin(\phi_3 - \varphi_{SR})]\} \tag{6.3}$$

The bus voltages and phase angles of all the power system buses are constrained by the following set of algebraic power balance equations:

$$\begin{cases} P_{L3}+\sum_{j=1}^{N+n} B_{3j}V_3V_j\sin(\phi_3-\phi_j)+B_{SH}V_3V_{SH}\sin(\phi_3-\varphi_{SH})-B_{SR}V_3V_{SR}\sin(\phi_3-\varphi_{SR})=0 \\ P_{L4}+\sum_{j=1}^{N+n} B_{4j}V_4V_j\sin(\phi_4-\phi_j)+B_{SR}V_4V_{SR}\sin(\phi_4-\varphi_{SR})=0 \\ -Q_{L3}+\sum_{j=1}^{N+n} B_{3j}V_3V_j\cos(\phi_3-\phi_j)+B_{SH}V_3V_{SH}\cos(\phi_3-\varphi_{SH})-B_{SR}V_3V_{SR}\cos(\phi_3-\varphi_{SR})=0 \\ -Q_{L4}+\sum_{j=1}^{N+n} B_{4j}V_4V_j\cos(\phi_4-\phi_j)-B_{SR}V_4V_{SR}\cos(\phi_4-\varphi_{SR})=0 \end{cases} \tag{6.4}$$

where P_{Li} and Q_{Li} are the active and reactive loads on the i^{th} bus and $V_j=E_j$; $\phi_j=\delta_j$ for $1\le j\le n$. In addition, N is the number of non-generator buses in the power system. $B_{SH}=1/jX_{SH}$; $B_{SR}=1/j(X_{SR}+X_{L2})$.

B. Nonlinear dynamic model

For the given power system, (6.1)-(6.4) form the set of algebraic-differential equations. Algebraic equations can be replaced by a set of differential equations as explained in section 5.2 by taking derivative of power balance equation.

$$\begin{cases} \frac{\partial P_i}{\partial t}=\frac{\partial P_i}{\partial V}*\dot{V}+\frac{\partial P_i}{\partial \phi}*\dot{\phi}+\frac{\partial P_i}{\partial \delta}*\dot{\delta}+\frac{\partial P_i}{\partial V_{dc}}*\dot{V}_{dc}+\frac{\partial P_i}{\partial m}*\dot{m}+\frac{\partial P_i}{\partial \varphi}*\dot{\varphi}=0 \\ \frac{\partial Q_i}{\partial t}=\frac{\partial Q_i}{\partial V}*\dot{V}+\frac{\partial Q_i}{\partial \phi}*\dot{\phi}+\frac{\partial Q_i}{\partial \delta}*\dot{\delta}+\frac{\partial Q_i}{\partial V_{dc}}*\dot{V}_{dc}+\frac{\partial Q_i}{\partial m}*\dot{m}+\frac{\partial Q_i}{\partial \varphi}*\dot{\varphi}=0 \end{cases} \tag{6.5}$$

where $i=n+1,...,n+N$; Differentiating (6.4) as explained by (6.5) we can get the new set of differential equation as

$$\begin{bmatrix} a_{11} & a_{12} & a_{13} & a_{14} \\ a_{21} & a_{22} & a_{23} & a_{24} \\ a_{31} & a_{32} & a_{33} & a_{33} \\ a_{41} & a_{42} & a_{43} & a_{44} \end{bmatrix} \begin{bmatrix} \dot{V}_3 \\ \dot{V}_4 \\ \dot{\phi}_3 \\ \dot{\phi}_4 \end{bmatrix} = -\begin{bmatrix} b_{11} & b_{12} & b_{13} \\ b_{21} & b_{22} & b_{23} \\ b_{31} & b_{32} & b_{33} \\ b_{41} & b_{42} & b_{43} \end{bmatrix} \begin{bmatrix} \dot{\delta}_1 \\ \dot{\delta}_2 \\ \dot{U}_{dc} \end{bmatrix} - \begin{bmatrix} g_{11} & g_{12} & g_{13} & g_{14} \\ g_{21} & g_{22} & g_{23} & g_{24} \\ g_{31} & g_{32} & g_{33} & g_{34} \\ g_{41} & g_{42} & g_{43} & g_{44} \end{bmatrix} \begin{bmatrix} \dot{m}_{SH} \\ \dot{\varphi}_{SH} \\ \dot{m}_{SR} \\ \dot{\varphi}_{SR} \end{bmatrix} \tag{6.6a}$$

Parameters $a_{11}.....a_{44}$, $b_{11}.....b_{43}$ and $g_{11}.....g_{44}$ are shown in the Appendix D. In (6.6a) $\dot{m}_{SH}$, $\dot{m}_{SR}$, $\dot{\varphi}_{SH}$ as well as $\dot{\varphi}_{SR}$ are the control inputs. Our aim is to define the control inputs. Once the control inputs are defined, the UPFC parameters m_{SH}, m_{SR}, φ_{SH} and φ_{SR} can be obtained by integrating the control inputs. Equation (6.6a) can be written in the simplified form as

$$[A]\left[\dot{x}\right] = -[B][\dot{\delta}] - [G]\left[\dot{u}\right] \tag{6.6b}$$

from this we can get $-[A]^{-1}[B] = [C]$ and $-[A]^{-1}[G] = [K]$ where $C \in R^{4\times 3}$; $K \in R^{4\times 4}$. By defining $r_1 = \dot{m}_{SH}$, $r_2 = \dot{\varphi}_{SH}$, $r_3 = \dot{m}_{SR}$ and $r_4 = \dot{\varphi}_{SR}$; and using equation (6.1), (6.3) and (6.6) we get the new nonlinear dynamic representation as shown in (6.7):

$$\begin{cases}
\dot{\delta}_i = \omega_i - \omega_0 \\
\dot{\omega}_i = \dfrac{1}{M_i}(P_{mi} - P_{ei} - D_i(\omega_i - \omega_0)/\omega_0) \\
\dot{E}_q^{'} = \dfrac{1}{T_{do}^{'}}[E_{fd} - (X_d - X_d^{'})I_d - E_q^{'}] \\
\dot{V}_{dc} = (P_{Shunt} - P_{Series})/C_{dc}V_{dc} \\
\dot{V}_3 = C_{11}\dot{\delta}_1 + C_{12}\dot{\delta}_2 + C_{13}\dot{V}_{dc} + K_{11}r_1 + K_{12}r_2 + K_{13}r_3 + K_{14}r_4 \\
\dot{V}_4 = C_{21}\dot{\delta}_1 + C_{22}\dot{\delta}_2 + C_{23}\dot{V}_{dc} + K_{21}r_1 + K_{22}r_2 + K_{23}r_3 + K_{24}r_4 \\
\dot{\phi}_3 = C_{31}\dot{\delta}_1 + C_{32}\dot{\delta}_2 + C_{33}\dot{V}_{dc} + K_{31}r_1 + K_{32}r_2 + K_{33}r_3 + K_{34}r_4 \\
\dot{\phi}_4 = C_{41}\dot{\delta}_1 + C_{42}\dot{\delta}_2 + C_{43}\dot{V}_{dc} + K_{41}r_1 + K_{42}r_2 + K_{43}r_3 + K_{44}r_4 \\
\dot{m}_{SH} = r_1 \\
\dot{\varphi}_{SH} = r_2 \\
\dot{m}_{SR} = r_3 \\
\dot{\varphi}_{SR} = r_4
\end{cases} \tag{6.7}$$

C. Problem formulation

In the two-area network, generator-1 is the machine being analyzed in detail, where as generator-2 is the machine away from the point of interest. Swing equations of generator-1 are adequate for the control formulation since only the generator speed variations are of concern. Let us start with the following coordinate transformation

$$[\delta_1 - \delta_0,\ \ \omega_1 - \omega_0,\ \ \ V_3 \sin(\delta_1 - \phi_3)] \tag{6.8}$$

where δ_0 and ω_0 are the pre fault load angle and speed of generator-1. The choice of x_3 renders the generator dynamic equation (6.1) in back stepping forms as explained in Chapter 5. Derivative of x_3 is

$$\dot{x}_3 = \dot{V}_3 \sin(\delta_1 - \phi_3) + V_3 \cos(\delta_1 - \phi_3)(\dot{\delta}_1 - \dot{\phi}_3) \tag{6.9}$$

Substitute values of $\dot{V}_3$, $\dot{\phi}_3$ and $\dot{\delta}_1$ from (6.7). We have

$$\dot{x}_3 = f_{T1} + L_1 r_1 + L_2 r_2 + L_3 r_3 + L_4 r_4 \tag{6.10}$$

where

$$L_1 = K_{11} \sin(\delta_1 - \phi_3) + K_{31} V_3 \cos(\delta_1 - \phi_3);\ \ L_2 = K_{12} \sin(\delta_1 - \phi_3) + K_{32} V_3 \cos(\delta_1 - \phi_3)$$

$$L_3 = K_{13} \sin(\delta_1 - \phi_3) + K_{33} V_3 \cos(\delta_1 - \phi_3);\ \ L_4 = K_{14} \sin(\delta_1 - \phi_3) + K_{34} V_3 \cos(\delta_1 - \phi_3)$$

By using equations (6.1), (6.7) and (6.9) a new set of state equation can be constructed as

$$\begin{cases} \dot{x}_1 = x_2 \\ \dot{x}_2 = \dfrac{P_{m1}}{M_1} - \dfrac{(B_{13} E_1)}{M_1} x_3 - \left(\dfrac{D_1}{M_1 \omega_0}\right) x_2 \\ \dot{x}_3 = f_{T1} + L_1 r_1 + L_2 r_2 + L_3 r_3 + L_4 r_4 \end{cases} \tag{6.11}$$

The above equation can be written as

$$\dot{x} = F(x, u) \tag{6.12}$$

D. Controller design

In (6.12), there are four control variables. These variables are r_1, r_2, r_3 and r_4. It is discussed in detail in the subsequent sections.

Control strategy for variables r_1 and r_2 of the shunt part of UPFC

The shunt part converter of a UPFC is able to provide reactive power compensation for the transmission system so as to regulate the voltage magnitude V_3 of node 3 (see Figure 6.2). In order to keep V_3 basically constant in the dynamic process, m_{SH} may be controlled by the strategy of proportional and integral (PI) control to regulate the voltage deviation of V_3 from its expected reference value V_{3ref}. As a result, the control law for the amplitude modulation index m_{SH} of shunt VSC can be logically given as

$$m_{SH} = (K_{P1} + \frac{K_{I1}}{s})(V_{3ref} - V_3) \tag{6.13}$$

The shunt part of a UPFC supplies active power to the DC-link capacitor C_{dc} to meet the demand of the series part. It is known that the direction of the exchange active power flow (P_{Shunt}) between shunt VSC and the AC power system can be changed by means of regulating the variable φ_{SH} , so as to control the active power getting into or out of the DC capacitor. In order to keep the DC capacitor voltage constant during the dynamic process, it is reasonable to adopt a conventional PI controller to regulate the dynamics of V_{dc} relative to its reference value V_{dcref} . That is, the control law for the variable φ_{SH} of the shunt part converter of a UPFC is in the form

$$\varphi_{SH} = (K_{P2} + \frac{K_{I2}}{s})(V_{dcref} - V_{dc}) \tag{6.14}$$

To avoid negative interactions among these controllers a multivariable controller is designed where the multivariable PI control law is

$$\begin{bmatrix} m_{SH} \\ \varphi_{SH} \end{bmatrix} = [C_P] \begin{bmatrix} V_{3ref} - V_3 \\ V_{dcref} - V_{dc} \end{bmatrix} + \begin{bmatrix} \frac{C_I}{s} \end{bmatrix} \begin{bmatrix} V_{3ref} - V_3 \\ V_{dcref} - V_{dc} \end{bmatrix} \tag{6.15}$$

where C_P, $C_I \in R^{2\times 2}$. The parameters of the multivariable PI controller are derived using the genetic algorithm explained in [65]. The parameters obtained are

$$C_P = \begin{bmatrix} 9.4 & 0.004 \\ 1.8 & 0.9 \end{bmatrix}; \quad C_I = \begin{bmatrix} 8.75 & 0.008 \\ 2.1 & 2.0 \end{bmatrix}$$

We can even develop multivariable PID controller. The details are given below. Since PID controller increases the noise level in practical application, most of the power system researchers are using PI controller. Even though there is a little improvement in the simulation results with PID, results with PI controller are shown in this thesis.

$$m_{SH} = (K_{P1} + \frac{K_{I1}}{s} + sK_{D1})(V_{3ref} - V_3) \qquad \varphi_{SH} = (K_{P2} + \frac{K_{I2}}{s} + sK_{D2})(V_{dcref} - V_{dc})$$

$$\begin{bmatrix} m_{SH} \\ \varphi_{SH} \end{bmatrix} = [C_P] \begin{bmatrix} V_{3ref} - V_3 \\ V_{dcref} - V_{dc} \end{bmatrix} + \begin{bmatrix} \frac{C_I}{s} \end{bmatrix} \begin{bmatrix} V_{3ref} - V_3 \\ V_{dcref} - V_{dc} \end{bmatrix} + [sC_D] \begin{bmatrix} V_{3ref} - V_3 \\ V_{dcref} - V_{dc} \end{bmatrix}$$

$$C_P = \begin{bmatrix} 7.4 & 0.39 \\ 0.35 & 4.9 \end{bmatrix}; \; C_I = \begin{bmatrix} 6.35 & 0.05 \\ 0.1 & 2.9 \end{bmatrix}; \; C_D = \begin{bmatrix} 5.75 & 0.15 \\ 0.1 & 6.09 \end{bmatrix}$$

Control strategy for variables r_3 and r_4 of the series part of UPFC

As shown in Figure 6.2, the series part of a UPFC generates an AC voltage source, whose magnitude and phase angles are restricted in the following set

$$S = \{(V_{SR}, \varphi_{SR}) \in R^2 | 0 \le V_{SR} \le V_{SR\max}, 0 \le \varphi_{SR} \le 2\pi\}$$

Control of UPFC injected power is essential for oscillation damping. One way of achieving this is by varying V_{SR} under constant phase angle φ_{SR}. This requires that

$$\dot{\varphi}_{SR} = r_4 = 0$$

With this assumption let us start the nonlinear control design by rewriting (6.11) as

$$\begin{cases} \dot{x}_1 = x_2 \\ \dot{x}_2 = \dfrac{P_{m1}}{M_1} - \dfrac{(B_{13}E_1)}{M_1} x_3 + \psi_2 x_2 \\ \dot{x}_3 = f_T + L_3 x_4 \end{cases} \tag{6.16}$$

where $f_T = (f_{T1} + L_1 r_1 + L_2 r_2)$ and $x_4 = r_3$ is the virtual control input, $\psi_2 = -D_1/(M_1\omega_0)$ is considered as an uncertain parameter, P_{m1}/M_1 and $(B_{13}E_1)/M_1$ are constants instead of functions of states. by assigning $f_1(x_1) = 0$; $\eta_1(x_1) = 1$; $\mu_1(x_1) = 0$; $\psi_1 = 0$; $f_2(x_1, x_2) = P_{m1}/M_1$; $\eta_2(x_1, x_2) = -(B_{13}E_1)/M_1$; $\mu_2(x_1, x_2) = x_2$; $\psi_2 = -D_1/(M_1\omega_0)$; $f_3(x_1, x_2, x_3) = f_T$; $\eta_3(x_1, x_2, x_3) = L_3$; $x_4 = r_3$; $\mu_3(x_1, x_2, x_3) = 0$; $\psi_3 = 0$

equation (6.16) can be transformed into standard parametric feedback form as shown

$$\dot{x}_i = f_i(x_1, .., x_i) + \eta_i(x_1, .., x_i) x_{i+1} + \mu_i^T(x_1, .., x_i)\psi_i \qquad (1 \le i \le n) \tag{6.17}$$

Here n represents the order of the system which equals to three for our case; and $x_{n+1} = r_3$. It can be inferred that f_i, η_i and μ_i are all smooth functions. Now the objective of our suggested controller is to design the control input r_3. Equation (6.16) thus becomes a special case of strict feedback form where back stepping can be used for the controller design.

A power system with a UPFC is a typical nonlinear system. Thus in order to achieve better control effectiveness, the control law for modulation index m_{SR} should be designed by adopting a nonlinear control approach. This can be achieved by defining an appropriate Lyapunov function. In equation (6.16) the control gain L_3 is bounded away from zero. Without loss of generality it will be assumed that $L_3 > 0$. Now using the same control technique explained in Chapter 5 section 3, the control signal can be derived.

Introducing K_δ as design constant, we write $z_1 = x_2 + K_\delta x_1$ which results in

$$\dot{x}_1 = z_1 - K_\delta x_1 \tag{6.18}$$

Differentiate z_1 we get, $\dot{z}_1 = \dot{x}_2 + K_\delta \dot{x}_1$ now substitute the value of $\dot{x}_2$ from (6.16)

$$\dot{z}_1 = \frac{P_{m1}}{M_1} + (K_\delta + \psi_2)x_2 - \frac{K_1}{M_1}x_3 \tag{6.19}$$

where $K_1 = B_{13}E_1$

by defining $z_2 = (x_3 - x_{3s})$, we have

$$\dot{z}_1 = \frac{P_{m1}}{M_1} + (K_\delta + \psi_2)x_2 - \frac{K_1}{M_1}(z_2 + x_{3s}) \tag{6.20}$$

similarly

$$\dot{z}_2 = f_T + L_3 r_3 - \dot{x}_{3s} \tag{6.21}$$

Now choose a Lyapunov function $L_f = \frac{x_1^2}{2} + \frac{z_1^2}{2} + \frac{z_2^2}{2}$

$$\frac{d}{dt}(L_f) = x_1\dot{x}_1 + z_1\dot{z}_1 + z_2\dot{z}_2 \tag{6.22}$$

$$\frac{d}{dt}(L_f) = -K_\delta x_1^2 + z_1[x_1 + \frac{P_{m1}}{M_1} + (K_\delta + \psi_2)x_2 - \frac{K_1}{M_1}x_{3s}] + z_2[\dot{z}_2 - \frac{K_1}{M_1}z_1] \tag{6.23}$$

The system will be asymptotically stable if RHS of the equation (6.23) is negative. This can be achieved by assuming

$$x_{3s} = \frac{M_1}{K_1}[x_1 + \frac{P_{m1}}{M_1} + (K_\delta + \psi_2)x_2 + K_T z_1] \tag{6.24}$$

$$\dot{z}_2 = \frac{K_1}{M_1}z_1 - K_S z_2 \tag{6.25}$$

with this the equation (6.23) become

$$\frac{d}{dt}(L_f) = -K_\delta x_1^2 - K_T z_1^2 - K_S z_2^2 < 0$$

We have to select the design constants (K_δ, K_T, K_S) in such a way that the eigen-values of the linear system have negative real parts.

Now by equating (6.21) and (6.25) we have

$$r_3 = \frac{1}{L_3}[\frac{K_1}{M_1} z_1 - K_s z_2 - f_T + \dot{x}_{3s}] \tag{6.26}$$

By differentiating equation (6.24) and using (6.16), (6.19) and the relation $z_2 = (x_3 - x_{3s})$, we can get

$$\dot{x}_{3s} = \frac{M_1}{K_1}\left\{ x_2 \left[1 + (K_\delta + \psi_2)(\psi_2 + K_T)\right] + \left(\frac{P_{m1}}{M_1} - \frac{K_1}{M_1} x_3 \right)(K_T + K_\delta + \psi_2) \right\} \tag{6.27}$$

To sum up, we have completed the hybrid controller design for a UPFC. The hybrid control strategy is proposed in combination with equations (6.15) and (6.26).

Adaptive law for uncertain parameter

Since the damping coefficient D_i is hard to be exactly measured, it is considered as uncertain parameter. Initial value of this uncertain parameter is considered as zero. This step is needed only to improve the efficiency of the controller. The adaptive law derived in Chapter 4 section 3 can be used here. The adaptive law for uncertain parameter is given by (4.25) and error dynamics is given by (4.26)

$$\dot{\hat{\psi}}_i = -\sum_{k=1}^{i} \frac{\partial \beta_i}{\partial x_k}[\, f_k(x_1,..,x_k) + \eta_k(x_1,..,x_k) x_{k+1} + \mu_i^T(x_1,..,x_k)(\hat{\psi}_i + \beta_i(x_1,...,x_i))] - \frac{\partial \mu_i}{\partial t} x_i \tag{6.28}$$

$$\dot{\varepsilon}_i = -\sum_{k=1}^{i} \frac{\partial \beta_i}{\partial x_k} \mu_k^T(x_1,..,x_k)\varepsilon_k \tag{6.29}$$

In each iteration, the estimator generates an error variable and a new estimate for the unknown parameter. The accuracy of the estimator is reduced considerably during faults

but improved quickly after fault clearance. The reduction in the accuracy is because of the complexity of the tracking task. The other reason is the selection of initial condition. The initial value of the unknown parameter is chosen to be zero, indicating no prior parameter knowledge. The accuracy of the estimator also depends on the value of adaption gain selected. For better accuracy, we need to choose adaption gain as small as possible, but a very small value of adaption gain will induce chattering in the presence of time delays.

6.3 Results and discussion

The block diagram representation of the proposed controller is shown in Figure 6.1. Together with hybrid control design for UPFC and adaptive law for uncertain parameter the system (6.17) is globally asymptotic stable and all the closed-loop signals like the system states and estimation errors (ε_i) will be bounded.

A. Dynamic performance of two-generator power system with proposed control

The nonlinear simulation to check the performance of the controllers is done on a two-area power system as shown in Figure 6.2. System parameters and initial conditions are same as given in Table 3.2. The design constants selected are $K_\delta = 0.1$, $K_T = 0.2$ and $K_S = 90$. In Figure 6.3, the reference AC voltage, V_{3ref}, is changed at 0.5s of the simulation from 1.018 to 1.0 pu. From Figure 6.3, it can be seen that performance of the AC voltage regulation is satisfactory. Corresponding load angle variation is shown in Figure 6.4.

The control performance of the DC voltage controller is shown in Figure 6.5. In the simulation the reference DC voltage, V_{dcref}, is changed at 0.5s of the simulation from 1.0 to 1.125 p. u. Load angle variation during the time of DC voltage change is shown in Figure 6.6. Performance of the DC voltage regulation is satisfactory.

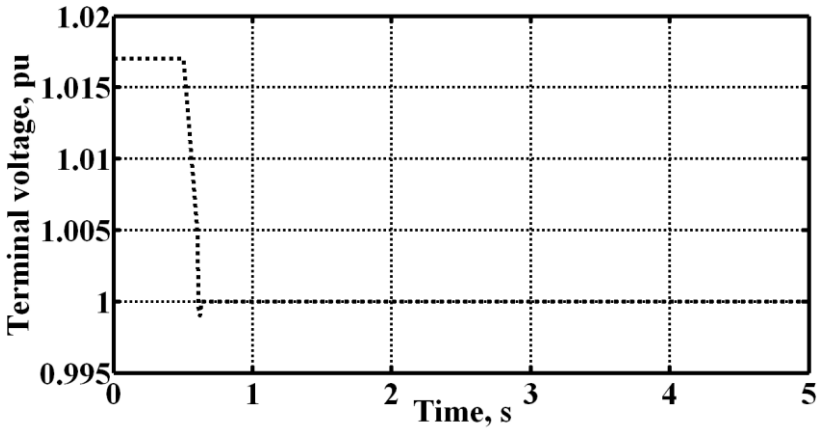

Figure 6.3: V**oltage (V_3) variation with PI AC voltage regulator at P_e=0.5, Q_e=0.3pu**

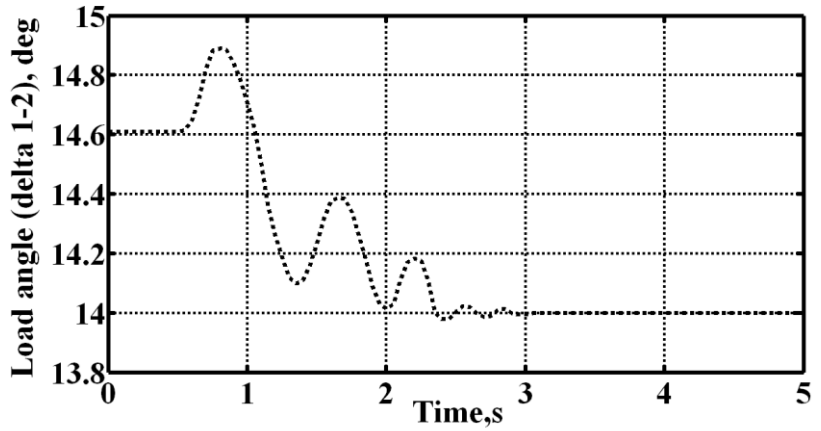

Figure 6.4: **Load angle variation during AC voltage regulation at P_e=0.5, Q_e=0.3pu**

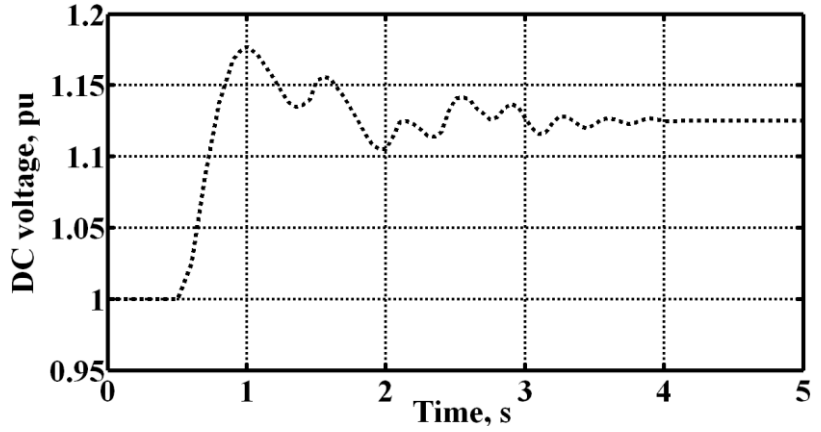

Figure 6.5: **DC voltage variation using PI DC voltage controller at P_e=0.5, Q_e=0.3pu**

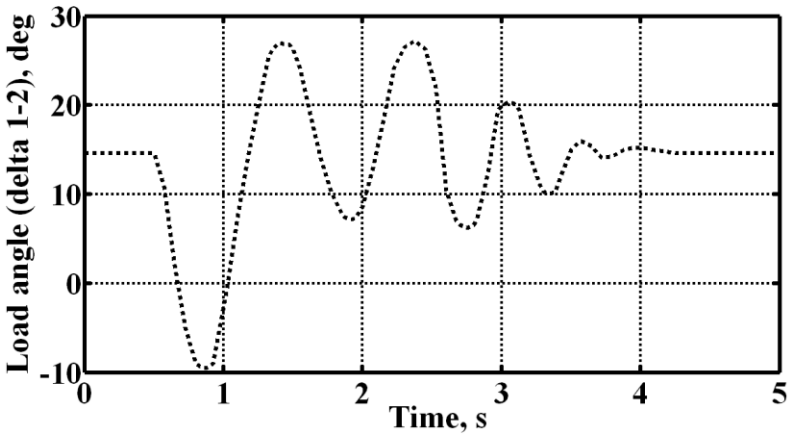

Figure 6.6: **Load angle variation during DC voltage regulation at P_e=0.5, Q_e=0.3pu**

Further, performance of the damping controller is analyzed. A three phase to ground fault occurs on point F. The fault cleared after 0.15s by opening of the faulted line. The UPFC placed at bus 3 is activated after fault clearance. Figure 6.7 shows the load angle variation between the two machines (δ_{12}). Figure 6.8 - Figure 6.11 show the changes in the angular speed, real power, terminal voltage (V_3) and uncertain parameter of the generator-1, respectively. The results are compared against the traditional Lead-Lag controller derived in Chapter 3. The eigen value for the inter-area mode is improved from -1.103 ± j 7.67 (Lead-Lag control) to -1.58 ± j 7.32 with the proposed hybrid controller.

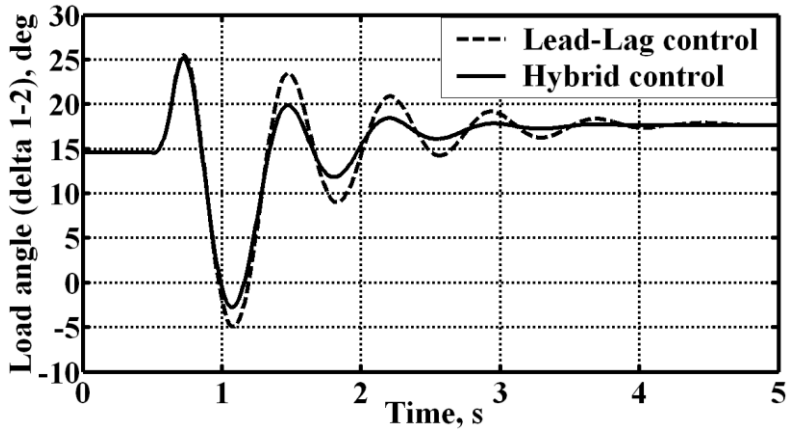

Figure 6.7: **Load angle variation with damping controller at P_e=0.5, Q_e=0.3pu**

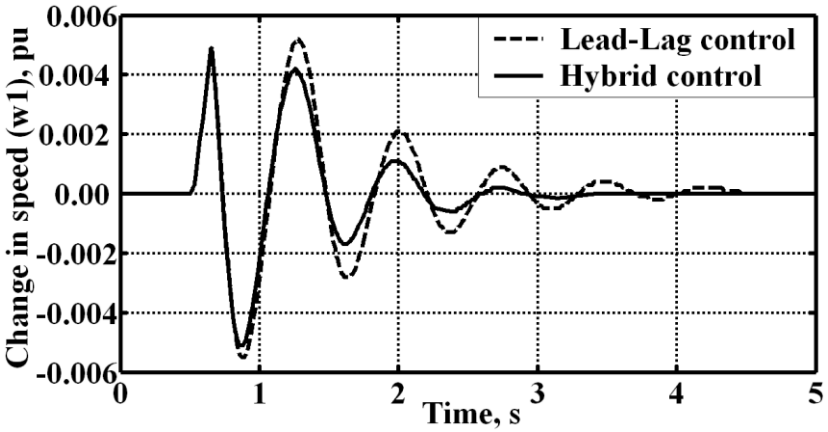

Figure 6.8: **Speed variation with damping controller at P_e=0.5, Q_e=0.3pu**

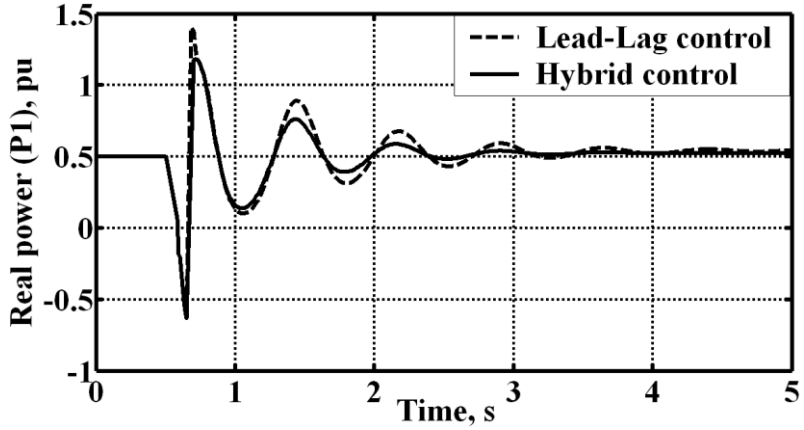

Figure 6.9: **Real power variation with damping controller at P_e=0.5, Q_e=0.3pu**

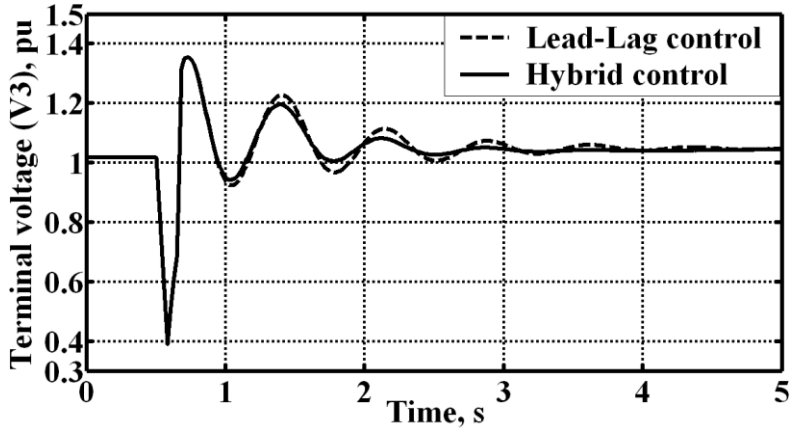

Figure 6.10: V**oltage (V_3) variation with damping controller at P_e=0.5, Q_e=0.3pu**

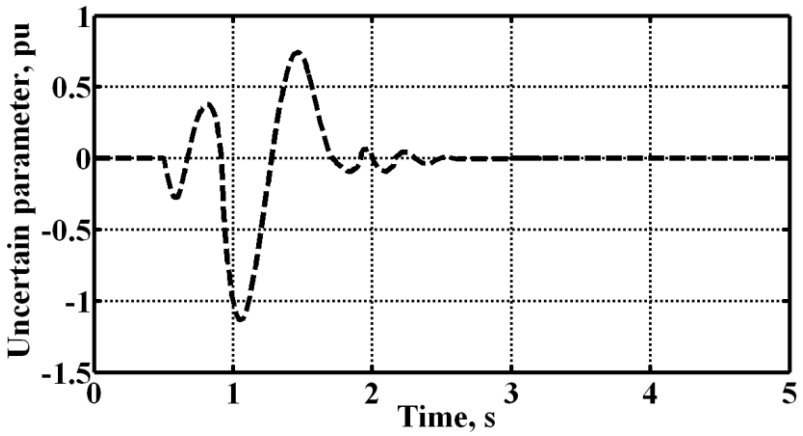

Figure 6.11: **Uncertain parameter (ψ_2) variation** at **P_e=0.5, Q_e=0.3pu**

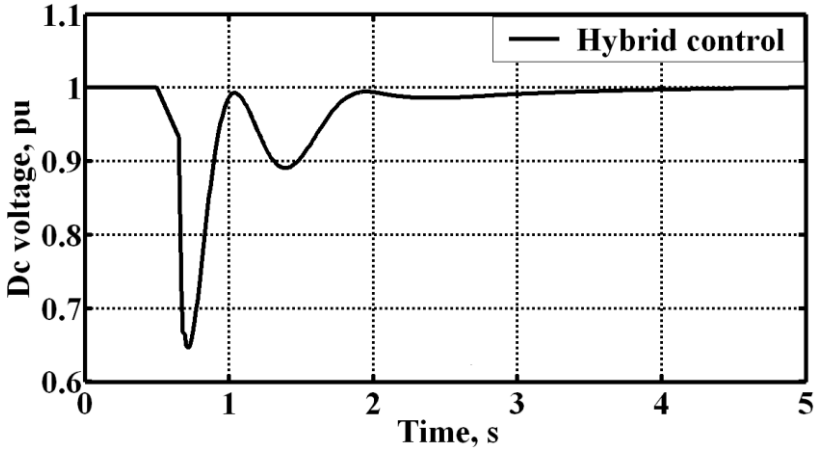

Figure 6.12: **DC voltage variation with damping controller at P_e=0.5, Q_e=0.3pu**

The above figures show that the stability of the system is improved considerably. Control performance for the damping controller, DC voltage regulator and AC voltage regulator are satisfactory with the three UPFC controllers installed and being in joint operation.

The designed controller with same parameters is now subjected to new operating conditions that show the proposed controller is independent of any particular operating

point. Angular speed variation of the generator-1 at P_e = 1.2 pu, P_e = 1.0 pu, P_e = 0.8 pu, P_e = 0.5 pu and P_e = 0.2 pu are shown in Figure 6.14 - Figure 6.17, respectively.

The hybrid controller shows robust dynamic performance under wide variations in loading condition, and provides a significant improvement in dynamic performance in terms of peak deviations.

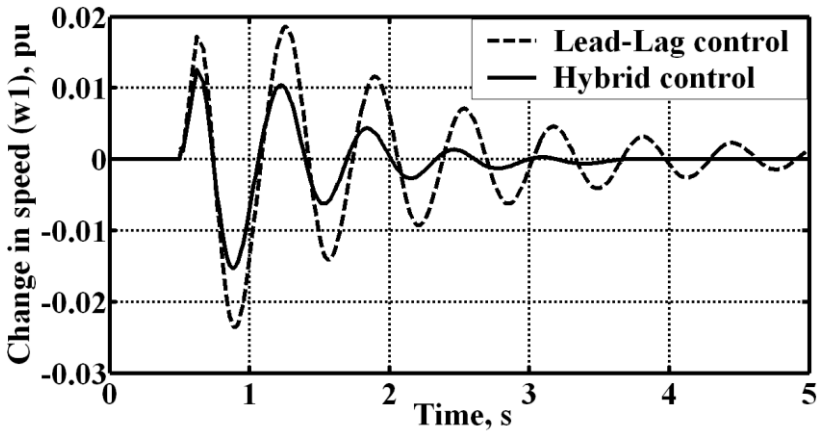

Figure 6.13: **Speed variation with damping controller at P_e = 1.2, Q_e=0.3pu**

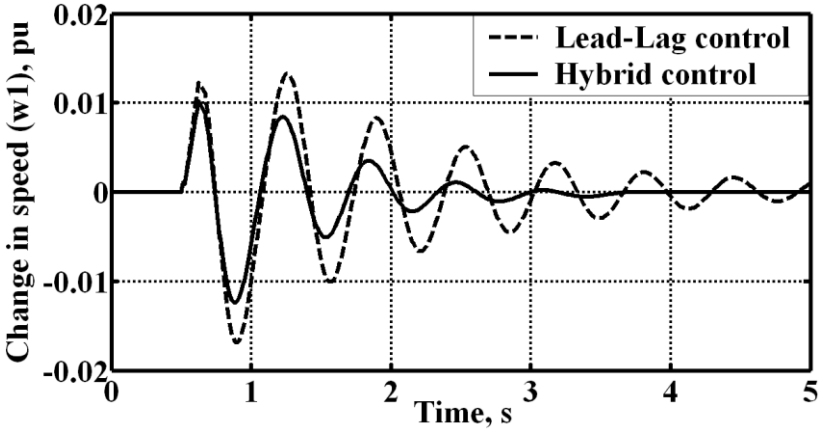

Figure 6.14: **Speed variation with damping controller at P_e = 1.0, Q_e=0.3pu**

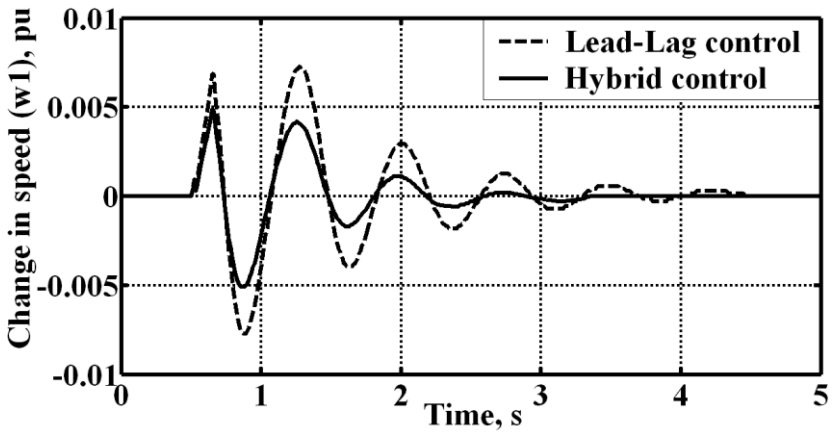

Figure 6.15: **Speed variation with damping controller at P_e = 0.8, Q_e=0.3pu**

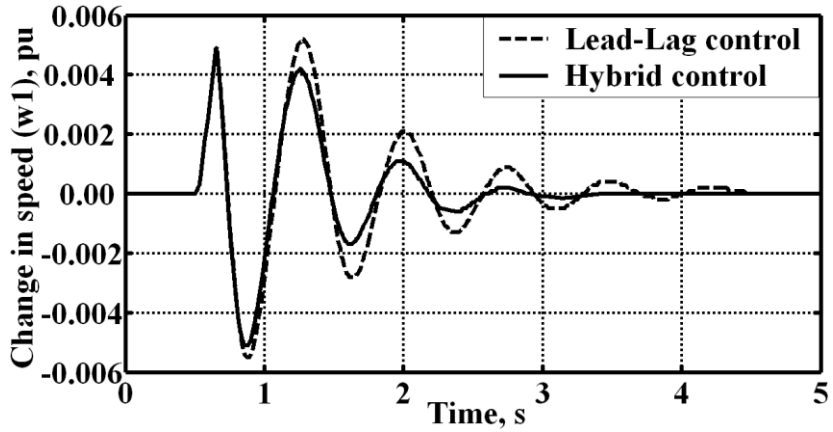

Figure 6.16: **Speed variation with damping controller at P_e = 0.5, Q_e=0.3pu**

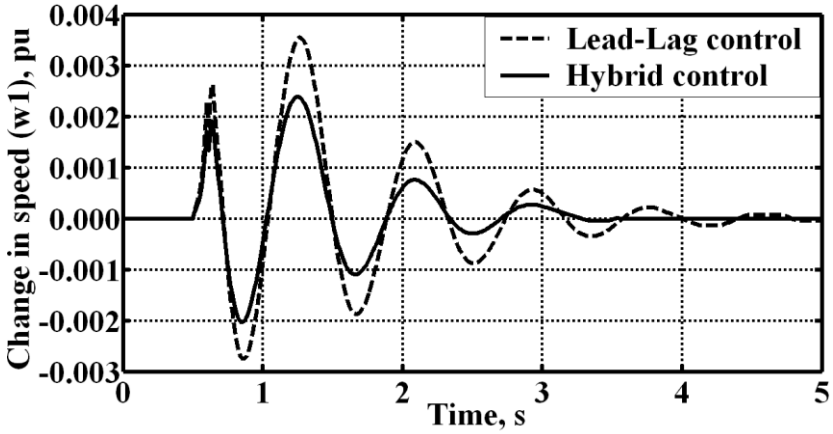

Figure 6.17: **Speed variation with damping controller at P_e = 0.2, Q_e=0.3pu**

The load angle variation at different operating points with Lag / Lead power factors are shown below. The operating points are $P_1 = 1.0,\ 0.8,\ 0.2\,pu$.

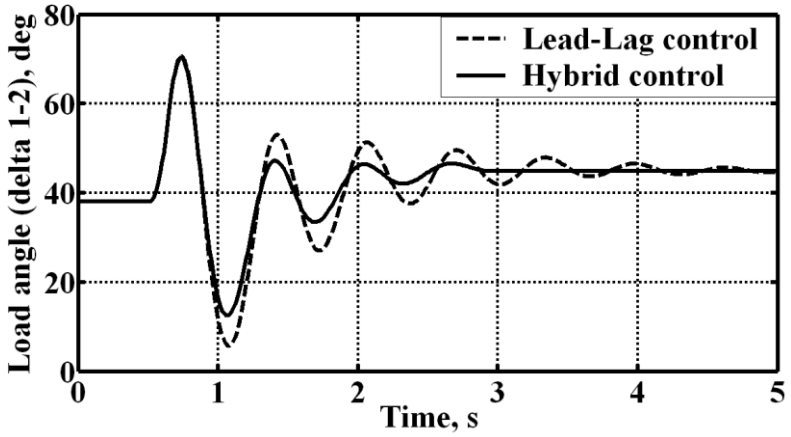

Figure 6.18: **Load angle variation at P_e=1.0, Q_e=0.3pu**

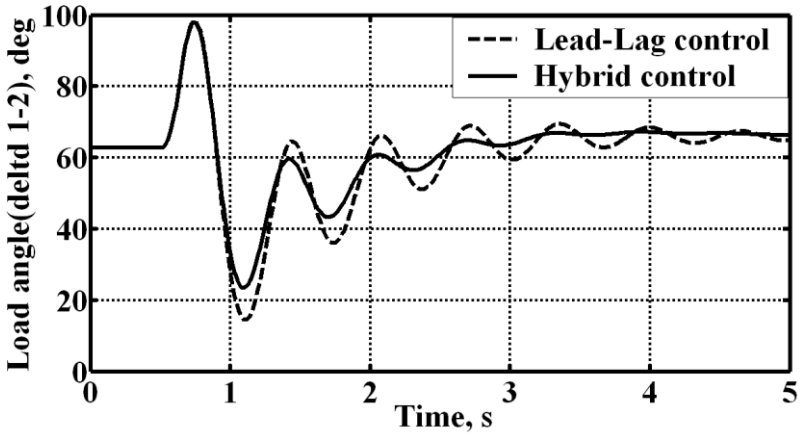

Figure 6.19: **Load angle variation at P_e=1.0, Q_e=-0.3pu**

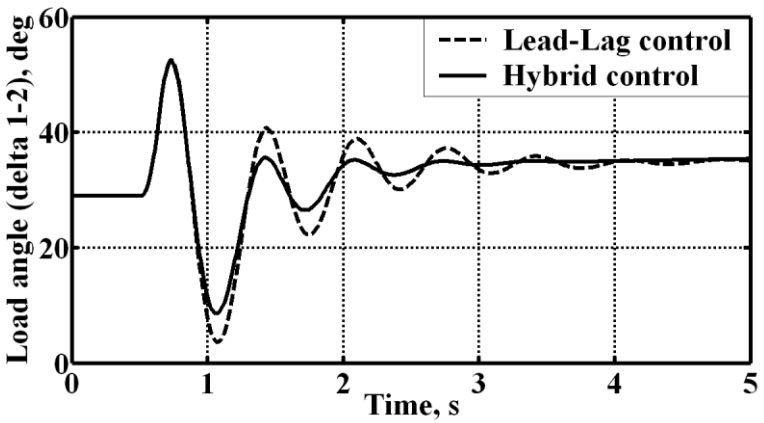

Figure 6.20: **Load angle variation at P_e=0.8, Q_e=0.3pu**

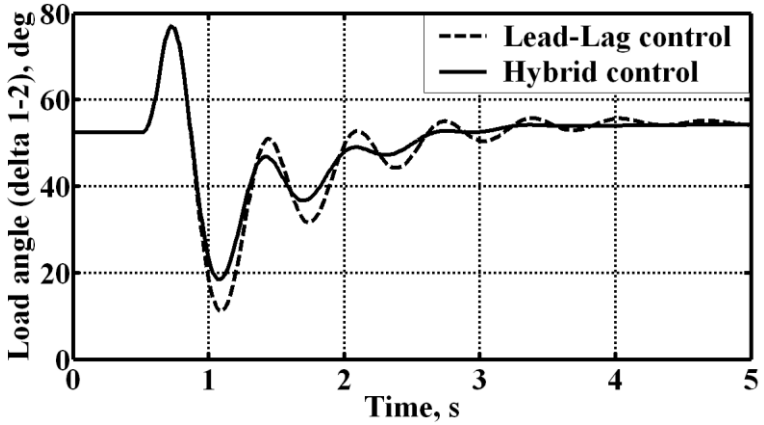

Figure 6.21: **Load angle variation at P_e=0.8, Q_e=-0.3pu**

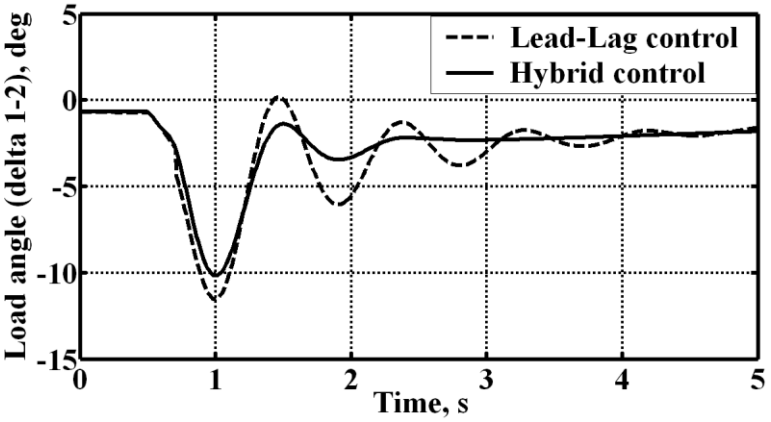

Figure 6.22: **Load angle variation at P_e=0.2, Q_e=0.3pu**

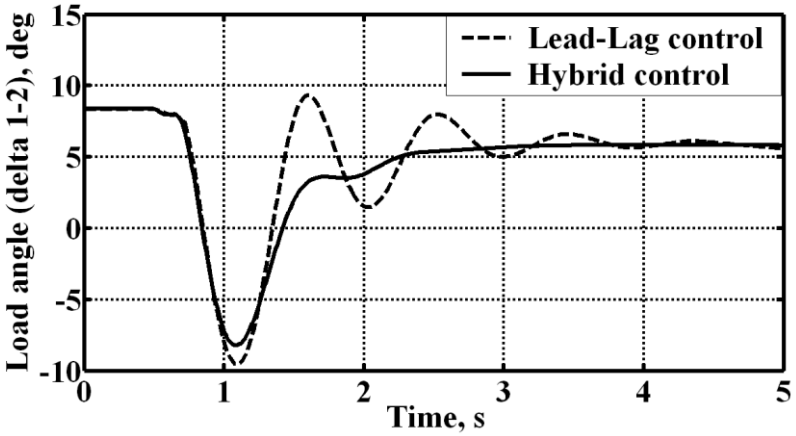

Figure 6.23: **Load angle variation at P_e=0.2, Q_e=-0.3pu**

B. Dynamic performance of three machine-nine bus system with proposed control

The same controller is experimented on a three-machine nine bus WSCC power system [6]. The shunt transformer of the UPFC is connected to bus 9 and series transformer between buses 9 and 6. The single-line diagram of the test system is as shown in Figure 6.24.

Selection of UPFC Suitable Location:

The locations of the UPFC device in the power system are obtained on the basis of static and/or dynamic performances. There are several methods for finding locations of UPFC in vertically integrated systems but little attention has been devoted to power, systems under network contingency. It is proposed to improve the performance of the system by selecting suitable locations for UPFC using all of its benefits under network contingencies. For a given contingency the possible locations of UPFC are analyzed. A contingency may involve a line having UPFC. Thus a location for UPFC is selected based on the best performance of the system. This UPFC may take care of many network contingencies. The following are the major steps involved in the approach for selection of UPFC location under a given network contingency.

Step I: Identify the transmission corridors for the given network.

Step 2: Select some transmission lines as suitable locations for each transmission corridor.

Step 3: Perform the power flow/dynamic stability analysis with UPFC connected in selected line for each transmission corridor for a given network contingency.

Step 4: Compute settling time from the dynamic performance graph.

Step 5: Prepare a list indicating location of UPFC, the value of settling time.

Step 6: From the above list we can identify the most suitable location for UPFC, which gives quicker settling**.**

The main advantage of keeping UPFC, between bus bars 9 and 6 is that the control of heavily loaded generator (G_2) can be achieved. The locally measured signals from generator 2 can be used easily for simulation. Inter-area mode of oscillations can be easily damped as the UPFC is placed between transmission lines.

Table 6.1: **System eigen-values for the electromechanical modes**

	Eigen-values	Damping ratio	Frequency (Hz)
UPFC with Lead-Lag control	-0.89 ± j 12.66	0.0702	2.01
	-0.77 ± j 8.78	0.0876	1.397
UPFC with Hybrid Control			
	-1.61 ± j 12.37	0.1293	1.97
	-1.22 ± j 8.54	0.142	1.357

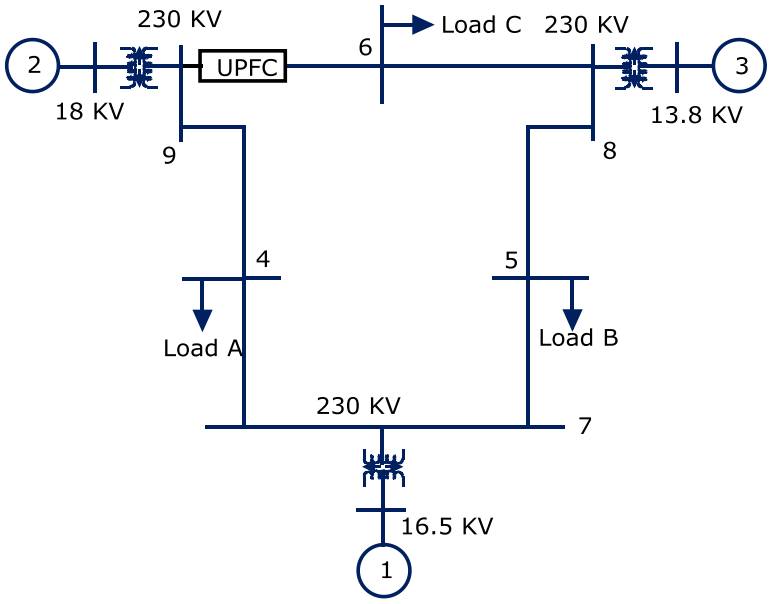

Figure 6.24: **Three machine nine bus system**

The eigen-values for the electromechanical mode of oscillation is given in Table 6.1. A computer simulation was performed on the test system. The fault considered here is a three phase to ground fault near bus 4 and cleared by opening the line between the buses 4–9 after an interval of 83ms. Several studies with various fault locations and different loading conditions were performed. However, due to limitations in space, only one set of results is presented here. Figure 6.25 - Figure 6.27 show the angular speed variation of the generators. The real power variations of the generators are shown in Figure 6.28 to Figure 6.30. Figure 6.31 and Figure 6.32 show the load angle variation of generator-2 and generator-3 with respect to generator-1.

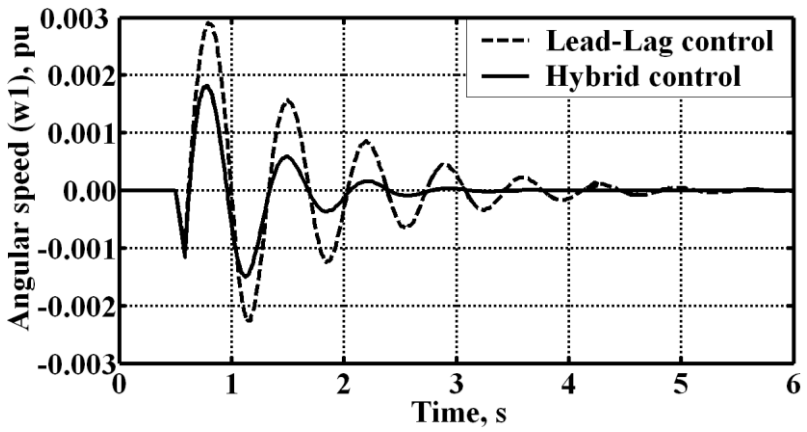

Figure 6.25: S**peed variation at P_1 = 0.72, Q_1=0.27, P_2 = 1.63, Q_2=0.1, P_3 = 0.85, Q_3= -0.11pu**

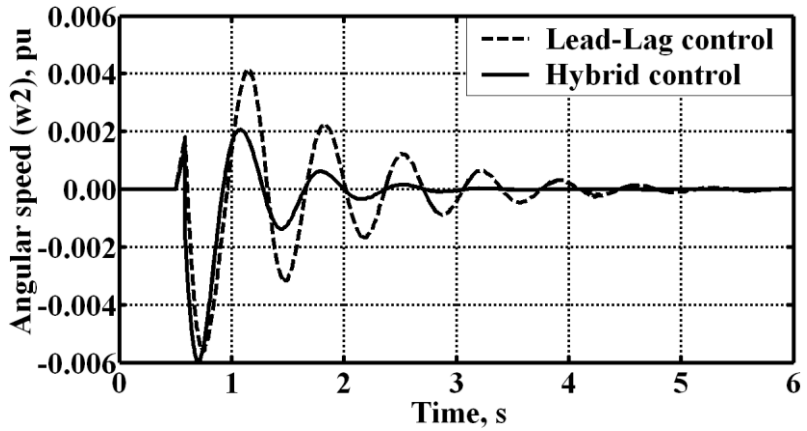

Figure 6.26: S**peed variation at P_1 = 0.72, Q_1=0.27, P_2 = 1.63, Q_2=0.1, P_3 = 0.85, Q_3= -0.11pu**

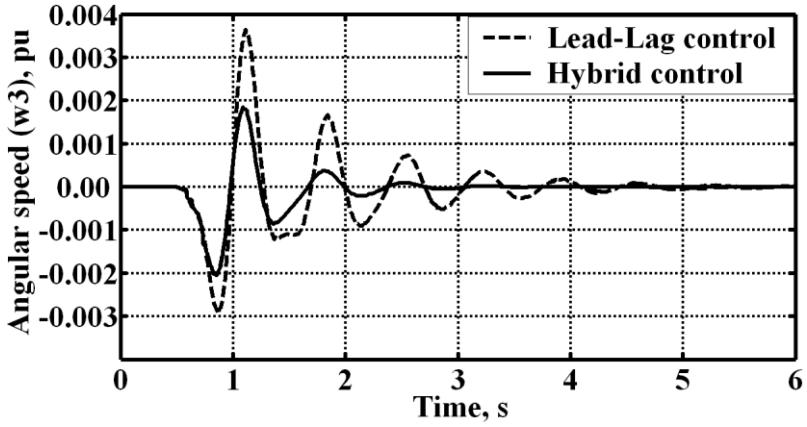

Figure 6.27: S**peed variation at P_1 = 0.72, Q_1=0.27, P_2 = 1.63, Q_2=0.1, P_3 = 0.85, Q_3= -0.11pu**

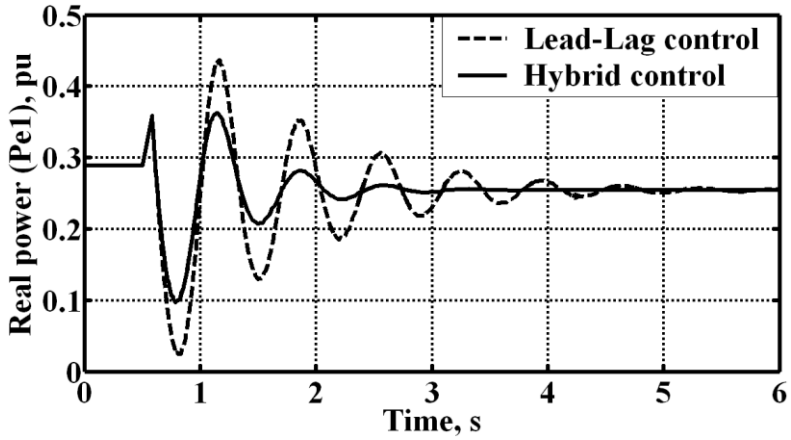

Figure 6.28: P**ower variation P_1 = 0.72, Q_1=0.27, P_2 = 1.63, Q_2=0.1, P_3 = 0.85, Q_3= -0.11pu**

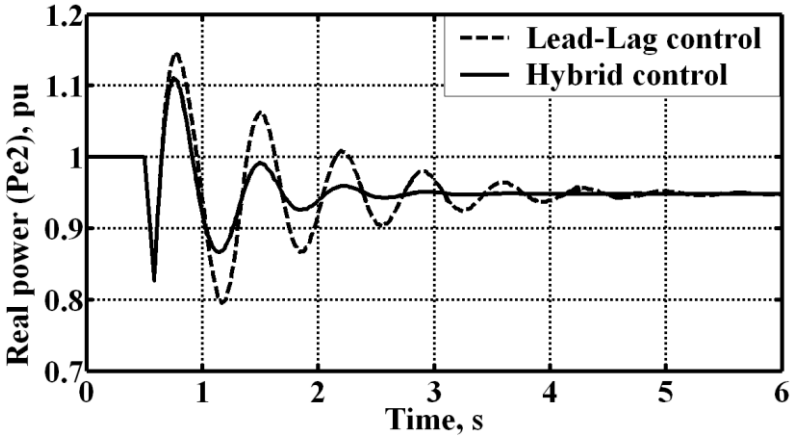

Figure 6.29: P**ower variation at P_1 = 0.72, Q_1=0.27, P_2 = 1.63, Q_2=0.1, P_3 = 0.85, Q_3= -0.11pu**

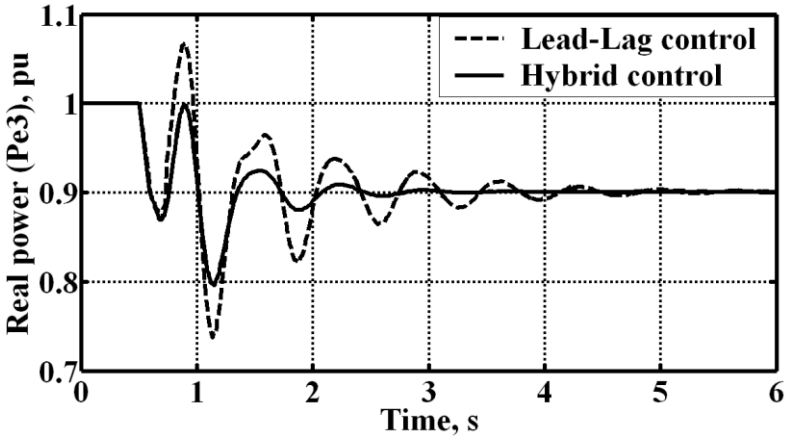

Figure 6.30: P**ower variation at P_1 = 0.72, Q_1=0.27, P_2 = 1.63, Q_2=0.1, P_3 = 0.85, Q_3= -0.11pu**

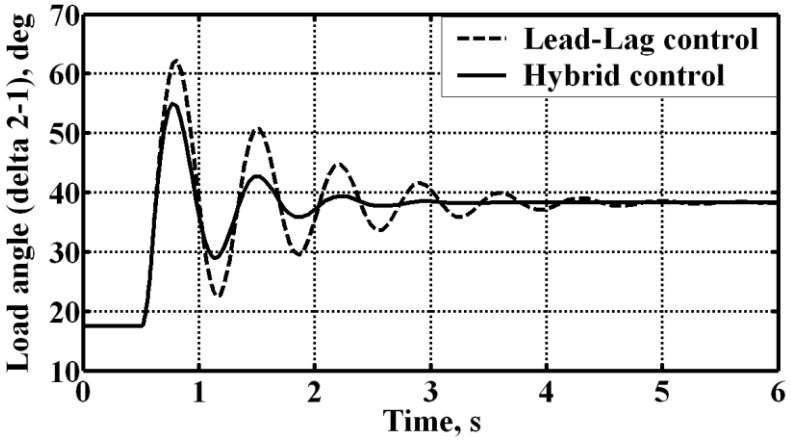

Figure 6.31: **Load angle (δ_{12}) at P_1 = 0.72, Q_1=0.27, P_2 = 1.63, Q_2=0.1, P_3 = 0.85, Q_3= -0.11pu**

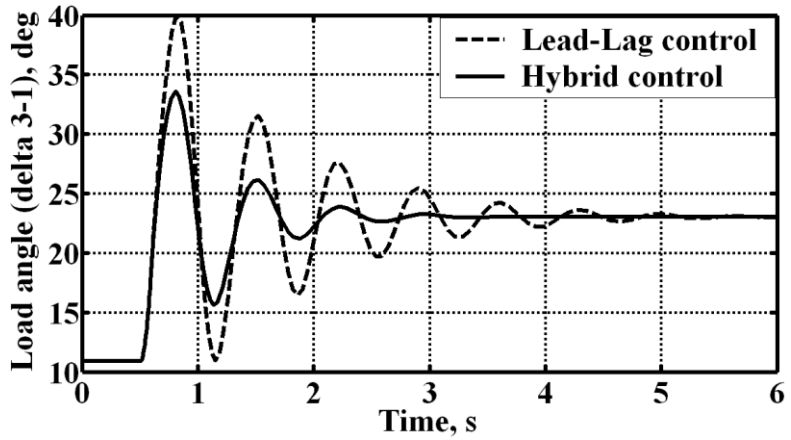

Figure 6.32: **Load angle (δ_{13}) at P_1 = 0.72, Q_1=0.27, P_2 = 1.63, Q_2=0.1, P_3 = 0.85, Q_3= -0.11pu**

C. Dynamic performance of four-generator two-area power system with proposed control

For inter-area mode analysis, the two-area and four machine test system shown in Figure 6.33, is considered [1]. A nonlinear simulation was performed for a large disturbance. A three phase to ground fault at bus 9 was applied for 100 ms. This is shown by the point 'F' in the Figure 6.33. The fault is cleared from the faulted line by opening the line between buses 8 and 9. Figure 6.34 - Figure 6.37 display a comparison between the

nonlinear simulations of the proposed hybrid controller with Lead-Lag controller examined for up to 10s. It is seen that the responses are very satisfactory.

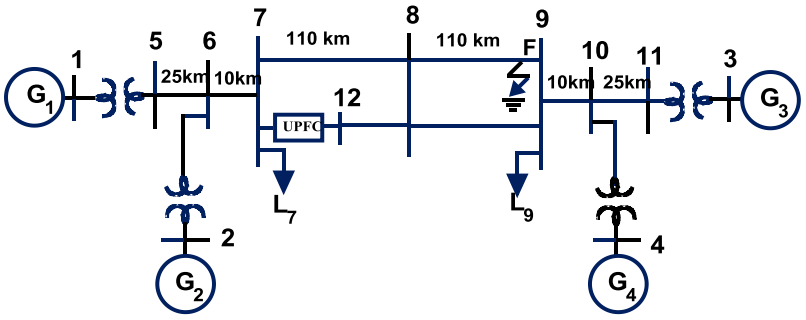

Figure 6.33: **Four generator power system**

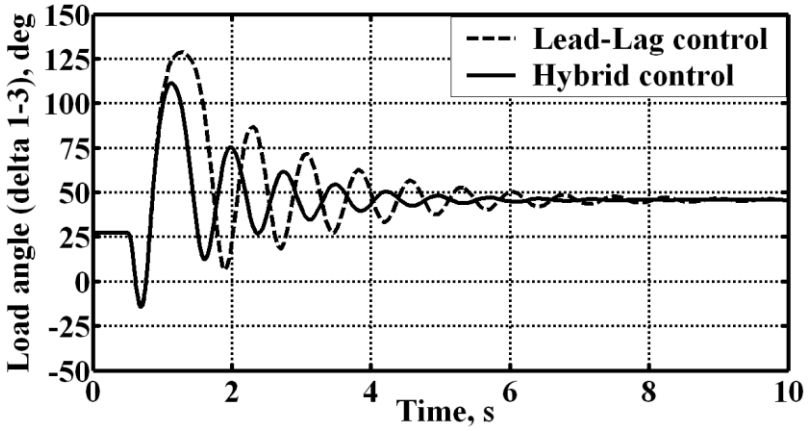

Figure 6.34: **Load angle ariation (δ_{13}) at P_1 = 7.0, Q_1=1.85, P_2 = 7.0, Q_2=2.35, P_3 = 7.2, Q_3= 1.76, P_4 = 7.0, Q_4=2.02pu**

Table 6.2 shows the improvement in the eigen-values of the electromechanical modes with the proposed controller. It can be seen from the Table 6.2 that the controller improves the damping of the inter-area mode between area 1 and area 2 only. Other local modes between generators of the same group are untouched which is very desirable to avoid interaction through action of controllers.

Table 6.2: **System eigen-values for the electromechanical modes**

	Eigen-values	Damping ratio	Frequency (Hz)
UPFC with Lead-Lag control	-0.63 ± j 3.47	0.1786	0.55
	-0.472 ± j 6.78	0.07	1.08
	-0.502 ± j 6.91	0.073	1.1
UPFC with Hybrid control	-0.968 ± j 3.17	0.292	0.5
	-0.478 ± j 6.74	0.07	1.07
	-0.508 ± j6.90	0.072	1.099

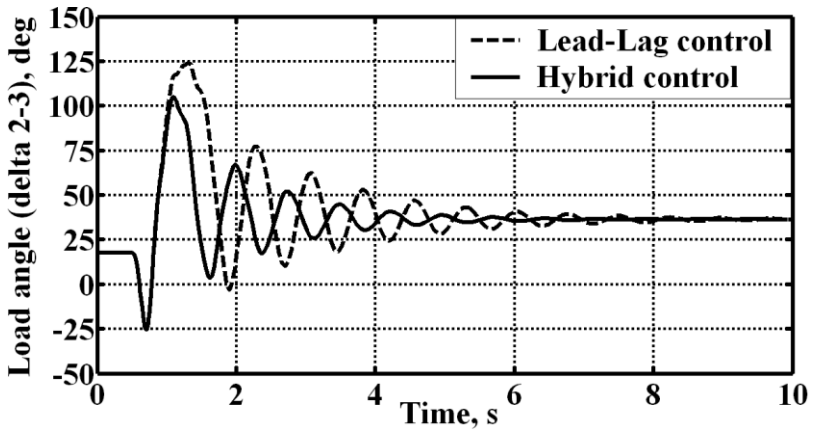

Figure 6.35: **Load angle variation (δ_{23}) at P_1 = 7.0, Q_1=1.85, P_2 = 7.0, Q_2=2.35, P_3 = 7.2, Q_3= 1.76, P_4 = 7.0, Q_4=2.02pu**

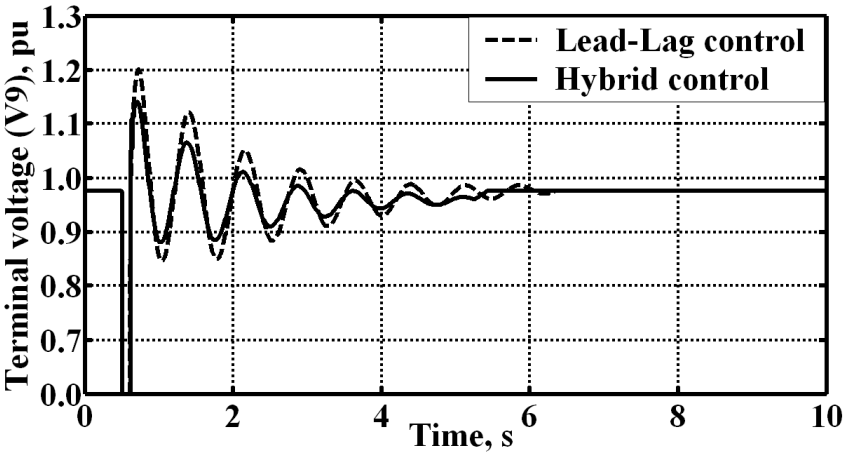

Figure 6.36: **Terminal voltage variation (V_9) at P_1 = 7.0, Q_1=1.85, P_2 = 7.0, Q_2=2.35, P_3 = 7.2, Q_3= 1.76, P_4 = 7.0, Q_4=2.02pu**

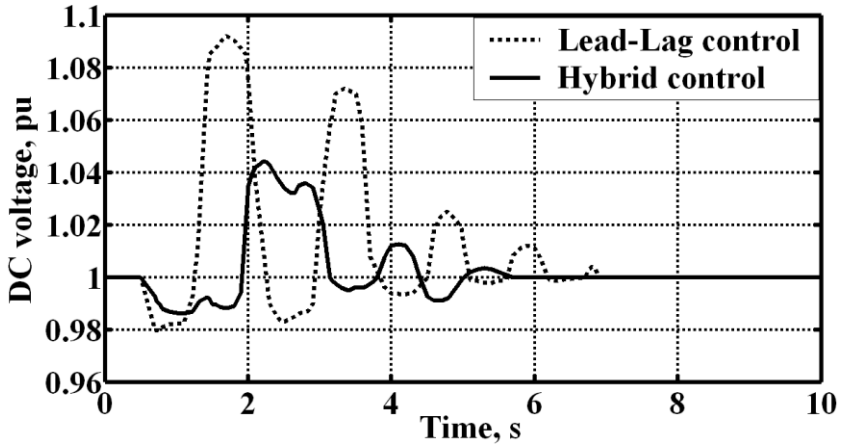

Figure 6.37: **Capacitor DC voltage (V_{dc}) at P_1 = 7.0, Q_1=1.85, P_2 = 7.0, Q_2=2.35, P_3 = 7.2, Q_3= 1.76, P_4 = 7.0, Q_4=2.02pu**

The above nonlinear computer analysis shows that the integrated linear and nonlinear control scheme is faster in damping inter-area oscillations and efficient in achieving voltage regulation.

The load angle variation with hybrid PID controller is shown below. Figure 6.38 shows that the PID hybrid controller is giving better result than PI hybrid controller. In Figure 6.39 the ripple content in the DC voltage is reduced considerably. Due to increase in the noise level while using PID for practical application, most of the researches are avoiding PID for power applications.

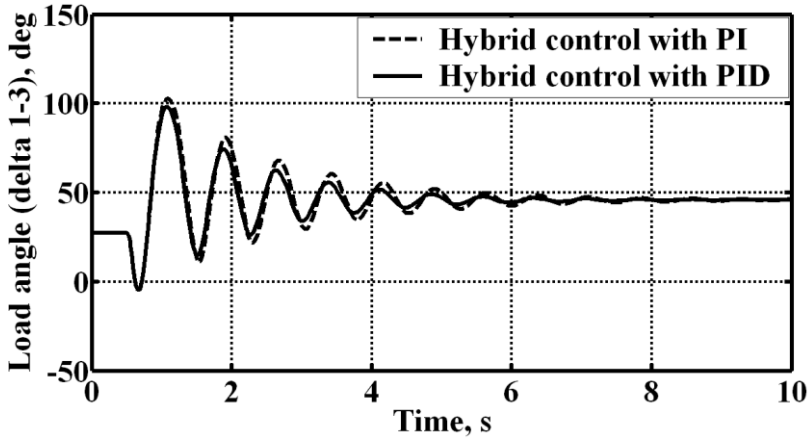

Figure 6.38: **Load angle variation (δ_{13}) with PI and PID controller**

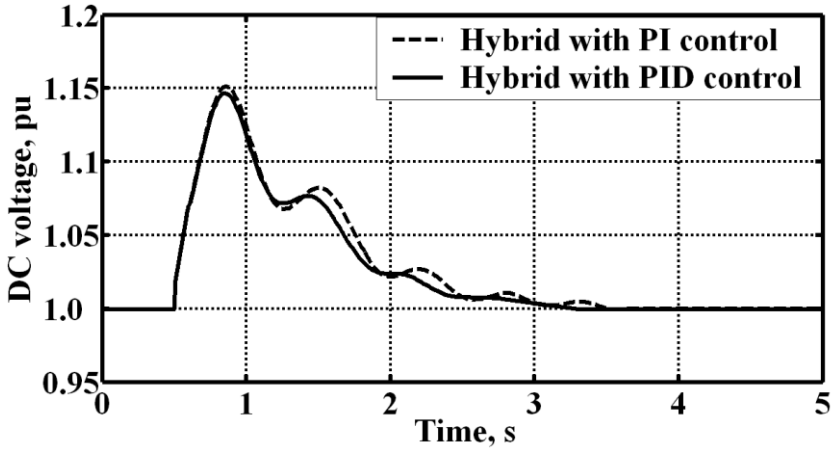

Figure 6.39: **Capacitor DC voltage (V_{dc})**

Chapter 7

Conclusions and Future Work

Chapter 7

Conclusions and Future Work

A general nonlinear dynamical model for power systems with UPFC as a stabilizing controller is introduced. This representation is appropriate to model a nonlinear power network with different FACTS devices. The advantage of this approach is that no algebraic equations are involved in the control design while the nonlinear behavior is retained. As demonstrated in Chapters 4, 5 and 6, this representation helps us to convert the nonlinear power system equations into standard parametric feedback form. Once the standard form is achieved, conventional and advanced nonlinear control techniques can be easily implemented. The net result is a power system dynamic representation that can be used for the design of a sophisticated FACTS damping controller.

A nonlinear control scheme is developed to stabilize and damp the oscillations resulting from a disturbance such as a three phase to ground fault. The nonlinear control scheme is independent of the operating point. We target the stability of the generators by defining an appropriate Lyapunov function. The analytical expression of the nonlinear control law for the UPFC is obtained using back stepping method. Then, combining the nonlinear control strategy with the linear one for the other variables, a complete linear and nonlinear stabilizing controller is obtained.

Finally, an adaptive law for estimating the uncertain parameters is derived to relax the need for approximating uncertain parameters such as damping coefficient, which is difficult to be measured precisely.

The small signal analysis shows that the damping ratio of the electro-mechanical mode has been improved from 0.142 to 0.211 with the new controller for a two area power system.

This improvement in the damping ratio reduces the settling time from 3.67s of the conventional control to 2.59s with the designed hybrid control.

In case of two-area four generators power system damping ratio of the inter-area mode between area-1 and area-2 has been improved from 0.1786 to 0.292 with a corresponding reduction in settling time. The settling time is reduced from 6.29s to 4.23s. Dynamic performance also shows a similar trend. Both these result shows that the proposed control strategy is more effective in improving system stability.

The linear control methods are applied to the linearized power system. This method, however, tacitly assumes that the network variables remain in the neighbourhood of the desired operating point. This is not true. Continuous load change would be experienced by the generators in a power system in their daily operation and when there is a fault in the power system, drastic changes can occur. As the system conditions shift from the operating point at which the controller was optimized, the linear controllers show poor performance. The linearized controllers can deliver best results in the loading conditions at which they are designed.

In future, studies may focus on design and implementation of a nonlinear control scheme with several FACTS devices in a multi-machine power system. The 68 bus NYPS-NETS test power system can be used for this purpose. Advanced random search on-line dynamic controllers like PSO, can be used for optimization.

Secondly, a hardware setup can be used to fully understand the dynamic performance of the multiple FACTS devices, which would validate software simulation.

References

References

[1] Kundur, P., “Power system stability and control”, McGraw-Hill, N.Y., 1994.

[2] Rogers, G., “Power system oscillations”, Kluwer Academic Publishers, USA, 2000.

[3] Hingorani, N. G., “Flexible AC transmission”, IEEE Spectrum, pp 40-45, 1993.

[4] Gyugyi, L., “Dynamic compensation of AC transmission lines by solid-state synchronous voltage sources”, IEEE Transactions on Power Delivery, vol.9, no. 2, pp. 904-911, 1994.

[5] Hingorani, N. G., Gyugyi, L., “Understanding FACTS: concepts and technology of flexible AC transmission systems”, New York: IEEE Press, 2000.

[6] Anderson, P. M., Fouad, A. A., “Power system control and stability”, Iowa State University Press, AMES, IOWA, U.S.A, 1977.

[7] Abido, M.A., Abdel-Magid, Y. L., “Analysis of power system stability enhancement via excitation and FACTs-based stabilizers”, Electric Power Components and Systems, vol. 32, no.1, pp. 75-91, 2004.

[8] Fregene, K., Kennedy, D., “Stabilizing control of a high-order generator model by adaptive feedback linearization”, IEEE Transactions on Energy Conversion, vol.18, no.1, pp. 149- 156, 2003.

[9] Sadegh Vaez-Zadeh, “ Robust power system stabilizers for enhancement of dynamic stability over a wide operating range”, Electric Power Components and Systems, vol. 29, no. 7, pp. 645-657, 2001.

[10] Shaoru, Z., Fang, Lin, L., “An improved simple adaptive control applied to power system stabilizer”, IEEE Transactions on Power Electronics, vol.24, no.2, pp.369-375, 2009.

[11] Peng, Z., Malik, O.P., "Design of an adaptive PSS based on recurrent adaptive control theory", IEEE Transactions on Energy Conversion, vol.24, no.4, pp.884-892, 2009.

[12] Larsen, E. V., Swann, D. A., "Applying power system stabilizers, Parts I-III", IEEE Transactions on Power Apparatus and Systems, Vol. 100, No. 6, pp 3017-3046,1981.

[13] Eliasson, B. E., Hill, D. J., "Damping structure and sensitivity in the NORDEL power system", IEEE Transactions on Power System, vol. 7, no. 1, pp 97-105, 1992.

[14] Klein, M., Rogers, G. J., Moorty, S., Kundur, P., "Analytical investigation of factors influencing power system stabilizers performance", IEEE Transactions on Energy Conversion, vol. 7, no. 3, pp 382-390, 1992.

[15] Hingorani, N. G., "FACTS-flexible AC transmission system", Proceedings of 5th International Conference on AC and DC Power Transmission-IEE Conference Publication,vol. 345, pp. 1–7, 1991.

[16] Hingorani, N. G., "High power electronics and flexible AC transmission system", IEEE Power Engineering Review, vol. 8, no. 7, pp. 3-4, 1988.

[17] Edris, A., et al., "Proposed terms and definitions for flexible AC transmission system (FACTS)", IEEE Transactions on Power Delivery, vol. 12, no. 4, pp. 1848–1852, 1997.

[18] IEEE Power Engineering Society, "FACTS Overview", IEEE Special Publication 95TP108, 1995.

[19] IEEE Power Engineering Society, "FACTS Applications", IEEE Special Publication 96TP116-0, 1996.

[20] Erinmez, I. A., Foss, A. M., "Static Synchronous Compensator (STATCOM)", Working Group 14.19, CIGRE Study Committee 14, Document No. 144, 1999.

[21] CIGRE Task Force 14-27, "Unified Power Flow Controller", CIGRE Technical Brochure, 1998.

[22] Mathur, R. M., Basati, R. S., "Thyristor-Based FACTS Controllers for Electrical Transmission Systems", IEEE Press Series in Power Engineering, 2002.

[23] Yong Hua Song, Allan T. Johns, "Flexible AC Transmission Systems (FACTS)", London, UK: IEE Press, 1999.

[24] Byerly, R. T., Poznaniak, D. T., Taylor, E. R., "Static reactive compensation for power transmission system", IEEE Transactions on Power Apparatus and Systems, vol. 101, no. 10, pp. 3997–4005, 1982.

[25] Hammad, A. E., "Analysis of power system stability enhancement by static VAR compensators", IEEE Transactions on Power Systems, vol. 1, no. 4, pp. 222–227, 1986.

[26] Padiyar, K. R., Varma, R. K., "Damping torque analysis of static VAR system oscillations", IEEE Transactions on Power Systems, vol. 6, no. 2, pp. 458–465, 1991.

[27] Wang, H. F., Swift, F. J., "Application of the Phillips-Heffron model in the analysis of the damping torque contribution to power systems by SVC damping control", International Journal of Electrical Power & Energy Systems, vol.18, no. 5, pp. 307–313, 1996.

[28] Wang, H. F., Swift, F. J., "Capability of the static VAR compensator in damping power system oscillations", IEE Proceedings on Generation Transmission and Distribution, vol. 143, no. 4, pp. 353–358, 1996.

[29] Pourbeik, P., Gibbard, M. J., "Damping and synchronizing torques induced on generators by FACTS stabilizers in multi-machine power systems", IEEE Transactions on Power Systems, vol. 11, no. 4, pp. 1920–1925, 1996.

[30] Dash, P. K., Panda, P. C., Sharaf, A. M., Hill, E. F., "Adaptive controller for static reactive power compensators in power systems", IEE Proceedings, Part-C, vol. 134, no. 3, pp. 256–264, 1987.

[31] Hsu, Y. Y., Cheng, C H., "Design of a static VAR compensator using model reference adaptive control", Electric Power Systems Research, vol. 13, pp. 129–138, 1987.

[32] Parniani, M., Iravani, M. R., "Optimal robust control design of static VAR compensators", IEE Proceedings on Generation Transmission and Distribution, vol. 145, no. 3, pp. 301–307, 1998.

[33] Dash, P. K., Sharaf, A. M., Hill, E. F., "An adaptive stabilizer for thyristor controlled static VAR compensators for power systems", IEEE Transactions on Power Systems, vol. 4, no. 2, pp. 403–410, 1989.

[34] Rao, P. S., Sen, I., "A QFT-based robust SVC controller for improving the dynamic stability of power systems", Electric Power Systems Research, vol. 46, pp. 213–219, 1998.

[35] Vidyasagar, M., Kimura, H., "Robust controllers for uncertain linear multivariable systems", Automatica, vol. 22, no. 1, pp. 85–94, 1986.

[36] Kwakernaak, H., "Robust control and H_∞ optimization-tutorial", Automatica, vol.29, no. 2, pp. 255–273, 1993.

[37] Noroozian, M., Andersson, G., "Damping of power system oscillations by use of controllable components", IEEE Transactions on Power Delivery, vol. 9, no. 4, pp. 2046–2054, 1994.

[38] Gronquist, J. F., Sethares, W. A., Alvarado, F. L., Lasseter, R. H., "Power oscillation damping control strategies for FACTS devices using locally measurable quantities", IEEE Transactions on Power Systems, vol. 10, no. 3, pp. 1598–1605, 1995.

[39] Larsen, E. V., Sanchez-Gasca, J. J., Chow, J. H., "Concepts for design of FACTS controllers to damp power swings", IEEE Transactions on Power Systems, vol. 10, no. 2, pp. 948–956, 1995.

[40] Smed, T., Andersson, G., "Utilizing HVDC to damp power oscillations", IEEE Transactions on Power Delivery, vol. 8, no. 2, pp. 620–627, 1993.

[41] Smed, T., "Feasible eigen value sensitivity for large power systems", IEEE Transactions on Power Systems, vol. 8, no. 2, pp. 555–563, 1993.

[42] Hanson, D. J., Woodhouse, M. L., Horwill, C., Monkhouse, D. R., Osborne, M. M., "STATCOM: a new era of reactive compensation", Power Engineering Journal, pp. 151–160, 2002.

[43] Wang, H. F., Li, H., Chen, H., "Application of cell immune response modeling to power system voltage control by STATCOM", IEE Proceedings on Generation Transmission and Distribution, vol. 149, no. 1, pp. 102–107, 2002.

[44] Abido, M. A., "Analysis and assessment of STATCOM-based damping stabilizers for power system stability enhancement", Electric Power Systems Research, vol. 73, no. 2, pp. 177–185, 2005.

[45] Haque, M. H., "Use of energy function to evaluate the additional damping provided by a STATCOM", Electric Power Systems Research, vol. 72, no. 2, pp. 195–202, 2004.

[46] Wang, H. F., **"**Static synchronous series compensation to damp power system oscillations", Electric Power Systems Research, vol. 54, no. 2, pp. 113–119, 2000.

[47] Kumkratug, P., Haque, M. H., "Improvement of stability region and damping of a power system by using SSSC", Proceedings of IEEE Power Engineering Society General Meeting, vol. 3, pp. 1417–1421, 2003.

[48] Edris, A., Mehraban, A.S., Rahman, M., Gyugyi, L., Arabi, S., Rietman, T., "Controlling the flow of real and reactive power", IEEE Computer Application in Power, pp. 20-25, 1998.

[49] Gyugyi, L., "A unified power flow control concept for flexible AC transmission Systems", IEE Conference Proceedings, vol. 139, no. 4, pp. 323-331, 1992.

[50] Gyugyi, L., Schauder, C.D., Williams, S.L., Rietman, T.R., Torgerson, D.R., Edris, A., "The unified power flow controller: a new approach to power transmission control", IEEE Transactions on Power Delivery, vol.10, no.2, pp.1085-1097, 1995.

[51] Farsangi, M.M., Song, Y.H., Lee, K.Y., "Choice of FACTS device control inputs for damping inter-area oscillations", IEEE Transactions on Power Systems, vol. 19, no. 2, pp. 1135-1143, 2004.

[52] Noroozian, M., Angquist, L., Ghandhari, M., Andersson, G., "Use of UPFC for optimal power flow control", IEEE Transactions on Power Delivery, vol.12, no.4, pp.1629-1634, 1997.

[53] Tambey, N., Kothari, M.L., "Damping of power system oscillations with unified power flow controller (UPFC)", IEE Proceedings on Generation, Transmission and Distribution, vol.150, no.2, pp. 129- 140, 2003.

[54] Wang, H. F., "A unified model for the analysis of FACTS devices in damping power system oscillations. III. unified power flow controller", IEEE Transactions on Power Delivery, vol.15, pp.978-983, Jul 2000.

[55] Wang, H.F., "Damping function of unified power flow controller," IEE Proceedings on Generation, Transmission and Distribution, vol.146, no.1, pp.81-87, 1999.

[56] Azbe, V., Gabrijel, U., Povh, D., Mihalic, R., "The energy function of a general multi-machine system with a unified power flow controller", IEEE Transactions on Power Systems, vol.20, no.3, pp. 1478- 1485, 2005.

[57] Noroozian, M., Ghandhari, M., Andersson, G., Gronquist, J., Hiskens, I., "A robust control strategy for shunt and series reactive compensators to damp electromechanical oscillations", IEEE Transactions on Power Delivery, vol.16, no.4, pp.812-817, 2001.

[58] Nabavi-Niaki, A., Iravani, M.R., "Steady-state and dynamic models of unified power flow controller (UPFC) for power system studies", IEEE Transactions of Power Systems, Vol. 11, No. 4, pp. 1937-1943, 1996.

[59] Wang, H.F., "Applications of modeling UPFC into multi-machine power systems", IEE Proceedings on Generation, Transmission and Distribution, Vol. 146, No. 3, pp. 306-312, 1999.

[60] Huang, Z., Ni, Y., Shen, C.M., Wu, F.F., Chen, S., Zhang, B., "Application of unified power flow controller in interconnected power systems -- modeling, interface, control strategy and case study", IEEE Transactions of Power Systems, Vol. 15, No. 2, pp. 817-824, 2000.

[61] Hammons, T. J., Winning, D. J., "Comparisons of synchronous machine models in the study of the transient behavior of electrical power system", IEE Proceedings, vol.118, no.10, pp.1442-1458, 1971.

[62] Prabhashankar, K., Janischewsy, J. W., "Digital simulation of multi-machine power systems for stability studies", IEEE Transactions on Power Apparatus and systems, vol. 87, no.1, pp.73-80, 1968.

[63] Mohan, N., Undeland, T. M., Robbins, W. P., "Power electronics: Converters, applications and design", Second ed: John Wiley & Sons, 1995.

[64] Brogan, W. L., "Modern control theory" Prentice Hall, 1985.

[65] Rajasekaran, S., Vijayalakshmi pai, G. A., "Neural networks, fuzzy logic and genetic algorithms: synthesis and applications," PHI Learning Pvt. Ltd. 2006.

[65] Goldberg, D. E., "Genetic Algorithms in search, optimization and machine learning" Addison-Wesley, 1989.

[66] Wang, K., Xin, H., Gan, D., Ni, Y., "Non-linear robust adaptive excitation controller design in power systems based on a new back-stepping method", IET Control Theory and Applications, vol.4, no.12, pp. 2947-2957, 2010.

[67] Mehraeen, S., Jagannathan, S., Crow, M. L., "Noval dynamic representation and control of power systems with FACTS devices," IEEE Transactions on Power Systems, vol.25, no.3, pp.1542-1554, 2010.

[68] Karagiannis D., Astolfi A., "Nonlinear adaptive control of systems in feedback form: an alternative to adaptive back-stepping", Syst. Control Lett., vol. 9, pp. 733-739, 2008.

[69] Khalil, H.K., "Nonlinear systems," Upper Saddle River, NJ: Prentice Hall, 2002.

Appendix

Appendix A.

$$M\Delta\dot{\omega} = W_1\Delta\delta + W_2\Delta\omega + W_3\Delta E_q^{'} + W_4\Delta V_{dc} + W_{uk}\Delta u_k$$

$$M\Delta\dot{\omega} - W_2\Delta\omega = W_1\Delta\delta + W_3\Delta E_q^{'} + W_4\Delta V_{dc} + W_{uk}\Delta u_k$$

$$(Ms - W_2)\Delta\omega = W_1\Delta\delta + W_3\Delta E_q^{'} + W_4\Delta V_{dc} + W_{uk}\Delta u_k$$

$$\Delta\omega = \frac{1}{(Ms - W_2)}(W_1\Delta\delta + W_3\Delta E_q^{'} + W_4\Delta V_{dc} + W_{uk}\Delta u_k)$$

Similarly

$$\Delta\dot{\delta} = \omega_0 I\Delta\omega\,; \qquad \Delta\delta = (\frac{\omega_0 I}{s})\Delta\omega$$

And

$$T_{do}^{'}\Delta\dot{E}_q^{'} = N_1\Delta\delta + N_3\Delta E_q^{'} + N_4\Delta V_{dc} + N_5\Delta E_{fd} + N_{uk}\Delta u_k$$

$$\Delta E_q^{'} = \frac{1}{(T_{do}^{'}s - N_3)}(N_1\Delta\delta + N_4\Delta V_{dc} + N_5\Delta E_{fd} + N_{uk}\Delta u_k)$$

Similarly we can derive that

$$\Delta V_{dc} = \frac{1}{(s - L_4)}(L_1\Delta\delta + L_3\Delta E_q^{'} + L_{uk}\Delta u_k)$$

$$\Delta E_{fd} = \frac{1}{(T_A s - S_5)}(S_1\Delta\delta + S_3\Delta E_q^{'} + S_4\Delta V_{dc} + S_{uk}\Delta u_k)$$

Appendix B.

Computation of parameters in Chapter 4

$X_{SRL} = X_{SR} + X_L$; $X_{SRLTd} = X_{SR} + X_L + X_t + X_d^{'}$; $X_{TSHd} = X_t + X_{SH} + X_d^{'}$; $X_{Td} = X_t + X_d^{'}$;

$X_{DT} = X_{TSHd} X_{SRL} + X_{SH} X_{Td}$; $X_{TSHq} = X_t + X_{SH} + X_q$

$X_{SRLTq} = X_{SR} + X_L + X_t + X_q$; $X_{Tq} = X_t + X_q$; $X_{QT} = X_{TSHq} X_{SRL} + X_{SH} X_{Tq}$

$a_{11} = (X_{SH} V_I \sin(\delta)) / X_{DT}$; $a_{12} = (X_{SRL} + X_{SH}) / X_{DT}$; $a_{22} = 0$

$a_{13} = -(m_{SH} \sin(\varphi_{SH}) X_{SRL} + m_{SR} \sin(\varphi_{SR}) X_{SH}) / 2X_{DT}$; $a_{21} = (X_{SH} V_I \cos(\delta)) / X_{QT}$;

$a_{23} = (X_{SRL} m_{SH} \cos(\varphi_{SH}) + X_{SH} m_{SR} \cos(\varphi_{SR})) / 2X_{QT}$; $b_{11} = -(X_{SRL} V_{dc} \sin(\varphi_{SH})) / 2X_{DT}$;

$b_{12} = -(X_{SRL} m_{SH} V_{dc} \cos(\varphi_{SH})) / 2X_{DT}$; $b_{13} = -(X_{SH} V_{dc} \sin(\varphi_{SR})) / 2X_{DT}$;

$b_{14} = -(X_{SH} m_{SR} V_{dc} \cos(\varphi_{SR})) / 2X_{DT}$; $b_{21} = (X_{SRL} V_{dc} \cos(\varphi_{SH})) / 2X_{QT}$;

$b_{22} = -(X_{SRL} m_{SH} V_{dc} \sin(\varphi_{SH})) / 2X_{QT}$; $b_{23} = (X_{SH} V_{dc} \cos(\varphi_{SR})) / 2X_{QT}$;

$b_{24} = -(X_{SH} m_{SR} V_{dc} \sin(\varphi_{SR})) / 2X_{QT}$

The functions $\alpha_i(\cdot)$ selected

$$\alpha_1 = \left(c_1 + \frac{3}{\rho\varsigma} \right) \tilde{x}_1; \qquad \alpha_2 = \eta_1(x_1)\tilde{x}_1 + \left(c_2 + \frac{2}{\rho\varsigma} \right) \tilde{x}_2 + \tilde{x}_2 \left(\frac{3}{\rho\varsigma} \right) \left(\frac{\partial \xi_2}{\partial x_1} \right)^2$$

$$\alpha_3 = \eta_2(x_1, x_2)\tilde{x}_2 + \left(c_3 + \frac{1}{\rho\varsigma} \right) \tilde{x}_3 + \tilde{x}_3 \left\{ \left(\frac{3}{\rho\varsigma} \right) \left(\frac{\partial \xi_3}{\partial x_1} \right)^2 + \left(\frac{2}{\rho\varsigma} \right) \left(\frac{\partial \xi_3}{\partial x_2} \right)^2 \right\}$$

In this c_1, c_2, c_3, ρ and ς are all positive constants

Appendix C.

Computation of parameters in Chapter 5

$$a_{11} = 2G_3V_3 + B_{31}E_1\sin(\phi_3 - \delta_1) + B_{34}V_4\sin(\phi_3 - \phi_4);$$

$$a_{12} = B_{34}V_3\sin(\phi_3 - \phi_4) + B_{34}(u_1\sin(\phi_3 - \phi_4) + u_2\cos(\phi_3 - \phi_4)); \quad a_{21} = B_{43}V_4\sin(\phi_4 - \phi_3);$$

$$a_{13} = B_{31}V_3E_1\cos(\phi_3 - \delta_1) + B_{34}V_3V_4\cos(\phi_3 - \phi_4) + B_{34}V_4(u_1\cos(\phi_3 - \phi_4) - u_2\sin(\phi_3 - \phi_4));$$

$$a_{14} = -B_{34}V_3V_4\cos(\phi_3 - \phi_4) - B_{34}V_4(u_1\cos(\phi_3 - \phi_4) - u_2\sin(\phi_3 - \phi_4));$$

$$a_{22} = 2G_4V_4 + B_{42}E_2\sin(\phi_4 - \delta_2) + B_{43}V_3\sin(\phi_4 - \phi_3) - B_{34}(u_1\sin(\phi_3 - \phi_4) + u_2\cos(\phi_3 - \phi_4))$$

$$a_{23} = -B_{43}V_4V_3\cos(\phi_4 - \phi_3) - B_{34}V_4(u_1\cos(\phi_3 - \phi_4) - u_2\sin(\phi_3 - \phi_4));$$

$$a_{24} = B_{42}V_4E_2\cos(\phi_4 - \delta_2) + B_{43}V_4V_3\cos(\phi_4 - \phi_3) + B_{34}V_4(u_1\cos(\phi_3 - \phi_4) - u_2\sin(\phi_3 - \phi_4))$$

$$a_{31} = -2B_3V_3 + B_{31}E_1\cos(\phi_3 - \delta_1) + 2B_{33}V_3 + B_{34}V_4\cos(\phi_3 - \phi_4) - B_{34}u_1;$$

$$a_{32} = B_{34}V_3\cos(\phi_3 - \phi_4); a_{33} = -B_{31}V_3E_1\sin(\phi_3 - \delta_1) - B_{34}V_3V_4\sin(\phi_3 - \phi_4)$$

$$a_{34} = B_{34}V_3V_4\sin(\phi_3 - \phi_4); a_{41} = B_{43}V_4\cos(\phi_4 - \phi_3);$$

$$a_{42} = -2B_4V_4 + B_{42}E_2\cos(\phi_4 - \delta_2) + B_{43}V_3\cos(\phi_4 - \phi_3) +$$

$$2B_{44}V_4 + B_{34}(u_1\cos(\phi_3 - \phi_4) - u_2\sin(\phi_3 - \phi_4))$$

$$a_{43} = B_{43}V_4V_3\sin(\phi_4 - \phi_3) - B_{34}V_4(u_1\sin(\phi_3 - \phi_4) + u_2\cos(\phi_3 - \phi_4))$$

$$a_{44} = -B_{42}V_4E_2\sin(\phi_4 - \delta_2) - B_{43}V_4V_3\sin(\phi_4 - \phi_3) + B_{34}V_4(u_1\sin(\phi_3 - \phi_4) + u_2\cos(\phi_3 - \phi_4))$$

$$b_{11} = -B_{31}V_3E_1\cos(\phi_3 - \delta_1); b_{12} = b_{21} = b_{32} = b_{41} = 0; \quad b_{22} = -B_{42}V_4E_2\cos(\phi_4 - \delta_2);$$

$$b_{31} = B_{31}V_3E_1\sin(\phi_3 - \delta_1); b_{42} = B_{42}V_4E_2\sin(\phi_4 - \delta_2)\ g_{11} = B_{34}V_4\sin(\phi_3 - \phi_4) = -g_{21} = -g_{42};$$

$$g_{12} = B_{34}V_4\cos(\phi_3 - \phi_4) = g_{41} = -g_{22}; \quad g_{31} = -B_{34}V_3$$

Appendix D.

Computation of parameters in Chapter 6

$$a_{11} = 2G_3V_3 + B_{31}E_1\sin(\phi_3-\delta_1) + V_4\sin(\phi_3-\phi_4)(B_{34}+B_{SR})$$

$$+B_{SH}V_{SH}\sin(\phi_3-\varphi_{SH}) - B_{SR}V_{SR}\sin(\phi_3-\varphi_{SR});\quad B_{34} = 1/\,jX_{L1};$$

$$a_{12} = V_3\sin(\phi_3-\phi_4)[B_{34}+B_{SR}];\quad a_{14} = -V_3V_4\cos(\phi_3-\phi_4)[B_{34}+B_{SR}];$$

$$a_{13} = B_{31}V_3E_1\cos(\phi_3-\delta_1) + V_3V_4\cos(\phi_3-\phi_4)[B_{34}+B_R] +$$

$$B_{SH}V_3V_{SH}\cos(\phi_3-\varphi_{SH}) - B_{SR}V_3V_{SR}\cos(\phi_3-\varphi_{SR});$$

$$a_{21} = V_4\sin(\phi_4-\phi_3)[B_{34}+B_R];\qquad a_{23} = -V_4V_3\cos(\phi_4-\phi_3)[B_{43}+B_{SR}];$$

$$a_{22} = 2G_4V_4 + B_{42}E_2\sin(\phi_4-\delta_2) + V_3\sin(\phi_4-\phi_3)[B_{43}+B_{SR}] + B_{SR}V_{SR}\sin(\phi_4-\varphi_{SR});$$

$$a_{24} = B_{42}V_4E_2\cos(\phi_4-\delta_2) + V_4V_3\cos(\phi_4-\phi_3)[B_{43}+B_{SR}] + B_{SR}V_4V_{SR}\cos(\phi_4-\varphi_{SR});$$

$$a_{31} = 2V_3[B_{33}-B_3] + B_{31}E_1\cos(\phi_3-\delta_1) + V_4\cos(\phi_3-\phi_4)[B_{34}+B_{SR}]$$

$$B_{SH}V_{SH}\cos(\phi_3-\varphi_{SH}) - B_{SR}V_{SR}\cos(\phi_3-\varphi_{SR});$$

$$a_{32} = V_3\cos(\phi_3-\phi_4)[B_{34}+B_{SR}];\qquad a_{34} = V_3V_4\sin(\phi_3-\phi_4)[B_{34}+B_{SR}];$$

$$a_{33} = -B_{31}V_3E_1\sin(\phi_3-\delta_1) - V_3V_4\sin(\phi_3-\phi_4)[B_{34}+B_{SR}]$$

$$-B_{SH}V_3V_{SH}\sin(\phi_3-\varphi_{SH}) + B_{SR}V_3V_{SR}\sin(\phi_3-\varphi_{SR});$$

$$a_{41} = V_4\cos(\phi_4-\phi_3)[B_{43}+B_{SR}];\quad a_{43} = V_4V_3\sin(\phi_4-\phi_3)[B_{34}+B_{SR}];$$

$$a_{42} = 2V_4[B_{44}-B_4] + B_{42}E_2\cos(\phi_4-\delta_2) + V_3\cos(\phi_4-\phi_3)[B_{43}+B_{SR}] +$$

$$B_{SR}V_{SR}\cos(\phi_4-\varphi_{SR});$$

$$a_{44} = -B_{42}V_4E_2\sin(\phi_4-\delta_2) - V_4V_3\sin(\phi_4-\phi_3)[B_{34}+B_{SR}] + B_{SR}V_{SR}V_4\sin(\phi_4-\varphi_{SR});$$

$$b_{11} = -B_{31}V_3E_1\cos(\phi_3 - \delta_1)\,; b_{12} = b_{21} = b_{32} = b_{41} = 0\,; \quad b_{22} = -B_{42}V_4E_2\cos(\phi_4 - \delta_2)\,;$$

$$b_{13} = (m_{SH}B_{SH}V_3\sin(\phi_3 - \varphi_{SH}) - m_{SR}B_{SR}V_3\sin(\phi_3 - \varphi_{SR}))/2\,;$$

$$b_{23} = (m_{SR}B_{SR}V_4\sin(\phi_4 - \varphi_{SR}))/2\,;$$

$$b_{31} = B_{31}V_3E_1\sin(\phi_3 - \delta_1)\,; b_{33} = (m_{SH}B_{SH}V_3\cos(\phi_3 - \varphi_{SH}) - m_{SR}B_{SR}V_3\cos(\phi_3 - \varphi_{SR}))/2\,;$$

$$b_{42} = B_{42}V_4E_2\sin(\phi_4 - \delta_2)\,; b_{43} = -(m_{SR}B_{SR}V_4\cos(\phi_4 - \varphi_{SR}))/2\,;$$

$$g_{11} = (B_{SH}V_3V_{dc}\sin(\phi_3 - \varphi_{SH}))/2\,; \quad g_{12} = -B_{SH}V_3V_{SH}\cos(\phi_3 - \varphi_{SH})\,;$$

$$g_{13} = -(B_{SR}V_3V_{dc}\sin(\phi_3 - \varphi_{SR}))/2\,; g_{14} = B_{SR}V_3V_{SR}\cos(\phi_3 - \varphi_{SR})\,;$$

$$g_{23} = (B_{SR}V_4V_{dc}\sin(\phi_4 - \varphi_{SR}))/2\,; g_{24} = -B_{SR}V_4V_{SR}\cos(\phi_4 - \varphi_{SR})\,; \quad g_{21} = g_{22} = 0\,;$$

$$g_{31} = (B_{SH}V_3V_{dc}\cos(\phi_3 - \varphi_{SH}))/2\,; g_{32} = B_{SH}V_3V_{SH}\sin(\phi_3 - \varphi_{SH})$$

$$g_{33} = -(B_{SR}V_3V_{dc}\cos(\phi_3 - \varphi_{SR}))/2\,; g_{34} = -B_{SR}V_3V_{SR}\sin(\phi_3 - \varphi_{SR})\,;$$

$$g_{43} = -(B_{SR}V_4V_{dc}\cos(\phi_4 - \varphi_{SR}))/2\,; g_{44} = -B_{SR}V_4V_{SR}\sin(\phi_4 - \varphi_{SR})\,; \quad g_{41} = g_{42} = 0\,;$$

$$L_1 = K_{11}\sin(\delta_1 - \phi_3) + K_{31}V_3\cos(\delta_1 - \phi_3)\,; L_2 = K_{12}\sin(\delta_1 - \phi_3) + K_{32}V_3\cos(\delta_1 - \phi_3)\,;$$

$$L_3 = K_{13}\sin(\delta_1 - \phi_3) + K_{33}V_3\cos(\delta_1 - \phi_3)\,; L_4 = K_{14}\sin(\delta_1 - \phi_3) + K_{34}V_3\cos(\delta_1 - \phi_3)$$

$$f_{T1} = (\omega_1 - \omega_0)\left\{C_{11}\sin(\delta_1 - \phi_3) + V_3\cos(\delta_1 - \phi_3)(1 - C_{31})\right\} +$$

$$(\omega_2 - \omega_0)(C_{12}\sin(\delta_1 - \phi_3) - C_{32}V_3\cos(\delta_1 - \phi_3)) + (C_{13}\sin(\delta_1 - \phi_3) + C_{33}V_3\cos(\delta_1 - \phi_3))\times$$

$$\left\{\frac{B_{SH}V_3V_{SH}\sin(\phi_3 - \varphi_{SH}) + B_{SR}V_{SR}\left[V_4\sin(\phi_4 - \varphi_{SR}) - V_3\sin(\phi_3 - \varphi_{SR})\right]}{C_{dc}V_{dc}}\right\}$$

Dissemination of the Work

Dissemination of the Work

[1] Therattil, Jose P., Panda, P. C., "Modeling and control of a multi-machine power system with FACTS controller," International Conference on Power and Energy Systems (ICPS-2011), Organized by Department of Electrical Engineering, IIT Madras, pp.1-6, 22-24 Dec. 2011.

[2] Therattil, Jose P., Panda, P.C., "Nonlinear model and control of a two area power system with unified power flow controller," Proceedings of the EE Centenary Conference, IISc, Bangalore, pp. 334-339, 15-17 Dec. 2011.

[3] Therattil, Jose P., Panda, P.C., "Transient stability enhancement of a power system with unified power flow controller using pole placement technique," Proc. 35th National system conference (NSC-2011) Organized by Department of Electrical Engineering, IIT Bhubaneswar, pp. 37-46, 9-11 Dec. 2011.

[4] Therattil, Jose P., Panda, P.C., "A nonlinear control to unified power flow controller for power oscillation damping," Proc. 3rd International conference on advances in energy research (ICAER-2011) Organized by Department of Energy Sciences and Engineering, IIT Bombay, 9-11 Dec. 2011.

[5] Therattil, Jose P., Panda, P.C., "A novel adaptive control for a power system with unified power flow controller," Proc. 3rd International conference on advances in energy research (ICAER-2011) Organized by Department of Energy Sciences and Engineering, IIT Bombay, 9-11 Dec. 2011.

[6] Therattil, Jose P., Panda, P.C., "Damping of power system oscillations using an advanced Unified Power Flow Controller," Power Electronics and Drive Systems (PEDS), 2011 IEEE Ninth International Conference on , pp.128-132, 5-8 Dec. 2011.

[7] Therattil, Jose P., Panda, P.C., "Dynamic stability enhancement using an adaptive Unified Power Flow Controller," TENCON 2011 - 2011 IEEE Region 10 Conference, pp.908-912, 21-24 Nov. 2011.

[8] Therattil, Jose P., Panda, P.C., "Improving dynamic stability of a power system using adaptive static synchronous series compensator," TENCON 2011 -IEEE Region 10 Conference, pp.928-932, 21-24 Nov. 2011.

[9] Therattil, Jose P., Panda, P.C., "Dynamic stability enhancement of a multi-area multi-terminal DC-AC system with self-tuning Static VAR Compensator," Power Electronics, Drives and Energy Systems (PEDES) & 2010 Power India, 2010 Joint International Conference on , pp.1-6, 20-23 Dec. 2010 (Organized by IIT Delhi).

[10] Therattil, Jose P., Panda, P.C., "Dynamic stability enhancement using self-tuning Static VAR Compensator," India Conference (INDICON), 2010 Annual IEEE, pp.1-5, 17-19 Dec. 2010.

[11] Therattil, Jose P., Panda, P. C., "Transient stability enhancement of a multi-machine power system with adaptive controlled static reactive power compensator," International conference on electrical power and energy systems (ICEPES-2010), 26-28 Aug. 2010. (MANIT Bhopal).

[12] Therattil, Jose P., Panda, P. C., "Transient stability enhancement of a multi-machine power system with admittance model static reactive power compensator," Communications in Computer and Information Science, 2010, Volume 102, part 1, pp.37- 41 (Springer Link).

[13] Narne, R., Panda, P. C., Therattil, Jose P., "Transient stability enhancement of SMIB system using PSS and TCSC-based controllers," Power Electronics and Drive Systems (PEDS), 2011 IEEE Ninth International Conference on , pp.214-218, 5-8 Dec. 2011.

[14] Laxmidhar, Sahu., Therattil, Jose P., Panda, P.C., "Study of shunt FACTS-based controllers effectiveness on multi-machine power system steady state operation," Advanced materials research, vol. 403-408, pp. 4926-4933, Nov. 2011.(Trans Tech publications, Switzerland)

[15] Narne, R., Therattil, Jose P., Sahu, L., Panda, P.C., "Dynamic Stability Enhancement Using Self-Tuning Static Synchronous Compensator," Process Automation, Control and Computing (PACC), 2011 International Conference on , pp.1-5, 20-22 July 2011.

Journals Published

[1] Therattil, Jose P., Panda, P.C., "Nonlinear Dynamic Modeling and Adaptive Control of a Power System with Unified Power Flow Controller," Electric Power Components and Systems, Vol. 40, No. 14, pp. 1544-1561, 2012.

Journals under review

[1] Therattil, Jose P., Panda, P.C., "Modeling and Control of a Multi-Area Power System with Unified Power Flow Controller," Sadhana - Academy Proceedings in Engineering Sciences, Springer, under review

[2] Therattil, Jose P., Panda, P.C., "Advanced Nonlinear Control for a Multi-Area Power System with Unified Power Flow Controller," Electric Power Components and Systems, Taylor & Francis, under review

[2] Therattil, Jose P., Panda, P.C., "Dynamic Modeling and Control of Multi-Machine Power System with FACTS Devices for Stability Enhancement," IEEE Transactions on Power Delivery, under review